

1982

Experimental study of flow in rectangular settling tanks.

Amal M. Moursi. El-Sabaky
University of Windsor

Follow this and additional works at: <http://scholar.uwindsor.ca/etd>

Recommended Citation

El-Sabaky, Amal M. Moursi, "Experimental study of flow in rectangular settling tanks." (1982). *Electronic Theses and Dissertations*. Paper 2030.

This online database contains the full-text of PhD dissertations and Masters' theses of University of Windsor students from 1954 forward. These documents are made available for personal study and research purposes only, in accordance with the Canadian Copyright Act and the Creative Commons license—CC BY-NC-ND (Attribution, Non-Commercial, No Derivative Works). Under this license, works must always be attributed to the copyright holder (original author), cannot be used for any commercial purposes, and may not be altered. Any other use would require the permission of the copyright holder. Students may inquire about withdrawing their dissertation and/or thesis from this database. For additional inquiries, please contact the repository administrator via email (scholarship@uwindsor.ca) or by telephone at 519-253-3000ext. 3208.

EXPERIMENTAL STUDY OF FLOW IN
RECTANGULAR SETTLING TANKS

by



Amal M. Moursi (El-Sebakhy)
B.Sc.

A Thesis

submitted to the Faculty of Graduate Studies through the
Department of Civil Engineering in Partial Fulfillment
of the requirements for the Degree of
Master of Applied Science at
The University of Windsor

Windsor, Ontario, Canada

1982

c Amal M. Moursi (El-Sebakhy) 1982
All Rights Reserved

778810

◦ To Ibrahim, my parents and Yossra

ABSTRACT

The behaviour of the flow in rectangular settling tanks is investigated experimentally under different flow conditions. A total of 13 configurations of rectangular settling tanks are tested using a Laser Doppler Anemometer to measure the mean and r.m.s. velocities throughout the tank. Statistical analysis is used to analyze the experimental data and to study the factors influencing the flow patterns, the size of eddies, potential core, growth of the boundary layer and the turbulence distribution within the tank.

The energy balance is investigated on the basis of measured velocity to discuss the internal mechanisms by which energy is lost in the basin. Mean kinetic energy and turbulent kinetic energy values are obtained by integrating the mean velocity and r.m.s. velocity profiles. Turbulent kinetic energy is used to represent the turbulence in the tanks.

A simplified differential transport equation for describing the general trend of the energy balance using the basic transport principles is developed. This equation uses the velocity and the mean kinetic energy fields as input to predict the turbulent kinetic energy within the tank.

The transport equation results compared reasonably well with the experimental data of this study.

ACKNOWLEDGEMENTS

The author wishes to express her sincere gratitude to her advisor, Dr. A. McCorquodale, for his guidance, suggestions and continuous encouragement throughout the preparation of this thesis.

The author would like to thank the hydraulic engineering staff members for their valuable courses. Thanks are due to Mr. F. Kiss and Mr. P. Feimer for their help in the experimental work.

The author is grateful to her husband, Ibrahim, for his assistance, guidance and encouragement.

Finally, the author wishes to express her sincere thanks to Mrs. A. Zeleney for typing this manuscript.

TABLE OF CONTENTS

DEDICATION.	iv
ABSTRACT.	v
ACKNOWLEDGEMENTS.	vi
LIST OF FIGURES	ix
LIST OF TABLES.	vi
I. INTRODUCTION	1
1.1 Objective	1
1.2 Definition of the Problem	1
1.3 The Approach in General	2
II. LITERATURE REVIEW.	4
2.1 Introduction.	4
2.2 Hydraulic Studies of Flow in Sedimentation Basins	5
2.3 Turbulence Studies and Their Application in Hydraulics and Settling Tanks	8
2.4 The Energy Equation	16
III. THE EXPERIMENTAL STUDIES	23
3.1 Objectives.	23
3.2 The Experimental Apparatus.	23
3.3 Experimental Procedure.	26
3.4 Experimental Ranges	28
3.5 Experimental Results.	28
IV. DATA REDUCTION AND ANALYSIS.	30
4.1 Introduction.	30
4.2 Presentation of Data in Terms of Dimensionless Variables.	30
4.2.1 Plotting the Mean Velocity and r.m.s. Profiles.	30
4.2.2 Mean Kinetic Energy and Turbulent Kinetic Energy Flux	32
4.3 Proposed Equation	34

4.4	Determination of the Constants (A, B)	37
4.5	Fitting of the Transport Equation	38
4.6	The Numerical Solution and Testing.	39
V.	DISCUSSION OF THE EXPERIMENTAL DATA AND EVALUATION OF THE TRANSPORT EQUATION	41
5.1	Introduction.	41
5.2	The Mean Velocity and r.m.s. Profiles.	41
5.3	Factors Influencing the Flow Patterns.	44
5.4	The Potential Core and Boundary Layer	47
5.5	Mean Kinetic Energy Profiles.	49
5.6	Comparison of the Transport Equation for the Turbulent Kinetic Energy with the Experimental Data.	50
5.7	Errors and Limitations of the Theory.	51
VI.	CONCLUSIONS	52
APPENDIX A	Tables.	127
APPENDIX B	Computer Programmes	157
NOMENCLATURE.	161
REFERENCES.	164
VITA AUCTORIS	168

LIST OF FIGURES

<u>Figure</u>		<u>Page</u>
3.1	Schematic Layout of Flume.	56
3.2	Laser Doppler Anemometer Arrangement (After Ref. 33).	57
3.3	Laser and Transmitting Optics.	58
3.4	Receiving Optics	59
3.5	Signal Processor and Oscilloscope.	60
3.6	Overall View of Test Facility.	60
4.1	Longitudinal velocity and r.m.s. profiles at X=5 cm, $q=53.9 \text{ cm}^3/\text{sec}/\text{cm}$, L=30 cm, G= 3 cm.	61
4.2	Longitudinal velocity and r.m.s. profiles at X=10 cm, $q=53.9 \text{ cm}^3/\text{sec}/\text{cm}$, L=30 cm, G=3 cm	62
4.3	Longitudinal velocity and r.m.s. profiles at at X=15 cm, $q=53.9 \text{ cm}^3/\text{sec}/\text{cm}$, L=30 cm, G=3 cm	63
4.4	Longitudinal velocity and r.m.s. profiles at X=20 cm, $q=53.9 \text{ cm}^3/\text{sec}/\text{cm}$, L=30 cm, G=3 cm	64
4.5	Longitudinal velocity and r.m.s. profiles at X=25 cm, $q=53.9 \text{ cm}^3/\text{sec}/\text{cm}$, L=30, G=3 cm	65
4.6	Longitudinal velocity and r.m.s profiles at X=5 cm, $q=53.9 \text{ cm}^3/\text{sec}/\text{cm}$, L=30 cm, G=5 cm	66
4.7	Longitudinal velocity and r.m.s. profiles at X=10 cm, $q=53.9 \text{ cm}^3/\text{sec}/\text{cm}$, L=30 cm, G=5 cm	67
4.8	Longitudinal velocity and r.m.s profiles at X=15 cm, $q=53.9 \text{ cm}^3/\text{sec}/\text{cm}$, L=30 cm, G=5 cm	68
4.9	Longitudinal velocity and r.m.s. profiles at X=20 cm, $q=53.9 \text{ cm}^3/\text{sec}/\text{cm}$, L=30 cm, G=5 cm	69

<u>Figure</u>	<u>Page</u>
4.10 Longitudinal velocity and r.m.s. profiles at X=25 cm, q=53.9cm ³ /sec/cm, L=30 cm, G=5 cm.	70
4.11 Longitudinal velocity and r.m.s. profiles at X=5 cm, q= 53.9 cm ³ /sec/cm, L=30 cm, G=7 cm.	71
4.12 Longitudinal velocity and r.m.s. profiles at X=10 cm, q=53.9 cm ³ /sec/cm, L=30 cm, G=7 cm.	72
4.13 Longitudinal velocity and r.m.s. profiles at X=15 cm, q=53.9 cm ³ /sec/cm, L=30 cm. G=7 cm.	73
4.14 Longitudinal velocity and r.m.s. profiles at X=20 cm, q=53.9 cm ³ /sec/cm, L=30 cm, G=7 cm.	74
4.15 Longitudinal velocity and r.m.s. profiles at X=25 cm, q=53.9 cm ³ /sec/cm, L=30 cm, G=7 cm.	75
4.16 Longitudinal velocity and r.m.s. profiles at X= 5 cm, q=111 cm ³ /sec/cm, L=40 cm, G=5 cm.	76
4.17 Longitudinal velocity and r.m.s. profiles at X=10 cm. q=111 cm ³ /sec/cm, L=40 cm, G=5 cm.	77
4.18 Longitudinal velocity and r.m.s. profiles at X= 15 cm, q=111 cm ³ /sec/cm, L=40 cm, G=5 cm.	78
4.19 Longitudinal velocity and r.m.s. profiles at X=20 cm, q=111cm ³ /sec/cm, L=40 cm, G=5 cm.	79
4.20 Longitudinal velocity and r.m.s. profiles at X=25 cm, q=111 cm ³ /sec/cm, L=40 cm, G=5 cm.	80
4.21 Variation of dimensionless mean kinetic energy with distance along the tank for (L=73 cm, G=3 cm, q=111 cm ³ /sec/cm)	81

<u>Figure</u>		<u>Page</u>
4.22	Variation of dimensionless mean kinetic energy with distance along the tank for (L=30 cm, G=3 cm, q=87.41 cm ³ /sec/cm)	82
4.23	Variation of dimensionless mean kinetic energy with distance along the tank for (L=30 cm, G=3, q=53.9 cm ³ /sec/cm)	82
4.24	Variation of dimensionless mean kinetic energy with distance along the tank for (L=40 cm, G=3 cm, q=61.74 cm ³ /sec/cm)	83
4.25	Variation of dimensionless mean kinetic energy with distance along the tank for (L=30 cm, G=5 cm, q=53.9 cm ³ /sec/cm)	83
4.26	Variation of dimensionless mean kinetic energy with distance along the tank for (L=40 cm, G=5, q=53.9 cm ³ /sec/cm)	84
4.27	Variation of dimensionless mean kinetic energy with distance along the tank for (L=30 cm, G=5cm, q=101.32 cm ³ /sec/cm)	84
4.28	Variation of dimensionless mean kinetic energy with distance along the tank for (L=73 cm, G=5 cm, q=147 cm ³ /sec/cm)	85
4.29	Variation of dimensionless mean kinetic energy with distance along the tank for (L=40 cm, G=5 cm, q=111 cm ³ /sec/cm)	85
4.30	Variation of dimensionless mean kinetic energy with distance along the tank for L=30 cm, G=7 cm, q=53.9 cm ³ /sec/cm)	86
4.31	Variation of dimensionless mean kinetic energy with distance along the tank for (L=30 cm, G=7 cm, q=106 cm ³ /sec/cm)	86
4.32	Variation of dimensionless mean kinetic energy with distance along the tank for L=40 cm, G=7 cm, q=53.9 cm ³ /sec/cm)	86
4.33	Variation of dimensionless turbulent kinetic energy with distance (L=30 cm, G=3 cm, q=87.41 cm ³ /sec/cm)	87

<u>Figure</u>		<u>Page</u>
4.34	Variation of dimensionless turbulent kinetic energy with distance (L=30 cm, G=3 cm, q=53.9 cm ³ /sec/cm)	88
4.35	Variation of dimensionless turbulent kinetic energy with distance (L=73 cm, G=3 cm, q=111 cm ³ /sec/cm).	89
4.36	Variation of dimensionless turbulent kinetic energy with distance (L=40 cm, G=3 cm, q=61.74 cm ³ /sec/cm),	90
4.37	Variation of dimensionless turbulent kinetic energy with distance (L=40 cm, G=5 cm, q=111 cm ³ /sec/cm).	91
4.38	Variation of dimensionless turbulent kinetic energy with distance (L=73 cm, G=5 cm, q=147 cm ³ /sec/cm).	92
4.39	Variation of dimensionless turbulent kinetic energy with distance (L=30 cm, G=5 cm, q=101.32 cm ³ /sec/cm)	93
4.40	Variation of dimensionless turbulent kinetic energy with distance (L=30 cm, G=5 cm, q=53.9 cm ³ /sec/cm)	94
4.41	Variation of dimensionless turbulent kinetic energy with distance (L=40 cm, G=5 cm, q=53.9 cm ³ /sec/cm)	95
4.42	Variation of dimensionless turbulent kinetic energy with distance (L=30 cm, G=7 cm, q=106 cm ³ /sec/cm).	96
4.43	Variation of dimensionless turbulent kinetic energy with distance (L=30 cm, G=7 cm, q=53.9 cm ³ /sec/cm)	97
4.44	Variation of dimensionless turbulent kinetic energy with distance (L=40 cm, G=7 cm, q=53.9 cm ³ /sec/cm)	98
4.45	Vertical strip of energy balance in a settling basin	99
4.46	Schematic representation for determining the Constants A, B	100

<u>Figure</u>		<u>Page</u>
4.47	The best fitting curve of mean kinetic energy.	101
5.1a, b	Flow characteristics (L=73 cm, G=3 cm, q=111 cm ³ /sec/cm)	102
5.2a, b	Flow characteristics (L=40 cm, G=3 cm, q= 61.74 cm ³ /sec/cm).	103
5.3a, b	Flow Characteristics (G=3 cm, L=30 cm, q=87.41 cm ³ /sec/cm)	104
5.4a, b	Flow characteristics (G=3 cm, L=30 cm, q= 53.9 cm ³ /sec/cm)	105
5.5a, b	Flow characteristics (G=5 cm, L=73 cm, q=147 cm ³ /sec/cm)	106
5.6a, b	Flow characteristics (G=5 cm, L=40 cm, q=111 cm ³ /sec/cm)	107
5.7a, b	Flow characteristics (G=5 cm, L=40 cm, q=53.9 cm ³ /sec/cm).	108
5.8a, b	Flow characteristics (G=5 cm, L=30 cm, q=101.32 cm ³ /sec/cm).	109
5.9a, b	Flow characteristics (G=5 cm, L=30 cm, q=53.9 cm ³ /sec/cm).	110
5.10 a,b	Flow characteristics (G=7 cm, L=40 cm, q=53.9 cm ³ /sec/cm).	111
5.11 a,b	Flow characteristics (G=7 cm, L=40 cm, q=106 cm ³ /sec/cm)	112
5.12 a,b	Flow characteristics (G=7 cm, L=30 cm, q=53.9 cm ³ /sec/cm)...	113
5.13	Effect of beam length on roller length.	114
5.14 a,b	Comparison of the general features of settling tank flow for (a) the present study, (b) Khattab, (c) McCorquodale.	115
5.15	Distribution of (r.m.s.) values for flow characteristics (L=73 cm, G=5 cm, q=147 cm ³ /sec/cm)	116

<u>Figure</u>	<u>Page</u>
5.16	Distribution of (r.m.s.) values for flow characteristics (L=73 cm, G=3 cm, q = 111. cm ³ /sec/cm) 116
5.17	Distribution of (r.m.s.) values for flow characteristics (L=30 cm, G=5 cm, q=101.32 cm ³ /sec/cm) 117
5.18	Distribution of (r.m.s.) values for flow characteristics (L=30 cm, G=7 cm, q=106 cm ³ /sec/cm) 117
5.19	Distribution of (r.m.s.) values for flow characteristics (L=30 cm, G=3 cm, q=53.9 cm ³ /sec/cm) 118
5.20	Distribution of (r.m.s.) values for flow characteristics (L=30 cm, G=3 cm, q=87.41 cm ³ /sec/cm) 118
5.21	Distribution of (r.m.s.) values for flow characteristics (L=30 cm, G=7 cm, q=53.9 cm ³ /sec/cm) 119
5.22	Distribution of (r.m.s.) values for flow characteristics (L=40 cm, G= cm, q=111 cm ³ /sec/cm) 119
5.23	Distribution of (r.m.s.) values for flow characteristics (L=40 cm, G=5 cm, q=53.9 cm ³ /sec/cm) 120
5.24	Distribution of (r.m.s.) values for flow characteristics (L=30 cm, G=5 cm, q=53.9 cm ³ /sec/cm) 120
5.25	Distribution of (r.m.s.) values for flow characteristics (L=40 cm, G=3 cm, q=61.74 cm ³ /sec/cm) 121
5.26	Definition sketch of plane turbulent wall jets. 122
5.27	Comparison of the slope of potential core. . 123
5.28	The effect of tank length on the length of the potential core. 124
5.29	Maximum calculated and measured values of turbulent kinetic energy. 125

LIST OF TABLES

<u>Table</u>	<u>Page</u>
3.1 Equipment Details.	127
3.2 Measured Longitudinal Mean Velocity and (r.m.s.) Profiles for, $q=61.74 \text{ cm}^3/\text{sec}/\text{cm}$ at $X = 0.0 \text{ cm}$	128
3.3 Measured Longitudinal Mean Velocity and (r.m.s.) Profiles for, $q=61.74 \text{ cm}^3/\text{sec}/\text{cm}$ at $X = 13 \text{ cm}$	129
3.4 Measured Longitudinal Mean Velocity and (r.m.s.) Profiles for, $q=61.74 \text{ cm}^3/\text{sec}/\text{cm}$ at $X = 23 \text{ cm}$	130
3.5 Measured Longitudinal Mean Velocity and (r.m.s.) Profiles for, $q=61.74 \text{ cm}^3/\text{sec}/\text{cm}$ at $X = 33 \text{ cm}$	131
3.6 Measured Longitudinal Mean Velocity and (r.m.s.) Profiles for, $q = 87.41 \text{ cm}^3/\text{sec}/\text{cm}$ at $X = 0.0 \text{ cm}$	132
3.7 Measured Longitudinal Mean Velocity and (r.m.s.) Profiles for, $q=87.41 \text{ cm}^3/\text{sec}/\text{cm}$ at $X = 13 \text{ cm}$	133
3.8 Measured Longitudinal Mean Velocity and (r.m.s.) Profiles for, $q=87.41 \text{ cm}^3/\text{sec}/\text{cm}$ at $X = 28 \text{ cm}$	134
3.9 Measured Longitudinal Mean Velocity and (r.m.s.) Profiles for, $q=111 \text{ cm}^3/\text{sec}/\text{cm}$ at $X = 0.0 \text{ cm}$	135
3.10 Measured Longitudinal Mean Velocity and (r.m.s.) Profiles for, $q=111 \text{ cm}^3/\text{sec}/\text{cm}$ at $X = 13 \text{ cm}$	136
3.11 Measured Longitudinal Mean Velocity and (r.m.s.) Profiles for, $q=111 \text{ cm}^3/\text{sec}/\text{cm}$ at $X = 28 \text{ cm}$	137
3.12 Measured Longitudinal Mean Velocity and (r.m.s.) Profiles for, $q=111 \text{ cm}^3/\text{sec}/\text{cm}$ at $X = 43 \text{ cm}$	138

<u>Table</u>	<u>Page</u>
3.13 Measured Longitudinal Mean Velocity and (r.m.s.) Profiles for, $q=111 \text{ cm}^3/\text{sec}/\text{cm}$ at $X = 63 \text{ cm}$	139
3.14 Measured Longitudinal Mean Velocity and (r.m.s.) Profiles for, $q=101.32 \text{ cm}^3/\text{sec}/\text{cm}$ at $X = 0:0 \text{ cm}$	140
3.15 Measured Longitudinal Mean Velocity and (r.m.s.) Profiles for, $q=101.32 \text{ cm}^3/\text{sec}/\text{cm}$ at $X = 13 \text{ cm}$	141
3.16 Measured Longitudinal Mean Velocity and (r.m.s.) Profiles for, $q=101.32 \text{ cm}^3/\text{sec}/\text{cm}$ at $X = 28 \text{ cm}$	142
3.17 Measured Longitudinal Mean Velocity and (r.m.s.) Profiles for, $q=111 \text{ cm}^3/\text{sec}/\text{cm}$ at $X = 8 \text{ cm}$	143
3.18 Measured Longitudinal Mean Velocity and (r.m.s.) Profiles for, $q=111 \text{ cm}^3/\text{sec}/\text{cm}$ at $X = 18 \text{ cm}$	144
3.19 Measured Longitudinal Mean Velocity and (r.m.s.) Profiles for, $q=111 \text{ cm}^3/\text{sec}/\text{cm}$ at $X = 28 \text{ cm}$	145
3.20 Measured Longitudinal Mean Velocity and (r.m.s.) Profiles for, $q=111 \text{ cm}^3/\text{sec}/\text{cm}$ at $X = 33 \text{ cm}$	146
3.21 Measured Longitudinal Mean Velocity and (r.m.s.) Profiles for, $q=147 \text{ cm}^3/\text{sec}/\text{cm}$ at $X = 8 \text{ cm}$	147
3.22 Measured Longitudinal Mean Velocity and (r.m.s.) Profiles for, $q=147 \text{ cm}^3/\text{sec}/\text{cm}$ at $X = 18 \text{ cm}$	148
3.23 Measured Longitudinal Mean Velocity and (r.m.s.) Profiles for, $q=147 \text{ cm}^3/\text{sec}/\text{cm}$ at $X = 28 \text{ cm}$	149
3.24 Measured Longitudinal Mean Velocity and (r.m.s.) Profiles for, $q=147 \text{ cm}^3/\text{sec}/\text{cm}$ at $X = 38 \text{ cm}$	150

<u>Table</u>	<u>Page</u>
3.25 Measured Longitudinal Mean Velocity and (r.m.s.) Profiles for, $q=147 \text{ cm}^3/\text{sec}/\text{cm}$ at $X = 70 \text{ cm}$	151
3.26 Measured Longitudinal Mean Velocity and (r.m.s.) Profiles for, $q=106 \text{ cm}^3/\text{sec}/\text{cm}$ at $X = 0.0 \text{ cm}$	152
3.27 Measured Longitudinal Mean Velocity and (r.m.s.) Profiles for, $q=106 \text{ cm}^3/\text{sec}/\text{cm}$ at $X = 18 \text{ cm}$	153
3.28 Measured Longitudinal Mean Velocity and (r.m.s.) Profiles for, $q=106 \text{ cm}^3/\text{sec}/\text{cm}$ at $X = 28 \text{ cm}$	154
4.1 Average Values of A's and B's for Different Flow Conditions	155

I. INTRODUCTION

1.1. Objective

The objective of this work is to study experimentally the hydraulics of rectangular settling tanks, and to develop a simplified transport equation to predict the turbulent kinetic energy in these tanks. In order to achieve this objective an experimental study of the flow under different conditions was necessary.

1.2 Definition of the Problem

Sedimentation is the most common process in the treatment of water and wastewater. Although first used in purification of raw water for water supply, sedimentation basins are found today more frequently in wastewater treatment plants. The study of flow behaviour in settling tanks has aroused considerable interest in recent years.

In an ideal sedimentation basin under the best conditions, every part of the fluid entering the unit is evenly distributed across the tank at inlet zone, and the flow advances with a uniform velocity distribution to the outlet. In a real basin, the kinetic energy of the flow entering the settling basin is lost mainly through eddies in the inlet zone. These generally result from the sudden

enlargement in flow section from the inlet section to the tank section. This phenomenon will cause re-circulation currents and dead space.

It is, therefore, of interest to discuss the internal mechanisms by which energy is lost in the basin. Turbulent kinetic energy is used to represent the turbulence in the tanks.

1.3 The Approach in General

In the project reported here, the behaviour of the flow in rectangular settling tanks is investigated for different tank configurations.

A total of 13 configurations of rectangular settling tanks were tested using a Laser Doppler Anemometer to measure the mean and r.m.s. velocities throughout the tank. Data measurements were analyzed using a computer programme and the CALCOMP Plotter to study the effect of tank length, gate opening and flowrates on velocity and turbulence distribution within the tank. Also the flow patterns, for the same configurations were presented to study the factors influencing the size of eddies, potential core and the growth of the boundary layer.

The energy balance was investigated on the basis of measured velocity. Mean kinetic energy and turbulent kinetic energy values were obtained by integrating the mean velocity and r.m.s. profiles.

A transport equation based on applying the basic principles for energy balance is developed; this equation uses the velocity and mean kinetic energy fields as input to predict the turbulent kinetic energy within the tank.

The rate at which the mean kinetic energy is converted into turbulence and the rate at which the turbulence energy is dissipated are developed using the experimental kinetic energy and turbulent kinetic energy data.

The transport equation is solved by using RUNGA-KUTTA method. To verify the transport equation, the results are compared with the experimental data for the present study for turbulent kinetic energy.

II. LITERATURE REVIEW

2.1 Introduction

Flow in settling tanks is a stratified, two-phase, turbulent flow. The factors affecting the removal process can be divided into three groups: (i) the characteristics of the suspended solids and the transporting liquid, (ii) hydraulic conditions within the clarifier due to its shape, inlet and outlet arrangements, and (iii) field conditions.

It is a difficult task to quantify the combined effects of all the factors on suspended solids removal. This has led researchers to study and quantify only a limited number of factors, while minimizing the effects of the other factors (17).

In this chapter the available literature related to the subject of this work, is presented. The review includes literature on:

- (a) hydraulics studies of flow in sedimentation basins,
- (b) turbulence studies in hydraulics and settling tanks, and
- (c) the energy transport equation.

2.2 Hydraulics Studies of Flow in Sedimentation Basins

The determination of the flow pattern in the settling tanks is the key to evaluating the performance for various tank configurations. Flow patterns may be generated by experimental model studies, direct field measurement, full-scale experimental studies, and mathematical modeling (37).

In 1967 Khattab (19) studied the flow pattern in circular sedimentation tanks; experimental work was carried out using a miniature flowmeter in measuring the velocities in large number of points at sections across the tank radius. Results were analyzed to study the effects of tank shape, inlet arrangements and flow rates on flow patterns.

Two types of flow patterns were obtained. In the first type, where no inlet baffles were present, the flow passed from the inlet to outlet weir at high velocity through the upper part of the tank inducing a large eddy in the lower part of the tank which rotated forward at the top. In deep tanks, small eddy took place near the inlet pipe and close to the tank floor, rotating backward at the top.

The second type, with an inlet baffle, the flow passed at high velocity throughout the lower part of the tank, inducing a large eddy in the upper part of the tank, rotating forward at the bottom. In deep tanks a small eddy was

induced at the bottom near the baffle. This eddy increased in size in sloping bottom tanks. This eddy rotates forward at the top.

In 1977, Larsen (21) published a comprehensive report on the hydraulic behaviour of the flow in rectangular settling basin. Detailed measurements of velocity distribution and concentration distribution have been reported from various rectangular tanks in Sweden.

In all basins tested the flow pattern consisted of a well developed bottom current and a return flow in the upper layers of the basins. Measurements in the established bottom current showed little variation across the basin. Thus, the assumption of two-dimensional flow is reasonable as regards the bottom current. Entrainment from the bottom current to return the current was noted by an increase in flowrate of the return flow in the directions of the inlets.

Based on these studies, he classified the settling basin into the following zones:

- (1) Inlet zone characterized by three-dimensional flow, mixing and entrainment of water with low concentrations of suspended matter.
- (2) Bottom current zone characterized by two-dimensional flow with velocities about ten times higher than the nominal velocity. In this zone

the bulk of the settling takes place.

- (3) Return current zone characterized by two-dimensional flow directed toward the inlet end with entrainment from bottom current.
- (4) Sludge zone beneath the bottom current zone.

Larsen also found turbulence intensities to range from 10%-20% (relative to the maximum mean value of velocities in the bottom current) throughout the basin, although even higher values were found in the inlet zone.

A settling tank flow does not readily lend itself to observation or measurement. Indirect methods of investigation such as tracer techniques have been used by many researchers, e.g., Camp (3), Morrill (28), Ingersoll et al. (18), El-baroudi (11,12), Hirsch (16), McCorquodale (23) and Crosby and Bender (7). Tracer methods are the most widely used and many tracers are available.

In 1972 Clements and Price (6) published a paper on "A two-float technique for examination of flow characteristics of sedimentation tanks." They emphasized that tracer methods do not reveal much information about the details of the internal flow pattern in a clarifier and in many cases have misled by giving invalid general criteria of the behaviour of the tank.

The float method described in his paper enabled both a practical measurement of the time-ratio of a full-scale

rectangular tank to be obtained and the flow pattern on plan to be drawn. The technique has already been used successfully by Price (30) on thirteen tanks at six different sewage works.

As indicated by Imam (17), the use of stochastic models is necessary in dealing with a random phenomenon of solid particle settlement in a turbulent flow.

Bayazit (1) applied a random walk model to the motion of a single small solid particle settling in a low Reynolds number turbulent open-channel flow.

Li and Shen (27) employed a random walk theory along with currently available Eulerian flow information to study a solid particle settlement in an open-channel.

2.3 Turbulence Studies and Their Application in Hydraulics and Settling Tanks

Turbulence provides many of the most challenging problems in hydraulics. The basic nature of the phenomenon of turbulence has been described by many researchers, e.g., Reynolds (34), Launder and Spalding (22), and Rodi (35).

As indicated by Rodi (35), turbulence is an eddying motion which, at the high Reynolds numbers usually prevailing, has a wide spectrum of eddy sizes and a corresponding spectrum of fluctuation frequencies. Its motion is always rotational and can be thought of as a tangle of vortex elements whose vorticity vectors can be aligned

in all directions and are highly unsteady.

The large eddies interact with the mean flow thereby extracting kinetic energy from the mean motion and feeding it into the large-scale turbulent motion. The eddies can be considered as vortex elements which stretch each other. Due to this vortex stretching, the energy is passed on to smaller and smaller eddies until viscous forces become active and dissipate the energy.

The results of an experimental investigation into the decay of turbulence in a flow behind a double grid of cylinders with the grids moving in opposite direction, were given by Ginevskii (14). It was shown that the distribution of the turbulence parameters behind such a grid is more uniform than for other known methods of generating turbulence.

The kinetic energy of the flow entering the settling basin is lost mainly through turbulent eddies in inlet zone.

Larsen (20, 21) studied the energy balance in a secondary settling tanks to assess the importance of various factors involved in the settling process. The major energy fluxes were: (i) kinetic energy associated with the inlets; (ii) potential energy due to the influent suspension having a higher density than the clarified liquid, (iii) energy transferred to the basin at the free surface due to wind shear, (iv) heat flux through sidewalls and potential energy due to atmospheric cooling at the surface, and (v)

energy flux associated with water surface slope. Sources (i) and (ii) were considered point sources of energy while (iii) to (v) were distributed over the entire surface.

Larsen made an order of magnitude study of the various energy inputs to a typical secondary settling basin and found that the energy of the effluent only amounts to a negligible amount compared to energy contributed to the basin. It was also shown that the energy fluxes related to inlet conditions are several orders of magnitude greater than energy flux and rate of energy loss assuming "ideal settling basin" conditions.

According to many researchers, e.g., Camp (3), Dobbins (8), Orton (29), McCorquodale (23), and Larsen (21), the design of inlets should be given attention as a consequence of the high flux of energy associated with the velocity of the influent.

Knowledge of the characteristics of turbulence is an important factor in many design and research projects in the fields of hydraulic and sanitary engineering. It is the mean motion, along with appropriate statistical characteristics of the turbulent fluctuations, that are normally of interest when a turbulent flow is studied. The root-mean-square of the fluctuations is a measure of fluctuation intensity. For brevity, it will be termed the r.m.s. value.

A three parameter model was derived by Schall, Ming Li and Simons (26, 36) predicting the root-mean-square (r.m.s.) values of turbulence for the vertical and longitudinal directions. They assumed a Gaussian distribution to describe the turbulent fluctuating velocities as a probabilistic approach to the problem. Further assumptions on the characteristics of flow were necessary to simplify the model: (1) the flow is steady and uniform in the ordinary sense, i.e., over a time period, (2) the fluctuating velocity in the streamwise direction is the result of momentum transfer only in the cross-streamwise Y direction. The influence in the transverse Z direction is neglected, (3) the mean flow velocity in the Y direction is zero across the entire flow depth, (4) the expected magnitude of the cross-stream fluctuating velocity is proportional to that of the streamwise fluctuating velocity, i.e.,

$$E[|V_i|] = CE [|U_i|] \quad (2.1)$$

in which $E[\cdot]$ = the expected magnitude of the absolute values of cross-stream and streamwise fluctuating flow velocities, respectively; and C is a constant.

The experimental data of McQuivey (24) and the split hot film data taken by Schall et al. (36) was used to evaluate the longitudinal and vertical r.m.s. values of velocity

in smooth boundary rectangular and trapezoidal channels.

A detailed experimental study of developing turbulent flow in a rectangular ducts was made by Melling and Whitelaw (25), using a Laser-Doppler anemometer. The purpose of the work were to obtain data of value to fluid mechanicians, particularly those interested in the development and testing of mathematical turbulence models, and to evaluate the performance of the anemometer. For the first purpose, contours of axial mean velocity and turbulence intensity were measured in the developing flow, and all three mean velocity components and five of the six Reynolds stresses were obtained in the nearly fully developed flow.

Increasing concern regarding the environmental effects of changes in flow patterns for bodies of water and streams demands that flow parameters characterizing turbulence be measured and understood.

Cenedese, Mele, and Morganti (5), obtained some information on the distribution of the velocity field in the turbulent shear flow generated by a square section body placed on the bottom of a two-dimensional turbulent flow. Intense velocity fluctuations were obtained on the walls of the obstacle bounding the flow. They emphasized that the magnitude and spectral distribution of fluctuations are of special interest for engineering problems. In a previous study (4), the velocity field, i.e.,

the mean horizontal component \bar{U} and the root-mean-square $\sqrt{u'^2}$ were analyzed and the modification of the power spectra of u' as a function of Strouhal number were determined.

The velocity values were obtained by a Laser anemometer, very low and negative velocity were measured using a frequency shift obtained by a Bragg cell (9).

Cenedese, et al. (5) presented the horizontal components of the flow mean velocity and of the root-mean-square of turbulent velocity on vertical profiles on the mid-point of the channel width.

Other studies were reported on a turbulent flow in a two-dimensional channel of aspect ratio 1:16 in which a square obstacle of half the channel height was used (10). A Laser Doppler anemometer was used to measure the mean longitudinal velocity fluctuations. The governing partial differential equations were solved numerically and results are described in the theoretical part of the paper. The calculations were compared with the measurements and demonstrated clearly that for turbulent flows with a separation, the present state of turbulence modelling results were in inaccurate predictions.

Turbulent flow with separation and recirculation over a double backward facing step has been investigated experimentally by Smith (40).

Temporal streamwise and cross-stream components of the velocity fluctuation together with turbulence kinetic energy and Reynolds shear stresses, were measured using a Laser Doppler anemometer, operating in the differential Doppler mode with forward scattering. Ordinary tap water was used in a closed loop flow system with a Reynolds number of 30, 210 and significant changes of flow patterns; an increase in turbulence kinetic energy, velocity fluctuations and shear stresses were observed downstream of the step expansion.

More recently, Griffith and Grimwood (15) presented the results of tests intended to evaluate the feasibility of using a modified commercially available electromagnetic current meter to measure parameters which would characterize turbulent flows from field measurements in rivers and lake inlets. The flows were characterized by the following parameters: (1) "Broadband" average r.m.s. of the fluctuating velocity $\sqrt{u'^2}$ (2) time average velocity resultant (D) as averaged over several seconds; (3) spectral composition from Fourier analysis of strip chart recordings; and (4) the ratio $\sqrt{u'^2}/D$ which is the modified turbulence intensity.

The influent upon entering the settling basin has the character of jet flow. The properties of jets have been studied by many researchers theoretically and by wind tunnel tests since the 1920's, but not until the 1950's

did jet mechanics become a familiar concept among hydraulic engineers (21).

In 1976 Rajaratnam (32) published a comprehensive book on "Turbulent Jets." The book covered many areas related to treatment of the mean flow characteristics of incompressible turbulent jets for use by engineers. He presented the typical experimental results connected with the similarity of the r.m.s. of the velocity fluctuations and turbulence shear-stress profiles.

Entrainment of ambient water and the energy dissipation associated with the flow are of particular interest in a jet flow.

Larsen (21), discussed these aspects for the case of three-dimensional (round) jets and two-dimensional (plane) jets of the same density as that of the ambient water.

If the inlet flow section to the settling tank is small compared to that flow section of the tank at the inlet, it can be represented as a submerged orifice discharging into a channel (19).

The flow immediately below a deeply submerged sluice gate was investigated experimentally by Rajaratnam and Subramanya (31). They analyzed the region of free mixing on the top of the potential core as a case of the free-jet boundary problem. The velocity distribution was found to be similar and it agreed well with Tollmien's solution.

The length characteristics of the diffusion region grow linearly with the longitudinal distance. It has also been indicated that the flow below the vena contracta could be treated as a case of the plane turbulent wall jet under an essentially zero pressure gradient.

2.4 The Energy Equation

The basic task of hydraulic engineering is that of predicting water-flow phenomena to describe the turbulent motion, and, because "Predictions" by way of experiments are usually very expensive; efficient calculation methods are in great practical demand. In order to account for the transport of turbulence, models have been developed which employ transport equations for quantities characterizing the turbulence.

The transport equation for the turbulence kinetic energy is the basis of rational representation of transport processes. The kinetic energy of the turbulent motion (per unit mass) is given by the expression,

$$k = 1/2 (\overline{u'^2} + \overline{v'^2} + \overline{w'^2}) \quad (2.2)$$

in which,

$\overline{u'^2}$, $\overline{v'^2}$, $\overline{w'^2}$ = mean-square fluctuating components of velocity in x, y, z directions.

According to this equation, k is a direct measure of

the intensity of the turbulence fluctuations in the three directions. If the velocity fluctuations are to be characterized by one scale, the physically most meaningful scale is \sqrt{k} . The energy k is contained mainly in the large-scale fluctuations. But how should the turbulence energy be determined?

Many researchers, e.g., Reynolds (34), Launder and Spalding (22), and Rodi (35) described, what Prandtl, Kolmogorov (and several others since) have suggested to determine the distribution of k by solving a differential transport equation with k as dependent variable. The equation enables account to be taken of the influence of neighbouring regions on the local turbulence energy.

As indicated by Reynolds (34), the form of the energy equation applicable to a plane, thin flow and with molecular diffusion neglected, the k equation, reads

$$\begin{aligned} \frac{Dk}{Dt} &= U \frac{\partial k}{\partial x} + v \frac{\partial k}{\partial y} \\ &= \overline{u'v'} \frac{\partial U}{\partial y} - \frac{\partial}{\partial y} \left[\overline{v' \left(\frac{P}{\sigma} + k \right)} \right] - \epsilon \end{aligned} \quad (2.3)$$

in which

U = the time-mean velocity in the x -direction

v = the time-mean velocity in the y -direction.

$\overline{u'v'}$ = the average value of the x - and y -components of the fluctuating velocity

p' = the fluctuations about the mean value of the time-mean pressure field.

For compactness, the kinetic energy is given by

$$k = \frac{1}{2} \overline{u_i'^2} = \frac{1}{2} \overline{q^2} \quad (2.4)$$

and the dissipation rate per unit mass by

$$\varepsilon = \frac{1}{2} \gamma \overline{\left(\frac{\partial u_i}{\partial x_i} + \frac{\partial u_k}{\partial x_k} \right)^2} \quad (2.5)$$

Lauder and Spalding (22) described the exact boundary-layer form of the k-equation as:

$$\rho \frac{Dk}{Dt} = - \frac{\partial}{\partial y} (\overline{\rho v' k'} + \overline{v' p'}) - \overline{\rho u' v'} \frac{\partial u}{\partial y} - \mu \Sigma \left(\frac{\partial u_i'}{\partial x_j} \right)^2 \quad (2.6)$$

Convective flux = diffusion + production - dissipation

in which

ρ = Density of fluid

v', u' = Fluctuating components of velocity in x and y directions

k' = The instantaneous value of turbulence energy

p' = Fluctuating pressure

$-\overline{u'v'}$ = Effective (kinematic) turbulent shear stress arising from correlation between velocities u' and v'

u = Streamwise velocity in boundary layer

μ = molecular viscosity

i, j = tensor-notation subscripts taking values 1, 2 or 3. u'_1 and u'_2 denote u' and v' respectively, x_1 denote x , etc.

They also demonstrated, the set of approximations made by Prandtl, Kolmogorov and by a number of other workers to simplify the turbulence correlations appearing on the right-hand side in the previous equation, in terms of quantities which are known or can be determined. The approximations were given by the expressions,

$$\bullet - (\rho \overline{v'k'} + \overline{p'v'}) = \text{constant} \times \rho k^{\frac{1}{2}} \ell \frac{\partial k}{\partial y} = \frac{\mu_t}{\sigma_k} \cdot \frac{\partial k}{\partial y} \quad (2.7)$$

$$\bullet - \overline{\rho u'v'} = \mu_t \frac{\partial u}{\partial y} \quad (2.8)$$

$$\bullet - \mu_{i,j} \sum_{i,j} \left(\frac{\partial u'_i}{\partial x_j} \right)^2 = \text{local isotropy} + c_D \frac{\rho k^{3/2}}{\ell} \quad (2.9)$$

in which

μ_t = Turbulent viscosity

σ_k = The effective Prandtl number for the diffusion of turbulence energy

C_D = Constant appearing in the dissipation term of turbulence energy equation

ℓ = Length scale of turbulence proportional to the size of the energy containing motions.

When the approximated forms of the terms are re-assembled the final equation becomes:

$$\rho \frac{Dk}{Dt} = \frac{\partial}{\partial y} \left(\frac{\mu_t}{\sigma_k} \frac{\partial k}{\partial y} \right) + \mu_t \left(\frac{\partial u}{\partial y} \right)^2 - c_D \frac{\rho k^{3/2}}{l} \quad (2.10)$$

The exact form of k equation can be derived from the Navier-Stokes equation. For high Reynolds number; Rodi (35) presented this equation as,

$$\underbrace{\frac{\partial k}{\partial t}}_{\text{rate of change}} + \underbrace{U_i \frac{\partial k}{\partial x_i}}_{\text{convective transport}} = \underbrace{\frac{\partial}{\partial x_i} \left[u_i \left(\frac{u_j u_j}{2} + \frac{P}{\rho} \right) \right]}_{\text{diffusive transport}} - \underbrace{\frac{\partial U_i}{\partial x_j} u_i u_j}_{\text{P=production by shear}}$$

$$\underbrace{-\beta g_i \overline{u_i \psi}}_{\text{G=buoyant production/destruction}} - \underbrace{\nu \frac{\partial u_i}{\partial x_j} \frac{\partial u_i}{\partial x_j}}_{\epsilon = \text{viscous dissipation}} \quad (2.11)$$

in which

- U_i = Instantaneous or mean velocity
- x_i = Co-ordinates in tensor notation
- u_i = Fluctuating velocity component in x_i direction
- g_i = The gravitational acceleration in direction x_i
- β = Volumetric expansion coefficient
- ψ = Fluctuating scalar quantity

The rate of change of k is balanced by the convective transport due to the mean motion, the diffusive transport due to velocity and pressure fluctuations, the production of k by interaction of Reynolds stresses and mean velocity

gradients, and the dissipation of k by viscous action into heat.

Rodi, also demonstrated the following model assumptions for the k -equation:

$$u_i \left(\frac{u_j u_j}{2} + \frac{p}{\rho} \right) = \frac{v_t}{\sigma_k} \frac{\partial k}{\partial x_i} \quad (2.12)$$

in which,

v_t = eddy (or turbulent) viscosity.

The diffusion flux of k is assumed proportional to the gradient of k , where σ_k is an empirical diffusion constant. The dissipation ϵ was modelled by the expression:

$$\epsilon = C_D \frac{k^{3/2}}{\ell} \quad (2.13)$$

where C_D is another empirical constant.

One-equation models are popular in the Soviet Union for determining the eddy viscosity and diffusivity of the vertical turbulent transport in large water bodies, but almost no comparisons with experiments have been reported so that the model performance is difficult to assess.

At present, two-equation models, and in particular the k - ϵ model, are the most widely-tested for hydraulic flow problems (22,35). Schamber and Larock in their article (38) described a numerical model which predicts

the velocity in sedimentation basin, the structure of the turbulence is represented by k - ϵ turbulence model.

More recently, Singhal and Spalding (39) presented numerical predictions of boundary layers exhibiting a large variety of streamwise pressure distributions, including those featured in the Stanford Conference on turbulent boundary layers. The model of turbulence employed was one in which the local statistic of turbulence was characterized by two quantities: the turbulence kinetic energy k and its dissipation rate ϵ . Transport equations for k and ϵ are solved simultaneously with that for the momentum of mean flow. The computed results are compared with the experimental data and the agreement was found to be good.

In 1976, Galin (13) developed a method for calculating the dissipation of turbulent energy on the basis of an approximate differential equation.

In the same year, Bradshaw (2), published a paper on "Turbulence Research Progress and Problems." His paper was an update of a review "The Understanding and Prediction of Turbulent Flow," published in 1972. The first part was a review of progress in calculation methods, and in experiments related to calculation methods, and the second part was a series of comments on topical problems which needed further study.

III. THE EXPERIMENTAL STUDIES

3.1 Objectives

The principal purposes of the following experimental programme, were to measure the velocity and turbulence fields throughout the tank length, as a guide in obtaining a gross picture of flow behaviour and to provide adequate evaluation of a transport equation for turbulent kinetic energy.

The use of a Laser Doppler Anemometer is particularly advantageous in this study in view of the low velocities and the unstable nature of turbulent flow.

3.2 The Experimental Apparatus

The tests were carried out in a recirculating flume made from plexiglass. The flume was 1.8 m long, by 0.5 m high and 0.125 ± 0.003 m wide. The flow entered the flume from the end where a 50 mm thick fibre filter was installed to damp out inflow turbulence. The water flowed under a round lip gate into the test section. The gate was shaped such that flow would be unidirectional at the inlet to the test section. The effluent from the test section was collected in a 0.75 m long by 0.6 m deep by 0.6 m wide plexiglas sump and recirculated to the flume through a 64 mm

diameter copper pipe. A 1/4 horsepower centrifugal pump was used to circulate tap water. Figure (3.1) shows a schematic layout and dimensions of the recirculating flume.

Inflow to the test section was controlled by a gate valve at the upstream end of the flume. Although the apparatus was originally equipped with an orificemeter for measuring flow, it was found that integration of the measured velocity distribution would yield more accurate results for the small flow-rates involved. The effluent weir at the end of the test section was calibrated to check the computed flow by measuring the head over the weir. The use of closed-loop flow circuit was necessary to attain temperature equilibrium and eliminate possible temperature effects on flow pattern.

A Laser Doppler Anemometer was used to measure velocity profiles because, (i) it requires small measuring volume as compared to propeller current meters, (ii) it is a non-intrusive method, (iii) it possesses a high absolute accuracy and it requires no calibration, and most important (iv) it is capable of accurately measuring reversed flow as well as r.m.s. values in a set direction. The side walls of the test section were constructed of plexiglass, 0.125 m apart, to permit the use of Laser Doppler Anemometer in its "Forward Scattered Mode," as shown in Fig. (3.2). Certain important details of the equipments used in these

experiments are given in Table (3.1). Rankin (33) used a Laser Doppler Anemometer arrangement that included a frequency shifter which enabled him to measure near-zero velocities. A similar arrangement was used in this experimental investigation to measure the negative back-flow velocities in the recirculating eddy.

The light from a 15 mW He-Ne Laser first passes through a polarization rotator and then an aperture before entering the beam splitter where it is divided into two equal parts 50 mm apart. The two beams enter the Acousto-optic cell housing where one beam is transmitted through the cell and the other through a path length equalizer. Both the shifted and unshifted beams are then focused onto the measurement point by the focusing lens. The scattered light from the intersection of the two laser beams is again focused onto the aperture of the photo detector (photo multiplier) which converts the light intensity variation into electrical variation. The shifted signal is passed through a high pass filter into the frequency tracker where frequency is converted into a proportional voltage. An oscilloscope was used to display the photo detector output signal.

A transverse mechanism was used to locate beam intersections to measure velocity at various points within the test section, and to construct the required velocity pro-

files. The Laser Doppler Anemometer components, transmitting optics and receiving optics were located on a horizontal frame which was perpendicular to the flume longitudinal-axis as shown in Figs. (3.3) to (3.5) inclusive. A limited adjustment in the frame direction (z-direction) was made possible by means of a plexiglass slide mechanism which was used for aligning the point of intersection onto the centreline of the flume. The entire frame was fastened onto a carriage that travelled on tracks in the x-direction. (flume centerline). In order to allow a third degree of freedom, the frame and tracks could move up and down (y-direction) by means of space frame and a hydraulic jack. Thus, the point of intersection of the two-laser beams could be located at any point (x, y, z) within the test section. The term "point of intersection" is used to refer to the small measuring volume which was an ellipsoid with minor and major axes, 0.078 mm and 0.315 mm respectively, in the present study (33). The overall view of test facility is shown in Fig. (3.6).

3.3 Experimental Procedure

The use of the Laser Doppler Anemometer requires knowledge of the laser light wavelength, focal distance of the lens and beam spacing. The fluid velocity, u , is related to the doppler frequency, f_d , according to

$$f_d = \frac{2u \sin K}{\lambda} \quad (3.1)$$

where λ is the laser light wavelength (=632.8 nm for air) and K is half the intersection angle (=13.76° for air). The ratio

$(\sin K/\lambda)$ is independent of the working medium. The tracker converts this frequency into a proportional voltage which is related to the fluid velocity at the measuring point by (33)

$$u = 6.651 (E - E_s) \quad (3.2)$$

where u is the longitudinal velocity in cm/sec, E is the output voltage to be read from the frequency tracker ($E = sf_d$, s is the range switch setting in volts/MHz), and E_s is the theoretical voltage that would be recorded when $u = 0$.

The measured water depth near the effluent weir was used to determine the head over the weir, and consequently the flow-rate, from the experimentally calibrated weir (17).

$$q = 17.25 h_w^{1.5} \quad (3.3)$$

where q is in $\text{cm}^3/\text{sec}/\text{cm}$ and h_w in cm. The measuring volume was located in the mid-width of the test section. A typical test was carried out as follows:

1. The sump tank was filled with tap water.
2. The Dual Beam Laser Doppler Anemometer arrangement was set up according to the operation manual supplied by the manufacturer.
3. The frequency shifter was set such that E_s was observed to be 1.0
4. The flowrate was set to approximately the desired value using the control valve.
5. The water depth was measured from the bottom at the "entrance gate" and also near the effluent weir.

6. Starting from the sections at the entrance gate and proceeding downstream, the measuring volume was traversed in the y-direction while voltage, rms voltage, and depth values were recorded.
7. Intervals of 10 mm were used in the y-direction while the intervals in the x-direction were 50 mm.
8. The test was repeated for different discharges, different gate openings and different lengths of the test section.

3.4 Experimental Ranges

The ranges of the experimental data are as follows:

Flowrate: $q = 53.9 \text{ cm}^3/\text{sec}/\text{cm}$ to $147 \text{ cm}^3/\text{sec}/\text{cm}$

Gate opening: $G = 3 \text{ cm}$ to 7 cm

Test sec. length $L = 30 \text{ cm}$ to 73 cm .

Water depth: $H = 10.7 \text{ cm}$ to 12.7 cm .

3.5 Experimental Results

The experimental data of a total of 130 profiles collected during this investigation are on file at the Civil Engineering Department, University of Windsor, and only samples of the data of the mean velocity and r.m.s. profiles are documented in Tables (3.2 to 3.28) in Appendix (A). All length dimensions are given in cm, the flowrate in $\text{cm}^3/\text{sec}/\text{cm}$, the mean velocity and r.m.s. values in cm/sec .

Tables (3.2 to 3.13) list the results of mean velocity and r.m.s. values for the gate opening, $G = 3$ cm, and the variables: flowrate, q , ranging between $61.74 \text{ cm}^3/\text{sec}/\text{cm}$ and $111 \text{ cm}^3/\text{sec}/\text{cm}$, length of test Section, L , ranging to between 30 cm and 73 cm.

Tables (3.14 to 3.25) present the velocity and r.m.s. distributions for the gate opening, $G = 5$ cm, and the variables: flowrate, q , ranging between $101.32 \text{ cm}^3/\text{sec}/\text{cm}$ and $147 \text{ cm}^3/\text{sec}/\text{cm}$, length of test section, L , ranging between 30 cm and 73 cm.

Tables (3.26 to 3.28) give the data of mean velocity and r.m.s. profiles for the gate opening, $G = 7$ cm, flow rate, $q = 106 \text{ cm}^3/\text{sec}/\text{cm}$, and the length of test section, $L = 30$ cm.

IV. DATA REDUCTION AND ANALYSIS

4.1 Introduction

A turbulent flow can be effectively studied by separating the fluid motion into a mean motion and a turbulent fluctuating motion. Flow variables such as velocity, U , are decomposed into a statistical average velocity, \bar{U} , and a turbulent fluctuating velocity, u' , i.e., $U = \bar{U} + u'$. The root-mean-square of the fluctuations is a measure of the fluctuation intensity. For brevity, the latter will be termed the r.m.s. value, and will be expressed as:

$$\text{r.m.s.} = (\overline{u'^2})^{1/2} \quad (4.1)$$

In this Chapter the experimental data for the mean velocity and r.m.s. values are analyzed to obtain the mean kinetic energy and turbulent kinetic energy profiles which are used to develop a transport equation predicting the turbulent kinetic energy.

4.2 Presentation of Data in terms of Dimensionless Variables

4.2.1 Plotting the Mean Velocity and r.m.s. Profiles

"CALCOMP Pen Plotter" was used for plotting the mean velocity and r.m.s. profiles using the data measurements.

The results of 13 tests of different tank lengths, gate openings, and different flowrate were collected and analyzed and are shown in tables and graphs. The samples of experimental values of mean velocity and r.m.s. are included in tabular form in Appendix (A). Mean velocity and r.m.s. profiles are obtained considering the average value at each level over the depth.

In all of the following graphs, Figs. (4.1 to 4.20) the velocity and r.m.s. values are normalized with the reference velocity, U_R , calculated at the gate, and plotted against the tank depth normalized with the gate opening which provides an excellent means of comparing profile shapes. The method of calculating U_R can be easily followed from one of the tables at the gate entrance in Appendix (A).

By integrating the velocity distribution using equal intervals and assuming that the reverse flow cancels an equivalent area of the forward flow, the area under any curve can be adjusted to be unity. Similarly the values of r.m.s. are corrected with the same ratio for each corresponding curve of \bar{U} .

Typical corrected values of \bar{U}/U_R and the r.m.s. profiles are plotted for different points throughout the tank depth normalized with the gate opening in Figs. (4.1 to 4.20) inclusive.

4.2.2 Mean Kinetic Energy and Turbulent Kinetic Energy Flux

The velocity profile data in this investigation is collected at sufficiently small vertical increments so that the basic definition could be used to determine the variation in the mean kinetic energy in x-direction. The mean kinetic energy flux per unit discharge that will be used here is defined below:

$$f_k = \int_0^y \bar{U}^3 dy / (q) \quad (4.2)$$

where

$$q = \text{the flowrate/unit width} = U_R \cdot G \quad (4.3)$$

G = the gate opening

U_R = the reference velocity calculated as the average value at the gate.

This equation is now approximated using the trapezoidal rule as shown below:

$$f_k = \frac{1}{q} \sum_{i=1}^{n-1} \left(\frac{\bar{U}_i^3 + \bar{U}_{i+1}^3}{2} \right) (\Delta y) \quad (4.4)$$

where, n is the number of data points (including the boundaries). The mean kinetic energy is made dimensionless by dividing it by the value at the gate, f_{k0} , i.e.:

$$f_{k0} = \frac{U_R^3 \cdot G}{(q)} \quad (4.5)$$

The same procedure are followed to determine the representative average turbulent kinetic energy flux/unit

discharge, $\overline{U'^2}$, which is defined as following:

$$\overline{U'^2} = \int_0^y \frac{\overline{(u'^2)} \bar{U} dy}{q} \quad (4.6)$$

where,

$\overline{u'^2}$ = the local mean-square of the turbulent
fluctuating (r.m.s.)²

\bar{U} = the mean velocity at a point in the x-direction.

(It is assumed that $\overline{u'^2} = \overline{v'^2}$ and $\overline{w'^2} = 0$)

Substituting the values of r.m.s. and mean velocity profiles into the integral equation (4.6) and performing the numerical integration, the following equation is obtained:

$$\overline{U'^2} = \frac{1}{q} \sum_{i=1}^{n-1} \left(\frac{\overline{(u'^2)} \cdot \bar{U}_i + \overline{(u'^2)} \cdot \bar{U}_{i+1}}{2} \right) (\Delta y) \quad (4.7)$$

where n is the number of data points.

The turbulent kinetic energy as well as the mean kinetic energy are made dimensionless by dividing by the value f_{k0} (Eq. 4.5). Dimensionless mean kinetic energy longitudinal profiles are presented in Figs. (4.21 to 4.32), and dimensionless turbulent kinetic energy longitudinal profiles are shown in Figs. (4.33 to 4.44).

4.3 Proposed Equation

The kinetic energy of the flow entering the settling basin is lost mainly through turbulent eddies in the inlet zone. But how should the turbulence energy be determined? Launder and Spalding (22), in their lectures on mathematical models of turbulence described a differential transport equation with k as dependent variable, as shown below:

$$\rho \frac{Dk}{Dt} = - \frac{\partial}{\partial y} (\overline{\rho v'k'} + \overline{v'p'}) - \overline{\rho u'v'} \frac{\partial u}{\partial y} - \mu \sum_{i,j} \left(\frac{\partial u'_i}{\partial x_j} \right)^2 \quad (4.8)$$

convective flux = diffusion + production-dissipation

where,

k' = the instantaneous value of turbulence energy.

Prandtl, Kolmogorov and a number of other workers used a modified form of Eq. (4.8) by making a set of approximations for the turbulence correlation appearing on the right-hand side. The set of approximations are shown below:

$$\bullet - (\overline{\rho v'k'} + \overline{v'p'}) = \text{constant} \times \rho k^2 \ell \frac{\partial k}{\partial y} = \frac{\mu_t}{\sigma_k} \cdot \frac{\partial k}{\partial y}$$

$$\bullet - \overline{\rho u'v'} = \mu_t \frac{\partial u}{\partial y}$$

$$\bullet - \mu \sum_{i,j} \left(\frac{\partial u'_i}{\partial x_j} \right)^2 + \text{local isotropy} + C_D \frac{\rho k^{3/2}}{\ell}$$

The modified equation is:

$$\rho \frac{Dk}{Dt} = \frac{\partial}{\partial y} \left(\frac{\mu_t}{\sigma_k} \frac{\partial k}{\partial y} \right) + \mu_t \left(\frac{\partial u}{\partial y} \right)^2 - c_D \frac{\rho k^{3/2}}{L} \quad (4.9)$$

This equation is for two-dimensional boundary-layer flows.

The present investigation is concerned with settling tank under steady state conditions, where $\frac{\delta k}{\delta t}$ can be set to zero in Eq. (4.9) ($\frac{\delta k}{\delta t}$ is an implicit part of $\frac{Dk}{Dt}$), the flow is depth averaged, the longitudinal diffusion is neglected and the net vertical diffusion is zero. The model to be described in this investigation determines one turbulence property from the solution of a differential transport equation based on these previous assumptions.

As a guide in obtaining a gross picture of flow behaviour in settling basins, it is instructive to look at the energy inputs into the basin. Energy flux into the control volume equals energy dissipation in the control volume plus energy flux out of it. Figure (4.45) shows schematic representation for energy balance in the settling basin.

A transport equation is developed using the basic transport principles and the terms shown in Fig.(4.45) as indicated below:

$$\begin{aligned} \text{Rate of accumulation} &= (\text{inflow} - \text{outflow}) + \text{generation rate} \\ &\quad \text{rate} \qquad \qquad \text{rate} \\ &\quad - \text{decay} \end{aligned}$$

$$(dx.H) \left(\frac{\partial \overline{U'^2}}{\partial t} \right) = -\overline{U}_m \frac{\partial \overline{U'^2}}{\partial x} (dx.H) - A \frac{\partial f_k}{\partial x} (dx.H) - B \frac{\overline{U'^2}}{\ell}^{3/2} (dx.H) \quad (4.10)$$

Substituting $\frac{\partial \overline{U'^2}}{\partial t} = 0$ (steady state) in Ecu. 4.10 and simplifying:

$$\overline{U}_m \frac{\partial \overline{U'^2}}{\partial x} = -A \frac{\partial f_k}{\partial x} (\overline{U}_O \cdot \frac{G}{H}) - B \frac{\overline{U'^2}}{\ell}^{3/2} \quad (4.11)$$

where,

$\ell \propto H$ = length scale of turbulence proportional to the size of energy containing motions

H = water depth of the tank

\overline{U}_m = depth averaged mean velocity

\overline{U}_O = depth averaged mean velocity at the gate

G = gate opening

f_k = mean kinetic energy flux

$\overline{U'^2}$ = representative turbulent kinetic energy.

The left side of Eq. (4.11) is the convective transport. The first term on the right is generally called the generation term. If one was to derive the equation for mean kinetic energy, he would find that the same term appears in that equation too, but with the sign reversed. So the generation term can be defined as the rate at which mean kinetic energy is converted into turbulence energy. And the last term can be taken as the rate at which turbulence energy is dissipated.

4.4 Determination of the Constants (A, B)

Before solving the previously developed equation, the constants A and B must be assigned.

The method of determining the constants A and B makes use of mean kinetic energy and turbulent kinetic energy profiles. The finite difference form of the equation that yields a good representation of the data from kinetic energy and turbulent kinetic energy curves is that presented below:

$$\bar{U}_m \left(\frac{\overline{U'^2_{i+1}} - \overline{U'^2_i}}{\Delta x} \right) = -A \left(\frac{f_{k_{i+1}} - f_{k_i}}{\Delta x} \right) \left(\frac{\bar{U}_0}{H} \right)^G - \frac{B}{\ell} \overline{U'^2}^{3/2} \quad (4.12)$$

where

$$\overline{U'^2} = \frac{1}{2} (\overline{U'^2_i} + \overline{U'^2_{i+1}})$$

Δx = the space increment.

Equation (4.12) is solved numerically to find the two constants A and B by arriving at the values in the equation separately. The equation is applied at the points (i), (i+1) and then at the points (i+1), (i+2) on curves 1 and 2, as shown in Fig. (4.46) and the two resulting algebraic equations are solved to get the two constants at the point (i+1). This process is repeated at all other points on the curves till all A's and B's of all sections are obtained.

A statistical analysis was made using the all dif-

ferent flow conditions using the mean kinetic energy and turbulent kinetic energy profiles, and finally the averages of all A's and B's were taken. The average values of A's and B's for different flow conditions are included in tabular form in Table (4.1) in Appendix (A).

4.5 Fitting of the Transport Equation

The present transport equation is developed to predict the turbulent kinetic energy, using the experimental mean kinetic energy profiles.

A statistical analysis is made of the calculated mean kinetic energy profiles presented in Figs. (4.21 to 4.32), in order to establish dimensionless equation to describe the mean kinetic energy profile. Figure (4.47) shows the best fit for dimensionless mean kinetic energy profiles.

It is found that the best equation to represent the dimensionless mean kinetic energy profile is:

$$\frac{f_k(x)}{f_{k0}} = C \left(\frac{x}{G}\right)^n + D \quad (4.13)$$

in which

$$\frac{f_k(x)}{f_{k0}} = \text{the dimensionless mean kinetic energy}$$

$$C = -0.36$$

$$D = 1.065$$

$$n = 0.371$$

where C, D and n are obtained from Fig. (4.47) which presents Eq. (4.13). Substitution of Eq. (4.13) into the transport Eq. (4.11) gives,

$$\bar{U}_m \frac{\delta \overline{U'^2}}{\delta x} = -A \frac{\delta}{\delta x} \left(C \left(\frac{x}{G} \right)^n + D \right) \left(\bar{U}_0 \cdot \frac{G}{H} \right) - B (\overline{U'^2})^{3/2} \quad (4.14)$$

4.6 The Numerical Solution and Testing

The proposed transport Eq. (4.12) is an ordinary first-order differential equation. This equation can be solved by Runge-Kutta method, using an initial value for turbulent kinetic energy $(\overline{U'^2})^n$ to calculate new value for $(\overline{U'^2})^{n+1}$ at step $x^{n+1} = x^n + \Delta x$.

The new value can be used as the initial value for the next step. The details of this method are given in Ref. (41).

The input data required for the transport equation are:

$\overline{U'^2}$ = initial value of turbulent kinetic energy

Δx = the space increment for the Runge-Kutta method

\bar{U}_m = depth averaged mean velocity.

The transport equation results for turbulent kinetic energy are predicted and compared with the corresponding experimental data of this study. The comparisons between the experimental and the numerical results are shown in

Figs. (4.33 to 4.44). The flow chart and the listing of the computer programmes are given in Appendix (B).

V. DISCUSSION OF THE EXPERIMENTAL DATA AND EVALUATION OF THE TRANSPORT EQUATION

5.1 Introduction

In this chapter the experimental measurements of velocity and turbulence distribution are discussed and compared with the corresponding experimental results from other researchers. The flow patterns, at different gate openings, flowrates and tank lengths, are presented to study the factors influencing the size of eddies, potential core and the growth of the boundary layer.

The mean kinetic energy and turbulent kinetic energy are investigated for different tank configurations, on the basis of measured velocity. Also a simplified transport equation for turbulent kinetic energy is compared with the experimental data of this study.

Finally, the sources of errors and the limitations of the theory are discussed.

5.2 The Mean Velocity and r.m.s. Profiles

The samples of velocity and r.m.s. data are included in Tables (3.2 to 3.28) in Appendix (A). Typical velocity and r.m.s. distributions are included in Figs. (4.1) to (4.20).

In all tests the velocity profile was characterized by well defined bottom current and a counter flow in upper layers of the basin.

Figures (4.1) to (4.5) show typical velocity profiles versus relative depth with the corresponding conditions at flowrate of $53.9 \text{ cm}^3/\text{sec}/\text{cm}$, length of test section of 30 cm, and gate opening of 3 cm. These figures show that the bottom current extended through the full length of the test section, i.e., there was no flow separation at the bed.

Figure (4.1) represents the mean velocity in the longitudinal direction and r.m.s. profiles close to the inlet. A bottom current of depth close to half of the tank depth is indicated. A well developed return flow occurred in the upper half of the tank. Figure (4.1) also shows measured r.m.s. velocities in the longitudinal direction; the r.m.s. values were found to be somewhat higher in this section than elsewhere in the tank (as a consequence of the jet flow).

As the velocity profile moved downstream towards the effluent weir, the depth of the bottom current was significantly increased as shown in Fig. (4.2) and Fig. (4.4) for $x = 10 \text{ cm}$ and $x = 20 \text{ cm}$ from the gate respectively. Velocities in the return current occupy a smaller portion of the depth.

With larger gate opening, the velocity profile was similar to that described for the previous case of 3 cm gate opening. The major change was in the layer thickness of the bottom current, as shown in Figs (4.6) to (4.10) of 5 cm gate opening and Figs. (4.11) to (4.15) of $G = 7$ cm.

The previous three cases, showed that the increase in the gate opening from 3 cm to 5 cm and then to 7 cm, resulted in a significant increase in the depth of bottom current for the same discharge. Velocities in the bottom current, however, were somewhat lower and counter flow velocities were also lower. The r.m.s. values were decreased by increasing the gate opening for the same discharge.

An increase in the flowrate to $111 \text{ cm}^3/\text{sec}/\text{cm}$ resulted in a significant increase of the values of the velocities in the bottom current as shown in Fig. (4.16) to Fig. (4.20). The return flow velocities were also higher. The highest turbulence measurements were in the inlet zone.

The experimental measurements of the r.m.s. values at the lower flowrate indicated that turbulence intensities were surprisingly uniform in the whole volume of the tank. At high flowrates, r.m.s. values were markedly influenced by the jet flow in the inlet zone.

The r.m.s. values were found to be in the range from 5% to 15% of mean velocities of the bottom current, these values are slightly lower than the turbulence measurements of Larsen (21).

Detailed measurements from this study gave results in general agreement with the experimental results of Khattab (19), McCorquodale (23), and Larsen (21).

5.3 Factors Influencing the Flow Patterns

A significant common feature of all experiments was that the flow passed through the lower part of the tank in high velocity region, and decreased from inlet to outlet zone. Because of the sudden enlargement from the inlet flow section to the tank section, eddies formed on the top of the forward flow zone. Figures (5.1b) to (5.12b) were obtained by dimensionless stream functions to analyze the factors influencing the flow patterns.

In an attempt to analyze the effects of these factors on the flow pattern, the test flow patterns were divided into three groups being dependent on the gate opening.

The first group had gate opening of 3 cm (see Figs. 5.1b to 5.4b). Figure (5.1b) shows a typical flow patterns calculated from the longitudinal velocity, \bar{U} , measured at various distance, x , from the tank entrance. The length of the test section, was 0.73 m, and the depth

varied between 0.119 to 0.12 m. The flowrate per unit width was $111 \text{ cm}^3/\text{sec}/\text{cm}$ which corresponds to a Reynolds number of 11100, based on average depth, velocity, and a kinematic molecular viscosity of $0.01 \text{ m}^2/\text{sec}$.

Under these flow conditions, Fig. (5.1b) shows that a large size eddy formed at the top of the forward flow zone. The eddy rotated forward at the inlet and extended from the inlet to about half the length of the test section, and about 4 times the tank depth at the baffle submergence.

Figures (5.2b to 5.4b) showed that these eddies decreased in size with the rate of flow. Figure (5.2b) represents the condition of flowrate equals of $61.74 \text{ cm}^3/\text{sec}/\text{cm}$, and the length of the test section was 0.4 m, the eddies extended from the inlet to about 90% of the test section length, and about 4.4 times the baffle height.

Figure (5.3b) shows a typical flow pattern for flowrate of $87.41 \text{ cm}^3/\text{sec}/\text{cm}$ with a Reynolds number of 8741. The length of the eddy is about 80% of the tank length, and 3 times the baffle height.

Figure (5.4b) represents flow pattern of $53.9 \text{ cm}^3/\text{sec}/\text{cm}$. The length of eddy extended to the whole tank length and is 3.9 times the baffle depth.

The second group of tests with $G = 5 \text{ cm}$, and the third group of $G = 7 \text{ cm}$, are shown in Figs. (5.5b) to

(5.12b). These figures also show that the flow patterns were in general, similar to those described in group 1 ($G = 3$ cm). Depths and lengths of eddies were inversely proportional to the gate opening.

The length of eddy, L_r/h_B , is plotted as a function of the tank length, L/h_B , and the baffle height ratio, h_B/H , ranging between 0.35 to 0.75 as shown in Fig. (5.13). Also Fig. (5.13) shows that for $6 < L/h_B < 10$, L_r/h_B varies between 4 and 5. For $L/h_B < 6$, $L_r/h_B < L/h_B$.

Figures (5.2b), (5.3b), (5.4b), (5.8b), and Fig. (5.9b), show that for a tank length less than approximate 0.3 m, weir effects will influence the flow pattern and eventually dominate over the other factors.

Figure (5.14) compares the general features of settling tank flow for earlier experimental work of Khattab (19), and McCorquodale (23), with the results from this study. It is noted that the main features of the flow pattern, i.e., the re-circulation and bottom flow are similar in all cases.

The error associated with the observed readings of the mean velocity and r.m.s. values is estimated to be $\pm 1\%$; the possible effect of this on the flow patterns, is indicated by the shaded areas in Fig. (5.1b) to (5.12b).

The r.m.s. values were used to obtain the corresponding turbulence distribution as shown in Figs. (5.15 to 5.25).

5.4 The Potential Core and Boundary Layer

The experimental observations of the mean velocity field indicate that, in the axial direction of the jet, one could divide the jet flow into two distinct regions: the development zone and the fully developed zone as shown in Fig. (5.26). As the turbulence penetrates inward towards the middle of the jet, a wedge is formed known as the potential core. The core of fluid with nearly constant maximum velocity is bounded by a mixing layer on the top, and a well shear layer on the bottom (32). In the second region, the turbulence has penetrated through the jet, and as a result, the potential core has disappeared.

The same hydraulic and geometrical data that were used for the preparation of the flow patterns, were used to determine the length of the potential core, L_p , and the growth of the boundary layer which are shown in Figs. (5.1a to 5.12a). These figures showed that the length of potential core, L_p , ranges between 2.57 and 5.67 times the gate opening.

Figure (5.27) shows a comparison between the slope of potential core by Rajaratnam (32) and the slope of

potential core with tank length, L/H , of the present study. Figure (5.27) also shows the scatter of experimental data and the difference between the value obtained by Rajaratnam (32) and the values of this study. However, the average value of the slope of the potential core from this study is in reasonable agreement with the value obtained by Rajaratnam and Subramanga (31).

The analysis also showed that the length of potential core, L_p , was influenced more by the baffle opening, G , than by any of the other factors.

As the gate opening became larger, smaller values of the ratio, L_p/G , were obtained. Figure (5.28) shows the general trend of the length of potential core, L_p/G , with the tank length, L/G , as a function of low Reynolds number, R_N , ranging between 5400 to 6200 and high Reynolds number ranging between 8740 to 14700. The length of potential core, L_p/G , increased with the tank length, L/G , for ($L/G < 15$) as indicated in Fig. (5.28) for both high Reynolds number and low Reynolds number.

Figures (5.1a to 5.12a) show that the boundary layer grows faster for larger gate opening for a fixed tank length and flowrate.

On the basis of this study it is not possible to reach a definite relationship between the rate of growth of boundary layer and the tank length or the rate of flow.

5.5 . Mean Kinetic Energy Profiles

The kinetic energy of the flow entering the settling tank is lost mainly through transformation to turbulent eddies in the inlet zone. The mean kinetic energy is decreased due to increasing the turbulent kinetic energy. This is denoted in Fig. (4.21) to Fig. (4.32) respectively by the rapid descent of the kinetic energy of the mean flow.

Figure (4.21) to Fig. (4.32), represent the variation of dimensionless mean kinetic energy with distance for different conditions of rate of flow, length of the tank, and gate opening. These figures show that the rates of energy dissipation are initially high and taper off with distance.

In the potential core the energy dissipation is small. In the outer region the loss of kinetic energy is high due to the high difference between the jet velocity and the mean velocity of the water into which it impinges.

In terms of kinetic energy it is advantageous to use a greater gate opening. The experimental observations in this study indicate that, if a smaller gate opening is used, the effect is that energy dissipation is substantially increased locally. This, however, means that inlet velocities become high with consequent adverse effects in the inlet zone. These effects may be detrimental, particularly

with fragile floc. It is, therefore, important to consider inlet design in the light of minimizing inlet velocities.

Figure (4.47) shows the curve fitting of mean kinetic energy for different tank configurations.

5.6 Comparison of the Transport Equation for the Turbulent Kinetic Energy with the Experimental Data

The proposed transport equation was compared with representative cases from the experimental results of the present study. The comparisons between the experimental and the predicted results are shown in Figs. (4.33 to 4.44).

The experimental data points were deduced from the measurements of r.m.s. velocities as explained in Chapter IV.

Most of the plots show a satisfactory agreement between the predicted values and the experimental data. However, there is a rather poor agreement in two cases as shown in Figs. (4.41) and (4.44). This may be due to three dimensional effects.

The peak value along the x-direction occurs because the energy has to diffuse in from regions where the turbulence energy is produced, i.e., the turbulent kinetic energy profile could be divided into two regions being dependent on the peak value as shown in Figs. (4.33 to 4.44)

The first region, before the maximum value occurs, represents the production zone in which the kinetic energy is transferred from the mean to the turbulent motions. The second region, after the maximum value occurs, represents the dissipation zone, in which the kinetic energy transfers from the turbulent motion into internal energy of the fluid.

In these zones the indicated process dominates over the other processes.

The maximum calculated and measured values of turbulent kinetic energy for each tank experiment are plotted in Fig. (5.29).

5.7 Errors and Limitations of the Theory

The errors and limitations of the theory may be discussed as follows: the proposed equation is not an exact model; it is a qualitative treatment of the transport equation which is used to explain the general trend. It is assumed that the flow is one dimensional, which is not strictly correct. It is assumed that the flow is not recirculating; inclusion of this effect would require an additional term. The effect of turbulence generation due to the boundary-layer is neglected. The effect of the weir is neglected and the flow is assumed to be under steady state conditions.

VI. CONCLUSIONS

From the analysis of the experimental data collected from a total of 13 configurations of rectangular settling tanks, for the mean velocity, turbulence distribution and flow patterns, the following conclusions are made:

(a) The experimental observation of the mean velocity field indicates that one could divide the jet flow at the flow development region into four zones: (i) the potential core with nearly constant maximum velocity which is bounded by, (ii) a mixing layer on the top, (iii) a shear layer on the bottom, and (iv) a zone of return flow which is formed on the top of the forward flow.

(b) The depth of the bottom current as well as the values of the velocities in the bottom current are functions of the gate opening, G , and the flowrate q . For the same flowrate q , the depth of the bottom current increases as, G , increases and the velocities in the bottom current decrease as, G , increases.

(c) An increase in the flowrate q , resulted in a significant increase in the values of the bottom velocities as well as the return flow velocities.

(d) The r.m.s. values were found to be somewhat higher in the sections close to the inlet than elsewhere as a con-

sequence of the jet flow.

(e) The r.m.s. values were found to be in the range from 5% to 15% of mean velocities of the bottom current. These values are slightly lower than the turbulence measurements of Larsen.

(f) The length of eddy, L_r/h_B , is plotted as a function of the tank length, L/h_B , and the baffle height ratio, h_B/H , ranging between 0.35 to 0.75. For $6 < L/R_B < 10$, L_r/h_B varies between 4 and 5. For $L/h_B < 6$, $L_r/h_B \leq L/h_B$.

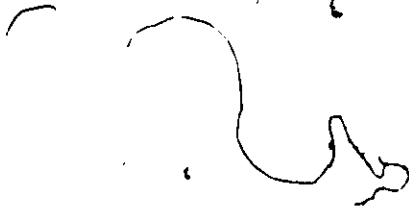
(g) The average value of the slope of the potential core from this study was found to be 0.093 for high Reynolds number and 0.097 for low Reynolds number. These values are in reasonable agreement with the values obtained by Rajaratham.

(h) The turbulent kinetic energy profiles were deduced from the measurements of r.m.s. velocities. The turbulent kinetic energy profile could be divided into two regions. The first region, before the maximum value occurs represents the production zone, and the second region, after the maximum value occurs, represents the dissipation zone.

(i) The length of potential core, L_p/G , is plotted as a function of the tank length, L/G , and Reynolds number ranging between 5400 to 14700. The length of potential core, L_p/G , was found to increase with the tank length, L/G for $L/G \leq 15$.

(j) The average value of the withdrawal zone $\approx 0.4H$, i.e., the influence of the weir extends 40% of the depth upstream of the weir.

A simplified differential transport equation for predicting the turbulent kinetic energy within the rectangular settling tanks using the velocity and mean kinetic energy as input, has been developed. The transport equation describes the general trend of the energy balance using the basic transport principles, and is verified reasonably well with the experimental data of this study.



FIGURES

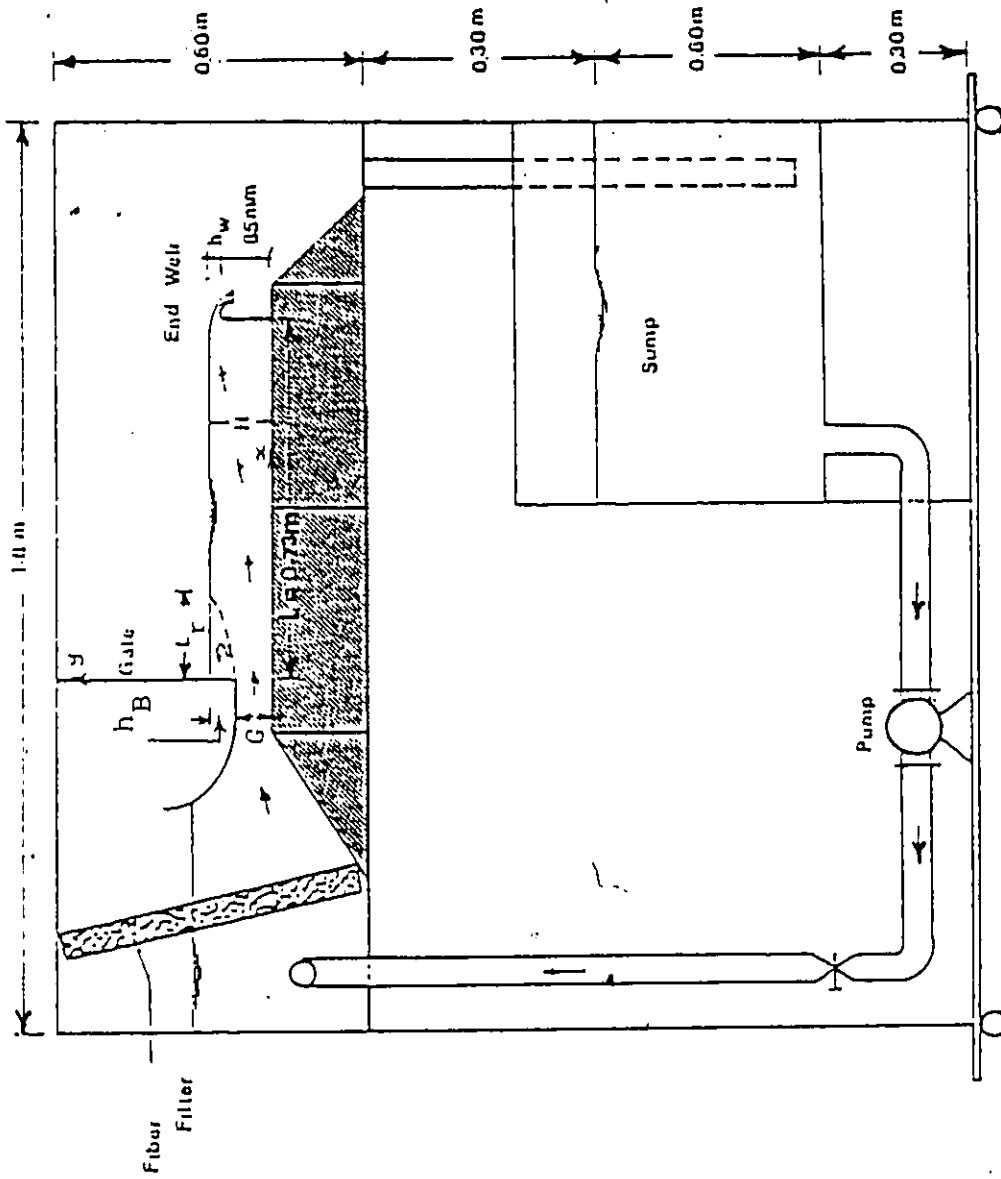
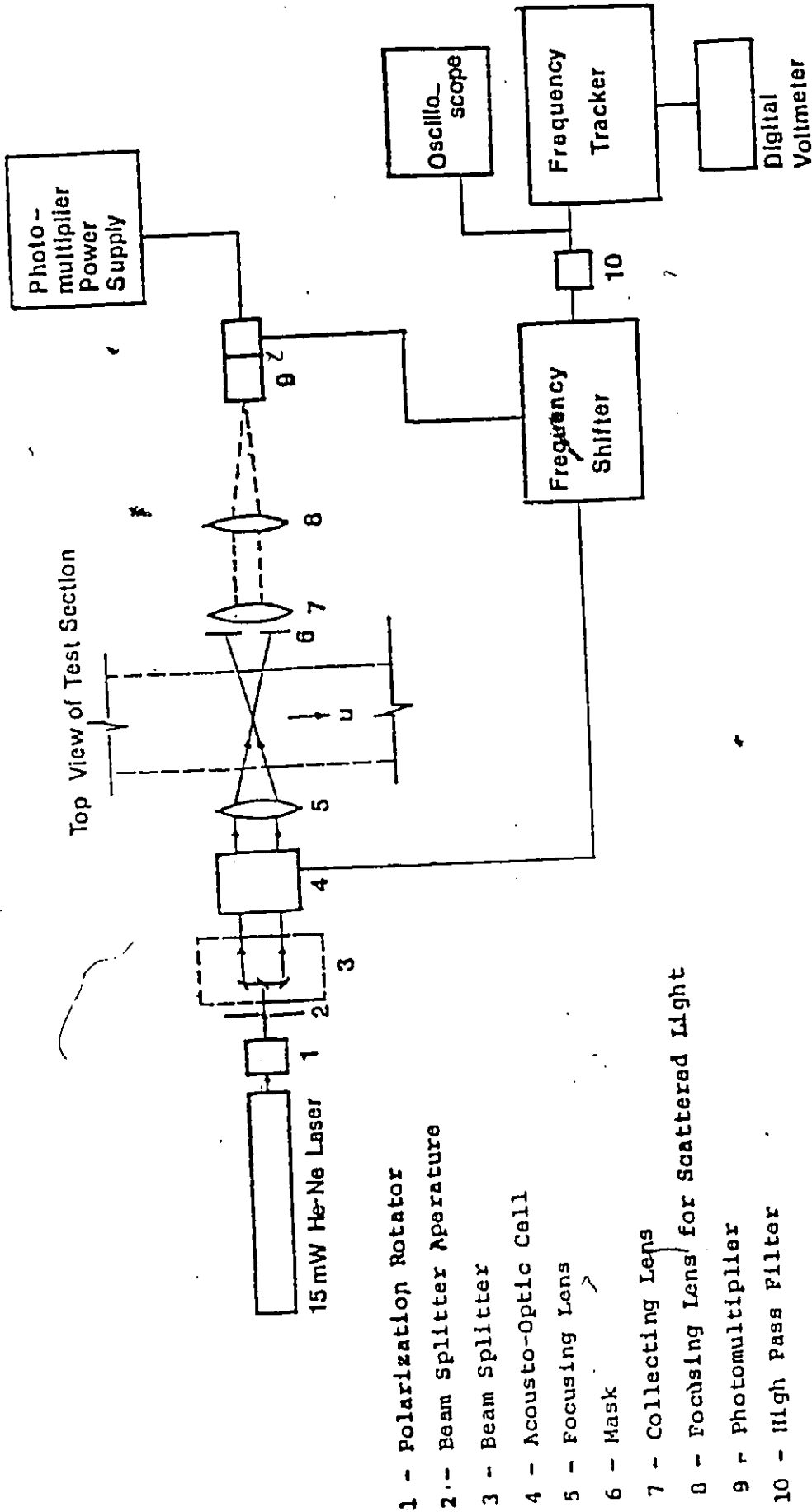


Fig. 3.1 Schematic layout of Flume.



- 1 - Polarization Rotator
- 2 - Beam Splitter Aperature
- 3 - Beam Splitter
- 4 - Acousto-Optic Cell
- 5 - Focusing Lens
- 6 - Mask
- 7 - Collecting Lens
- 8 - Focusing Lens for Scattered Light
- 9 - Photomultiplier
- 10 - High Pass Filter

Fig. 3.2 Laser Doppler Anemometer Arrangement. (After Ref. 33).

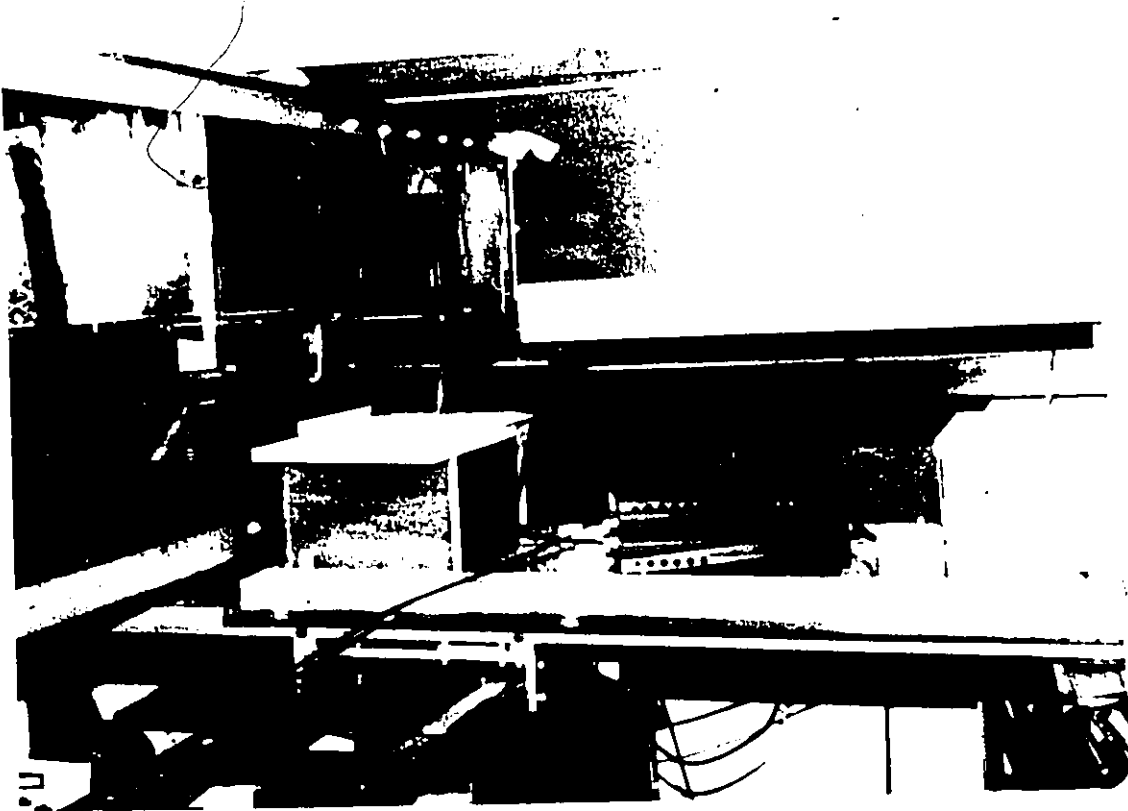


Fig. 3.3 Laser and Transmitting Optics

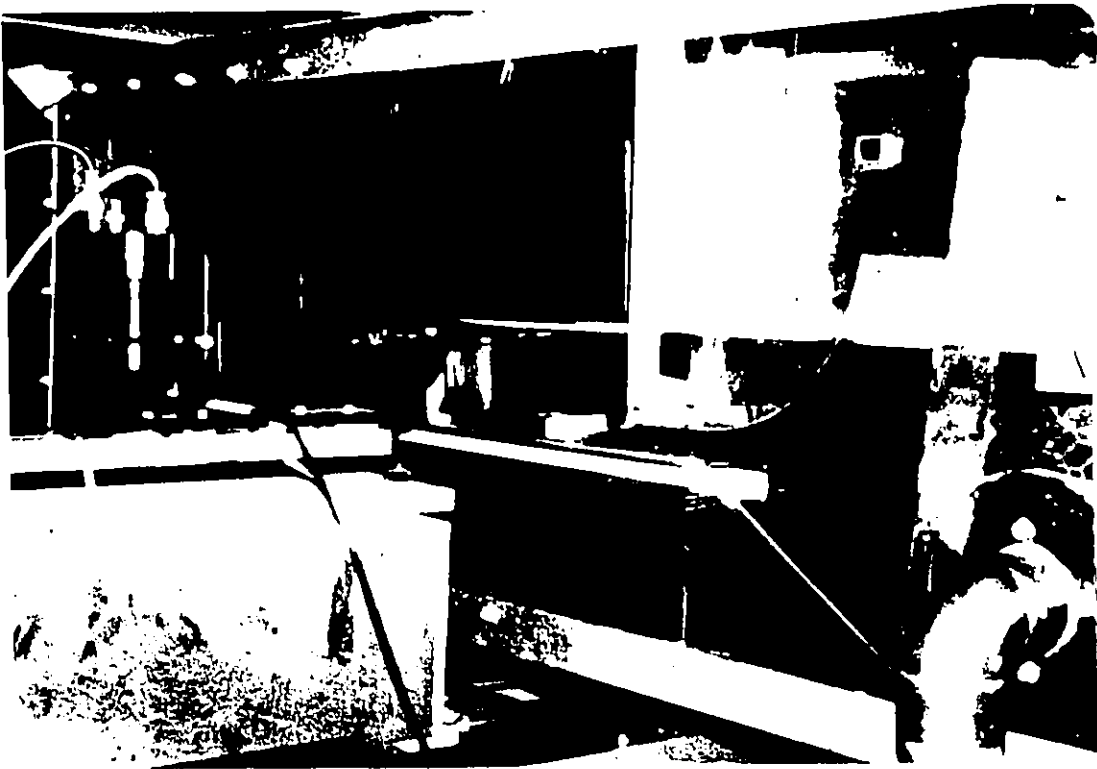


Fig. 3.4 Receiving Optics.

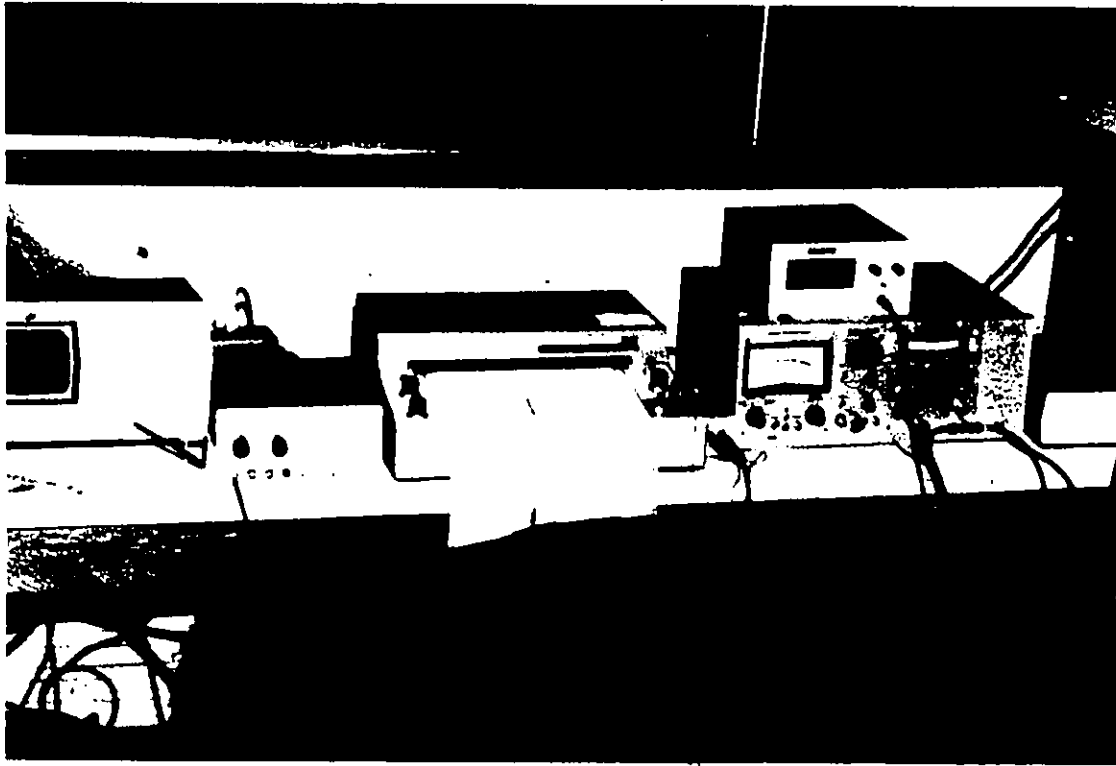


Fig. 3.5 Signal Processor and Oscilloscope.

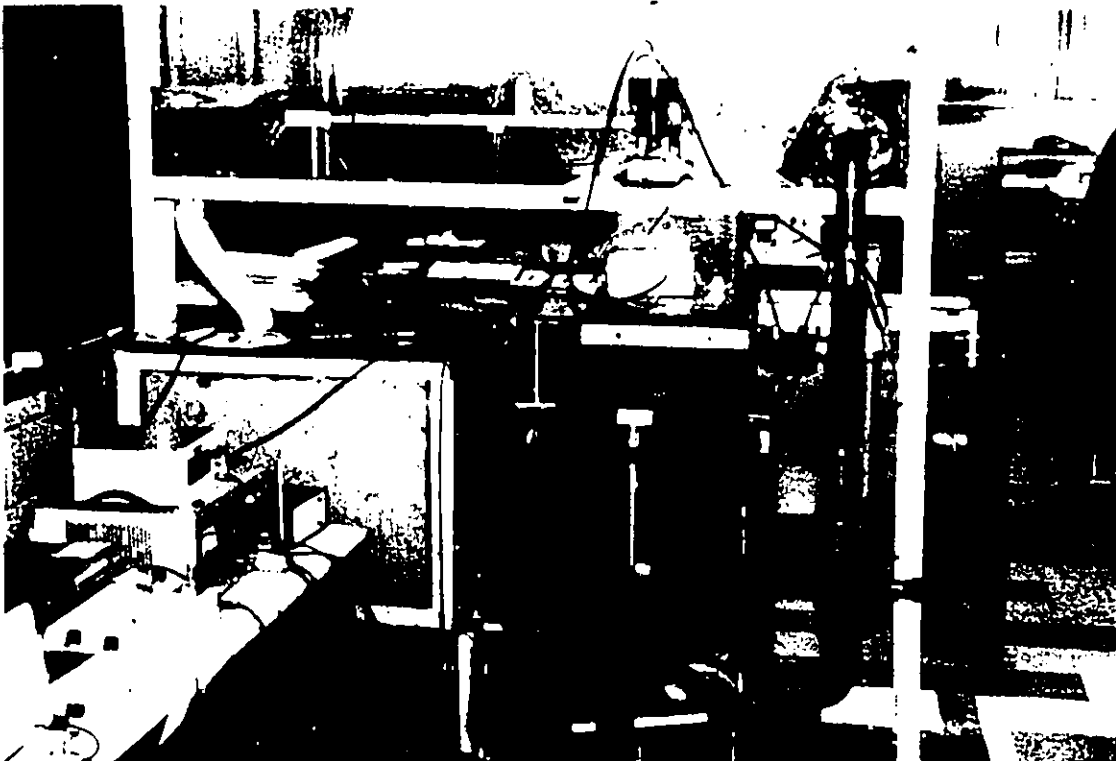


Fig. 3.6 Overall View of Test Facility.

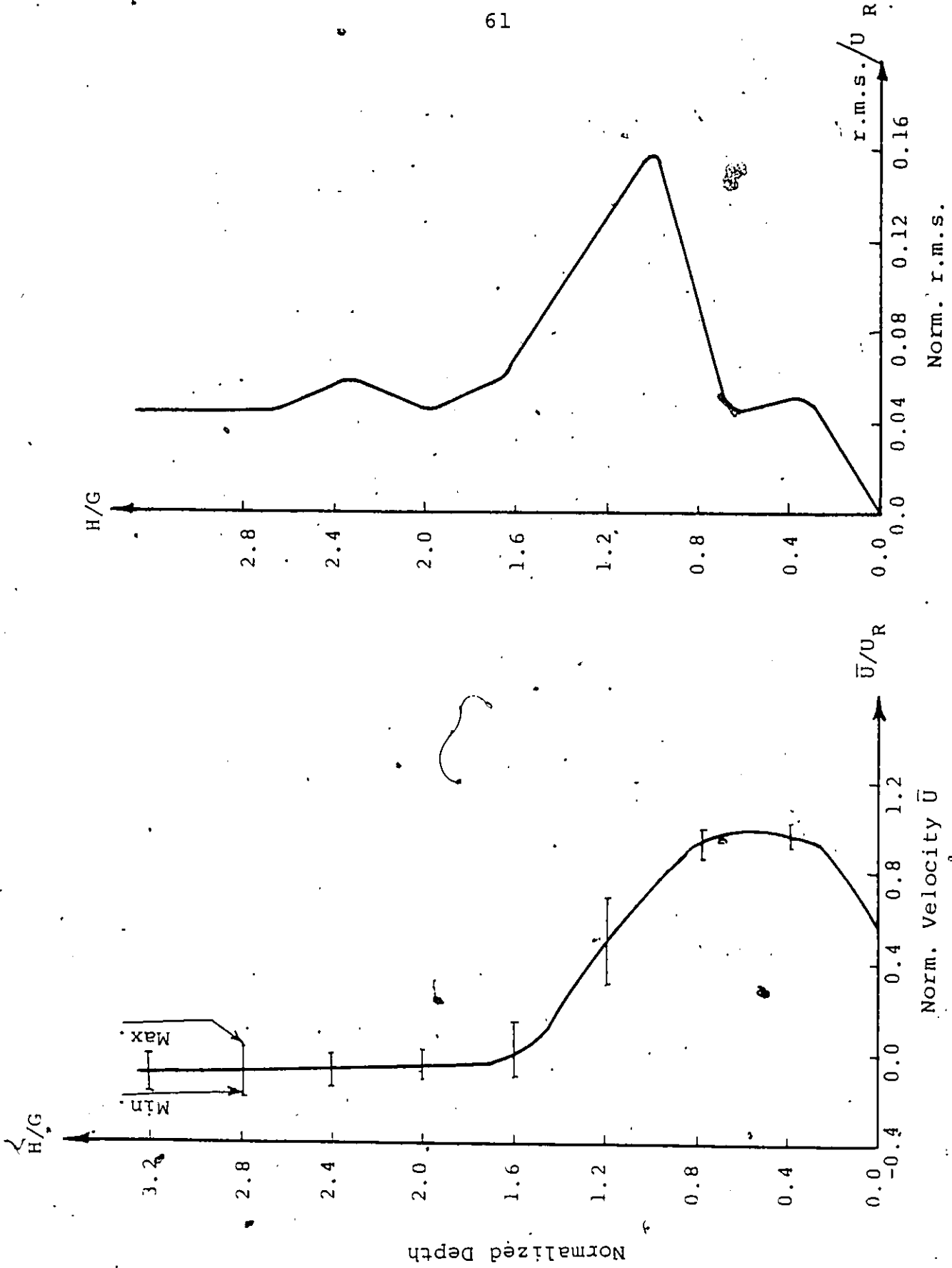


Fig. 4.1 Longitudinal velocity and r.m.s. profiles at $X = 5$ cm, $q = 53.9 \text{ cm}^3/\text{sec/cm}$
 $L = 30$ cm, $G = 3$ cm.

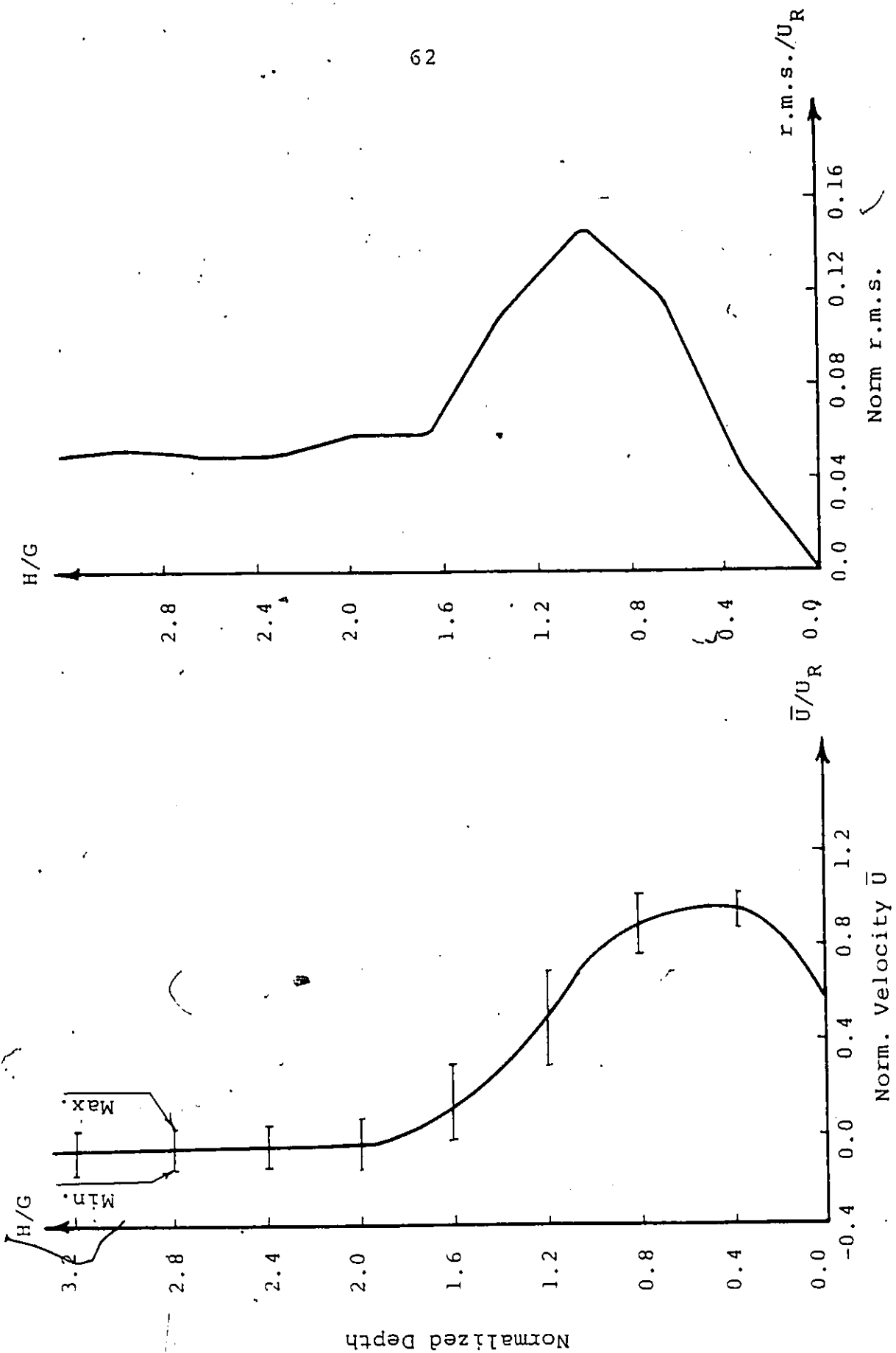


Fig. 4.2 Longitudinal velocity and r.m.s. profiles at $X = 10$ cm, $q = 53.9 \text{ cm}^3/\text{sec/cm}$, $L = 30$ cm, $G = 3$ cm.

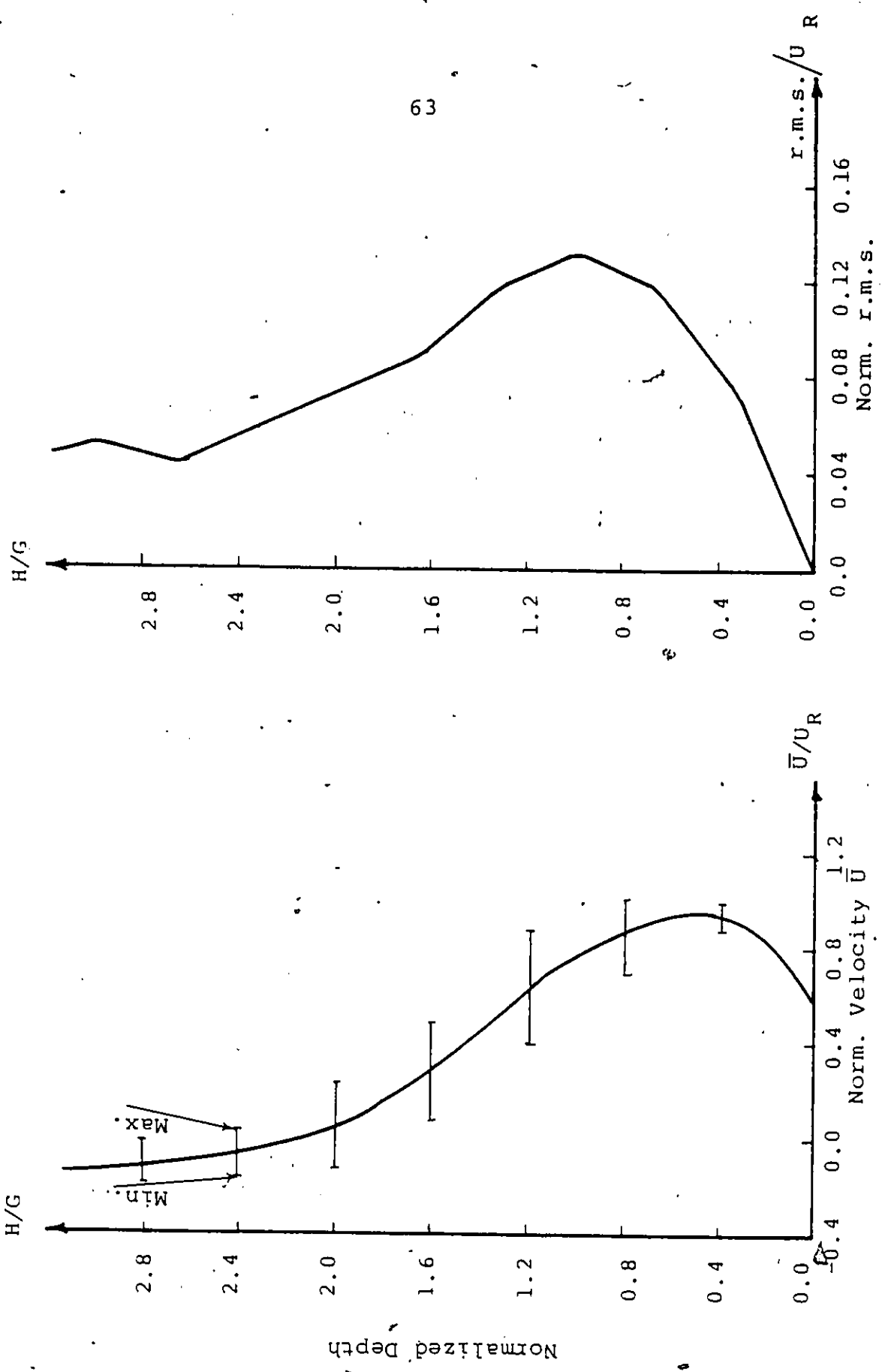


Fig. 4.3 Longitudinal velocity and r.m.s. profiles at $X = 15$ cm, $q = 53.9 \text{ cm}^3/\text{sec}/\text{cm}$, $L = 30 \text{ cm}$, $G = 3 \text{ cm}$.

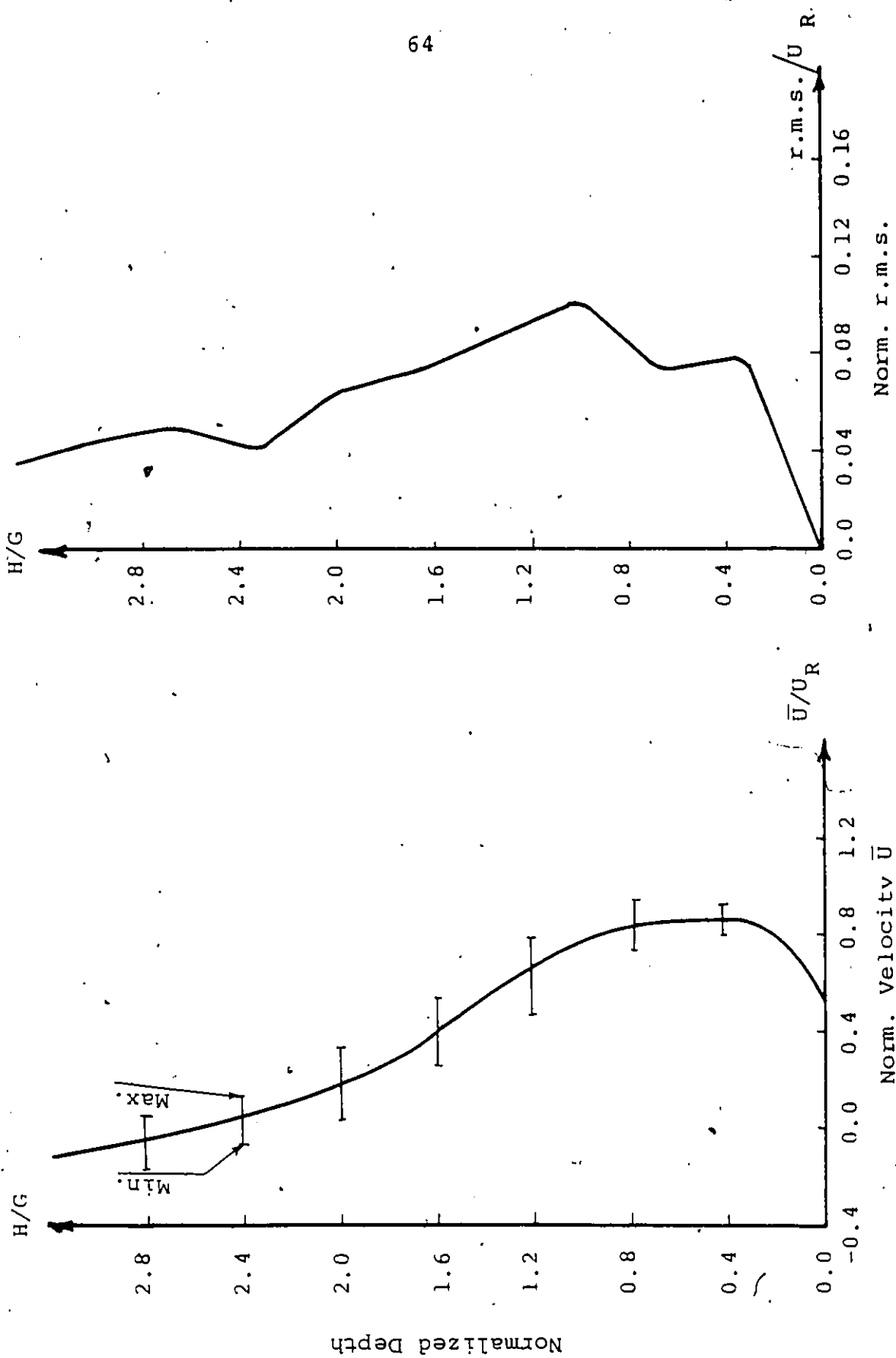


Fig. 4.4 Longitudinal velocity and r.m.s. profiles at $X = 20$ cm, $q = 53.9$ cm³/sec/cm, $L = 30$ cm, $G = 3$ cm.

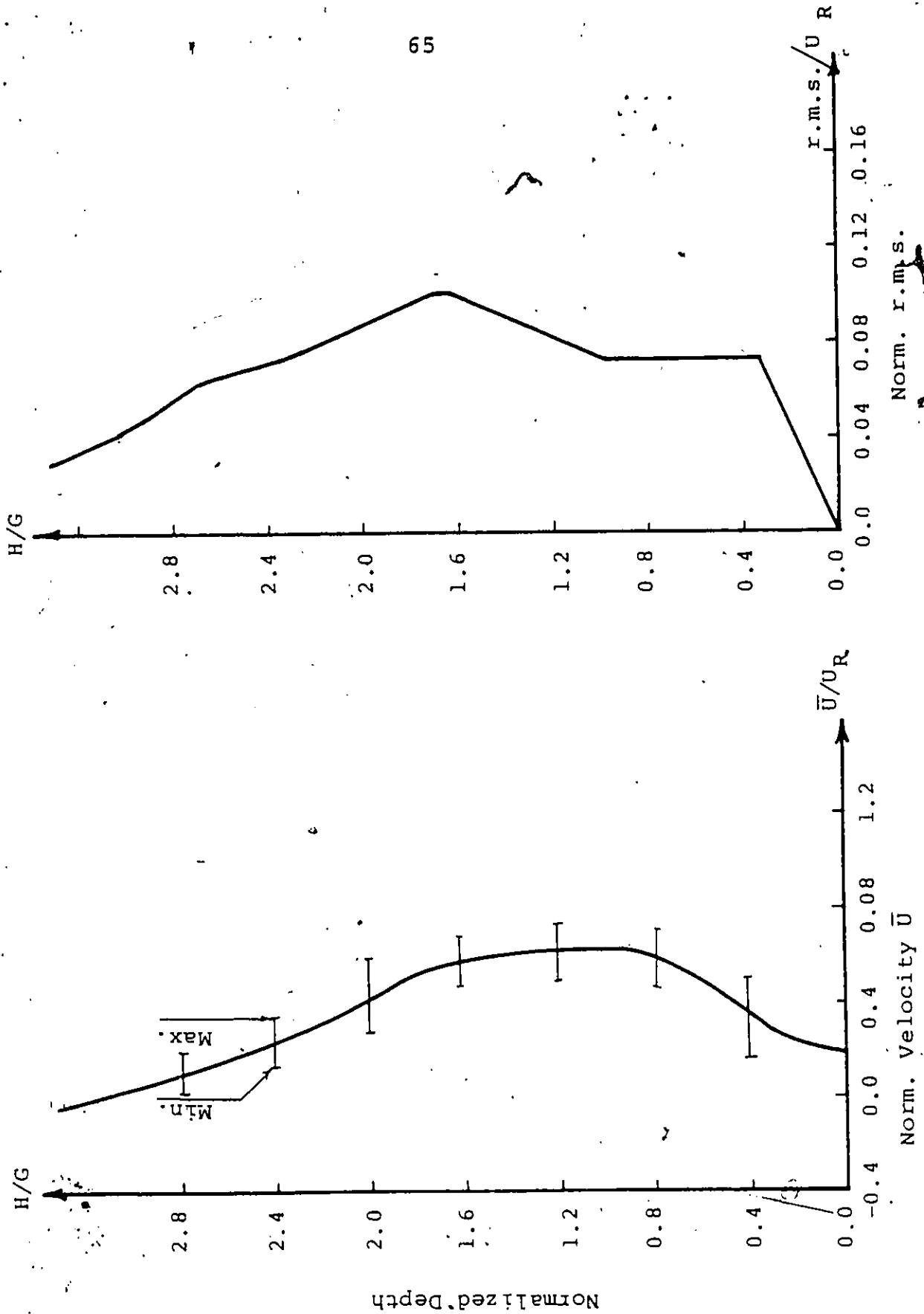


Fig. 4.5 Longitudinal velocity and r.m.s. profiles at $X_1 = 25$ cm, $q = 53.9$ cm³/sec/cm, $L = 30$ cm, $G = 3$ cm.

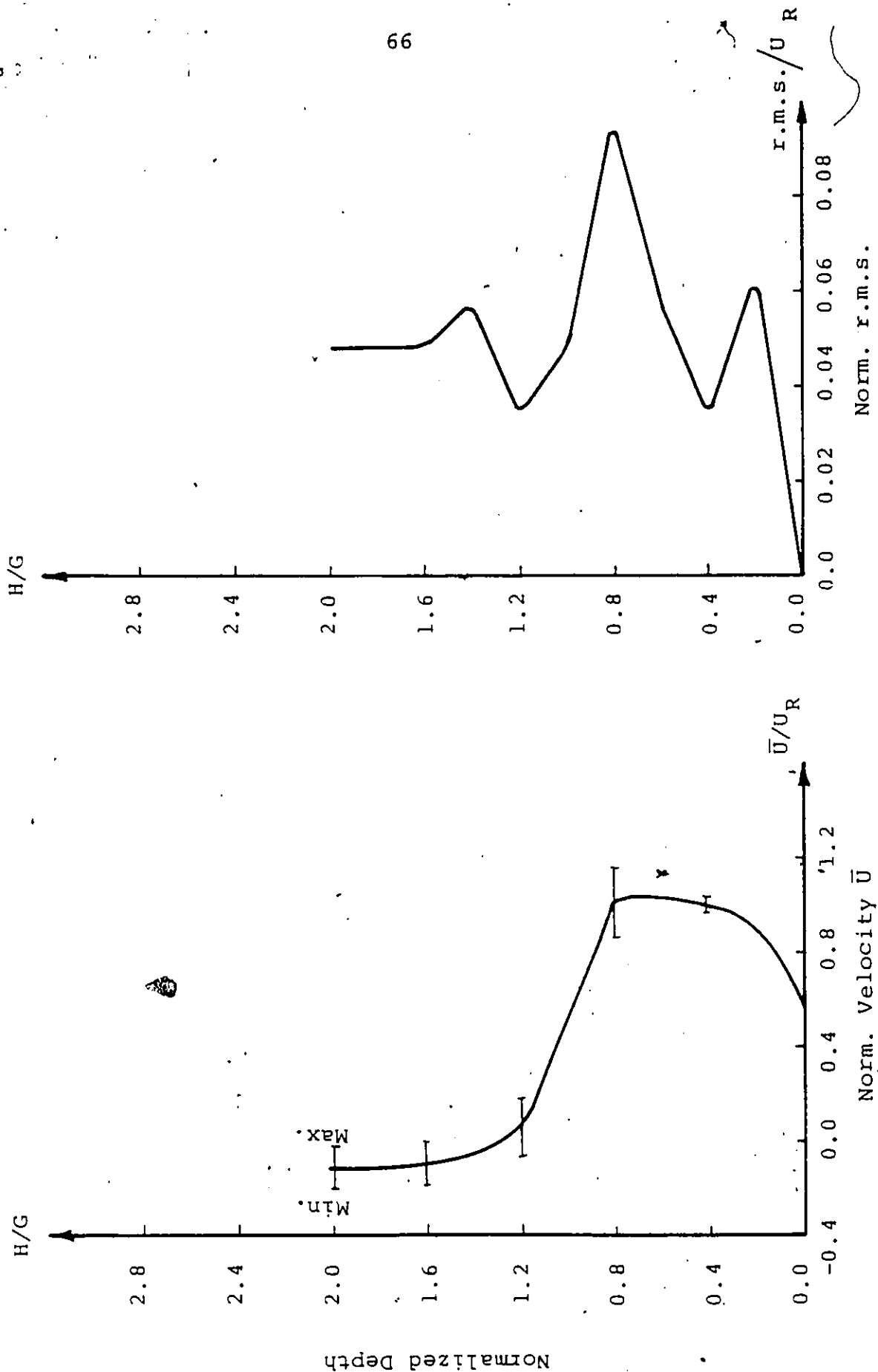


Fig. 4.6 Longitudinal velocity and r.m.s. profiles at $X = 5$ cm, $q = 53.9$ cm³/sec/cm
 $L = 30$ cm; $G = 5$ cm.

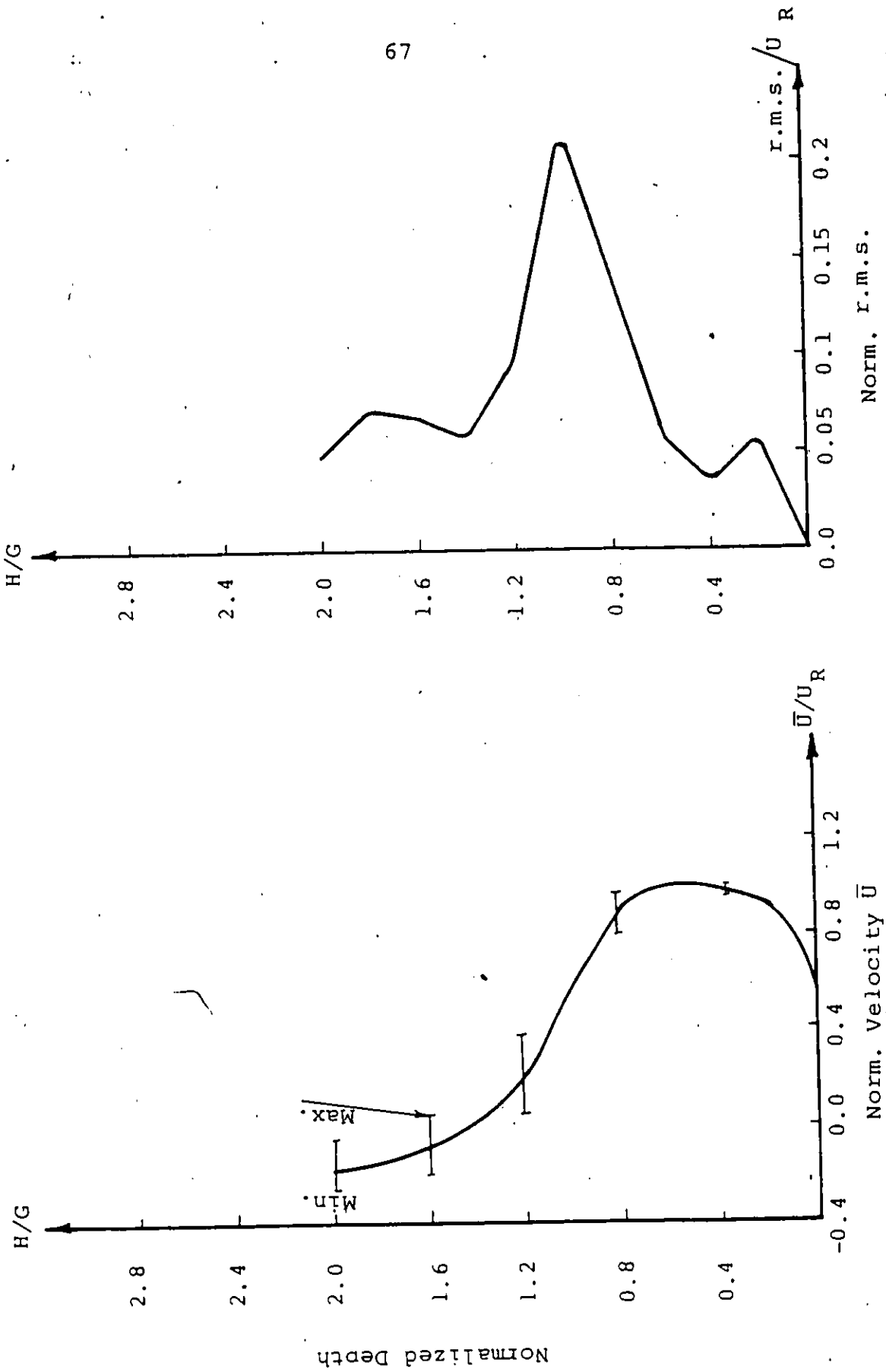


Fig. 4.7 Longitudinal velocity and r.m.s. profiles at $X = 10$ cm, $q = 53.9 \text{ cm}^3/\text{sec}/\text{cm}$
 $L = 30$ cm, $G = 5$ cm.

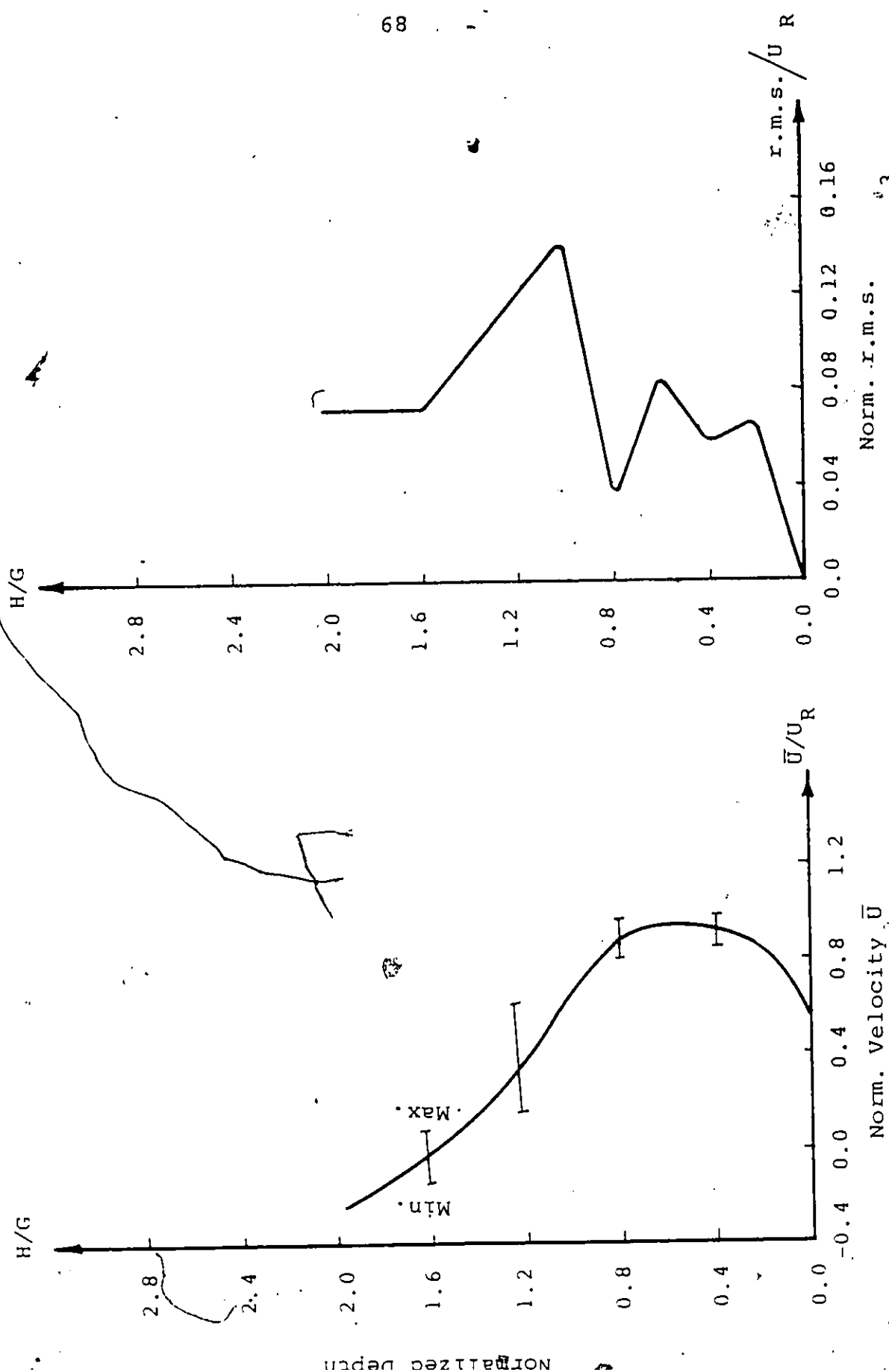


Fig. 4.8 Longitudinal velocity and r.m.s. profiles at $X = 15$ cm, $q = 53.9 \text{ cm}^3/\text{sec/cm}$, $L = 30$ cm, $G = 5$ cm.

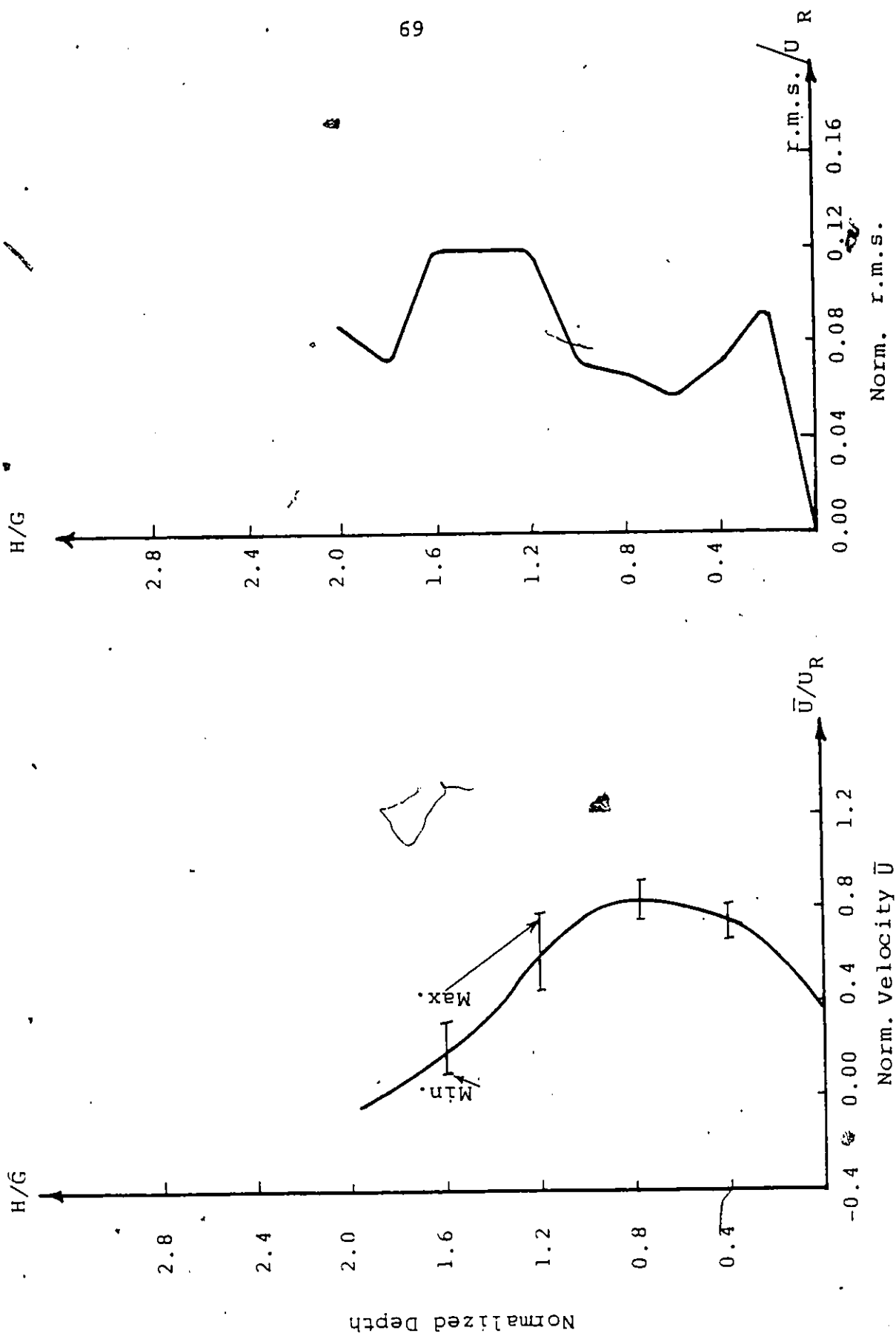


Fig. 4.9 Longitudinal velocity and r.m.s. profiles at $X = 20$ cm, $q = 53.9 \text{ cm}^3/\text{sec}/\text{cm}$
 $L = 30$ cm, $G = 5$ cm.

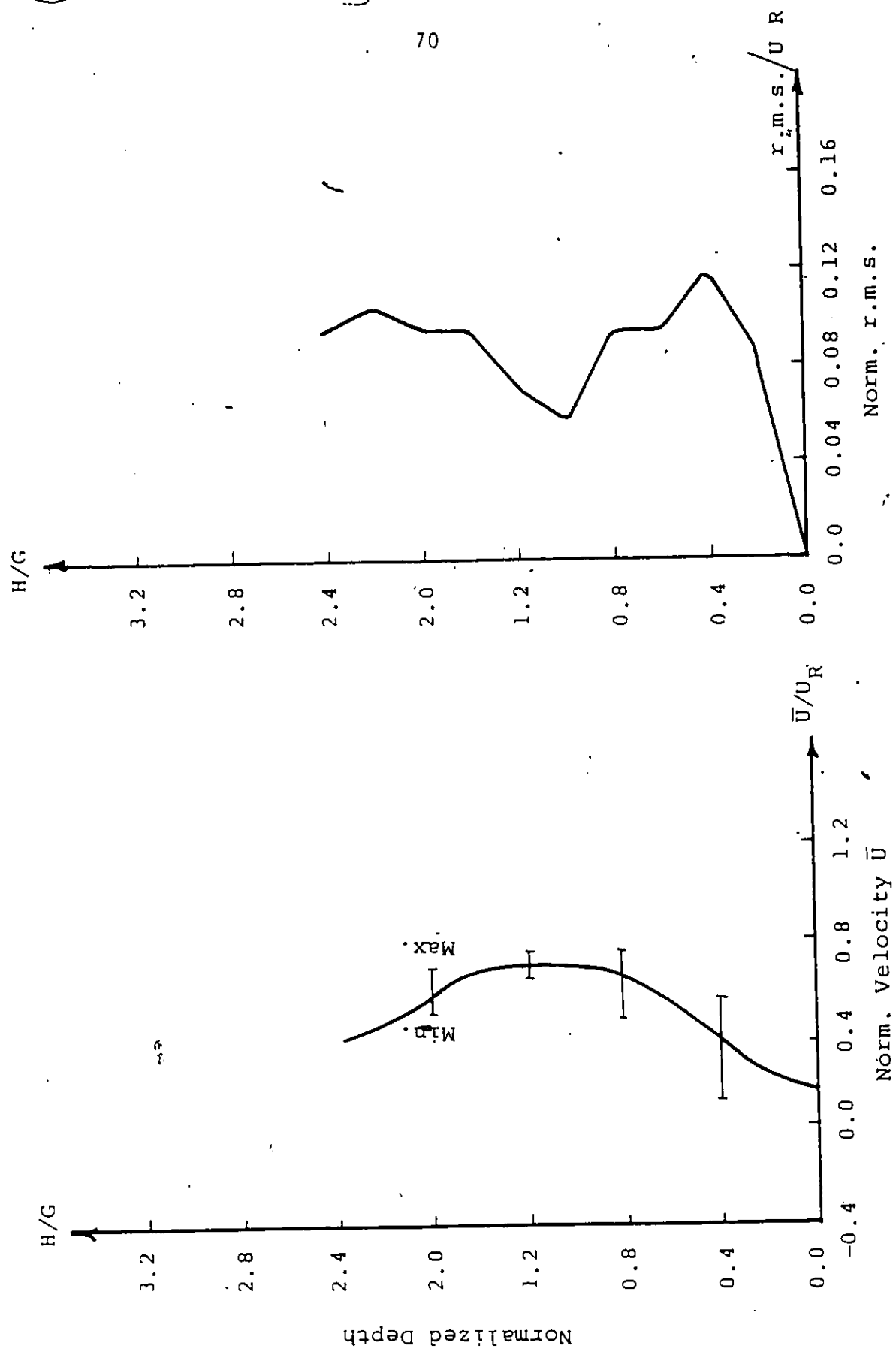


Fig. 4.10 Longitudinal velocity and r.m.s. profiles at $X = 25$ cm, $q = 53.9 \text{ cm}^3/\text{sec}/\text{cm}$
 $L = 30$ cm, $G = 5$ cm.

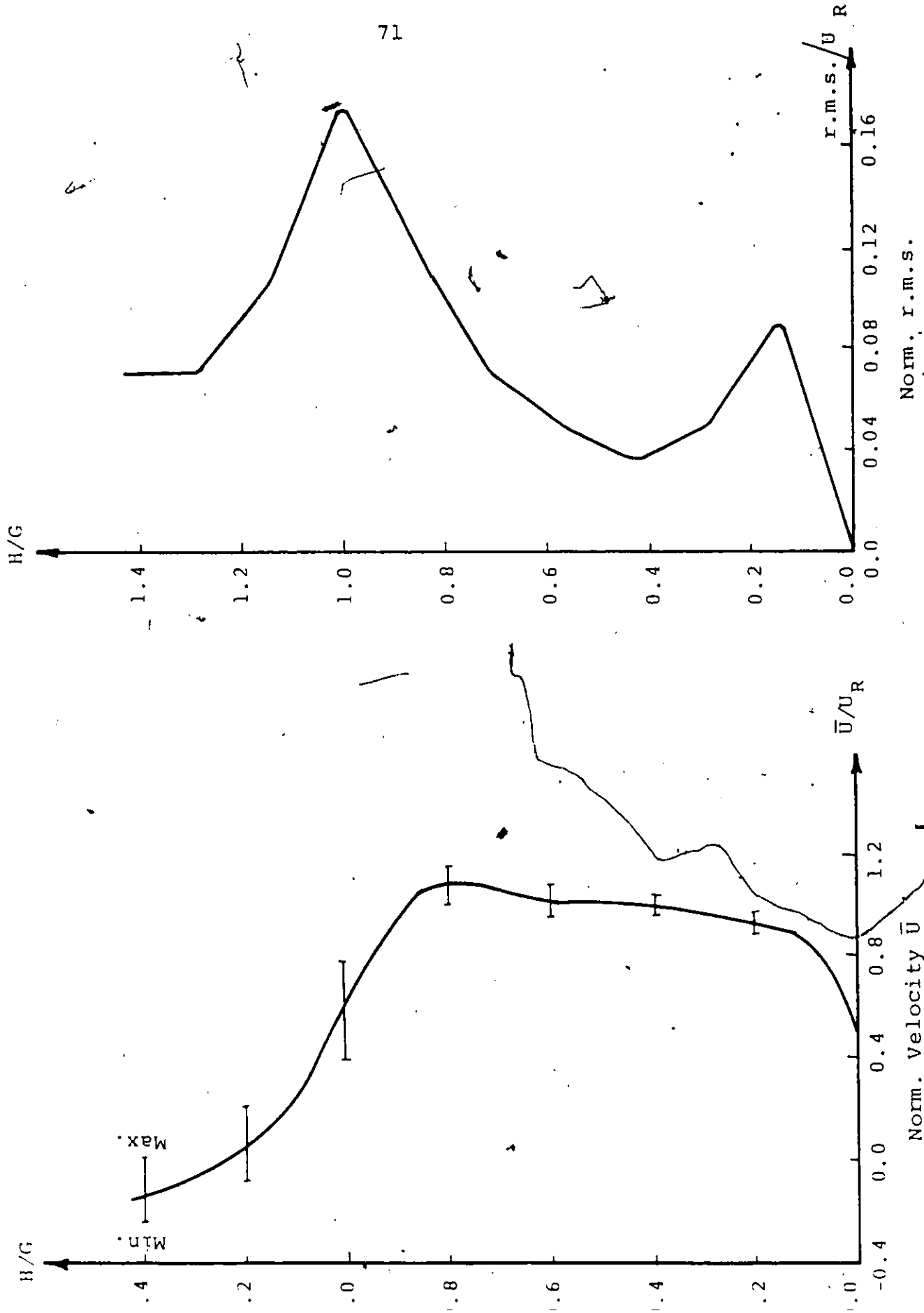
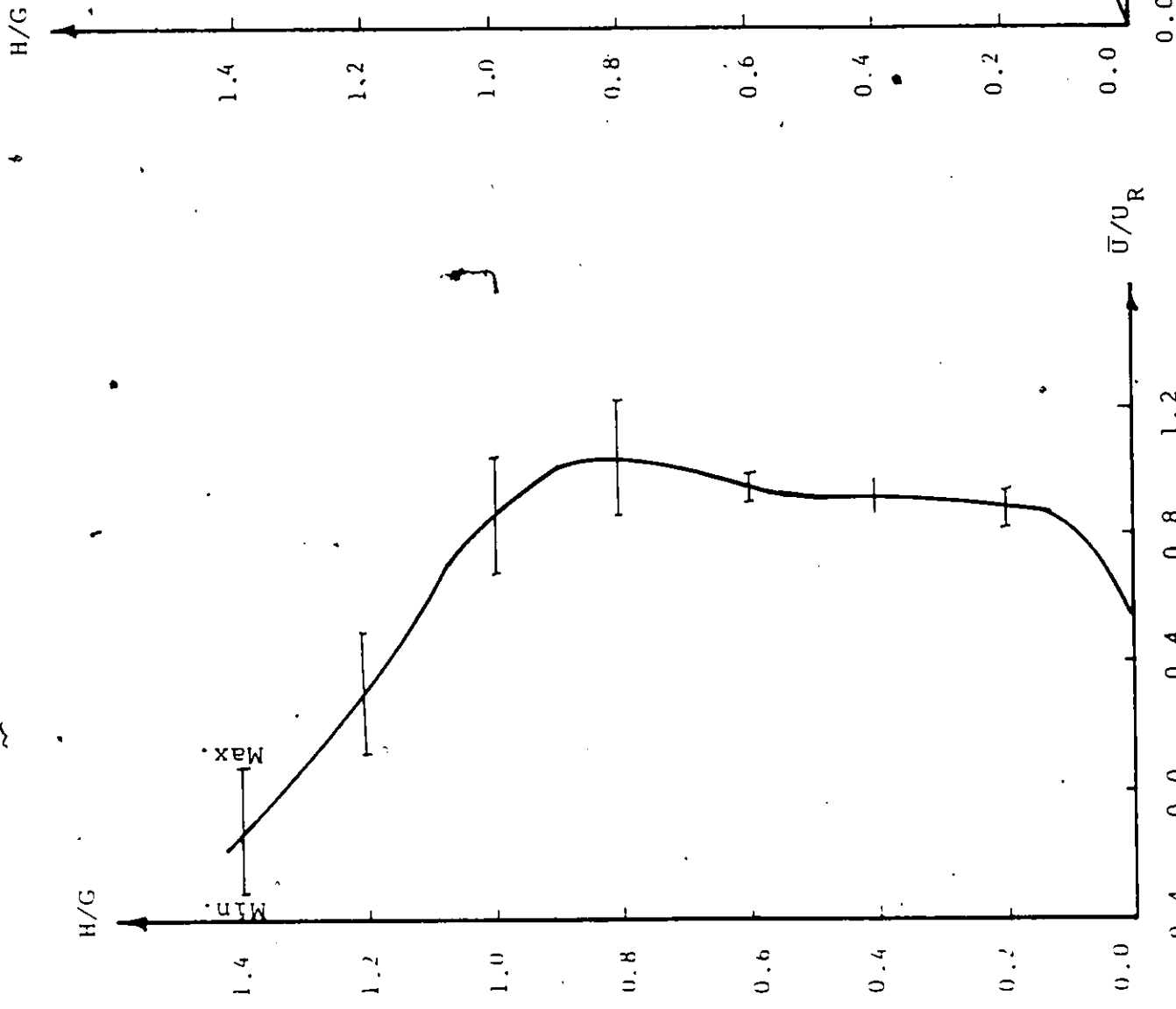


Fig. 4.11. Longitudinal velocity and r.m.s. profiles at $X = 5$ cm, $q = 53.9$ cm³/sec/cm



Norm. r.m.s.

r.m.s./U_R

Fig. 4.12 Longitudinal velocity and r.m.s. profiles at $X = 10$ cm, $\alpha = 53.9$ cm³/sec/cm
 $L = 30$ cm, $G = 7$ cm.

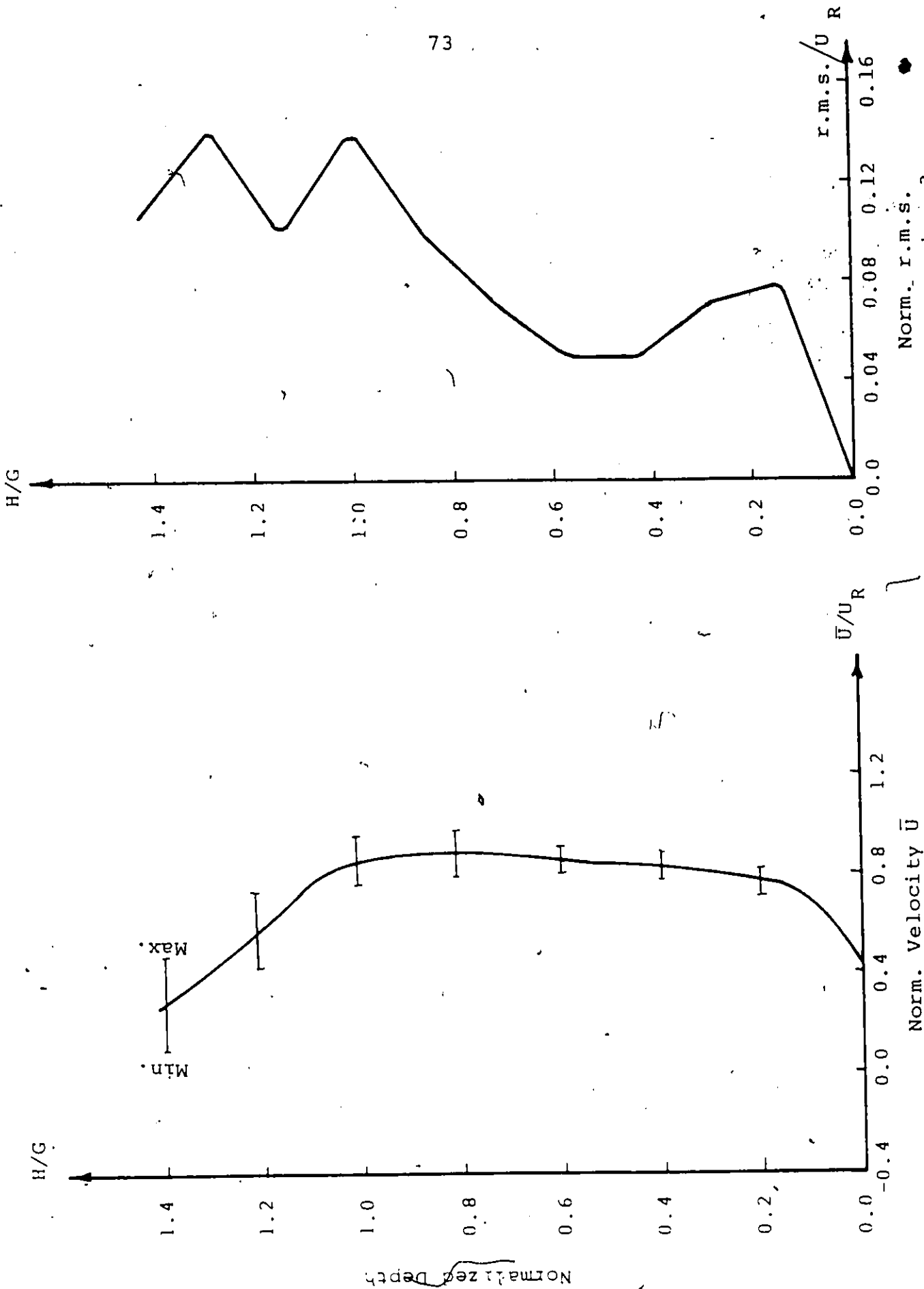


Fig. 4.13 Longitudinal velocity and r.m.s. profiles at $x = 15$ cm, $q = 53.9$ cm³/sec/cm, $L = 30$ cm, $G = 7$ cm.

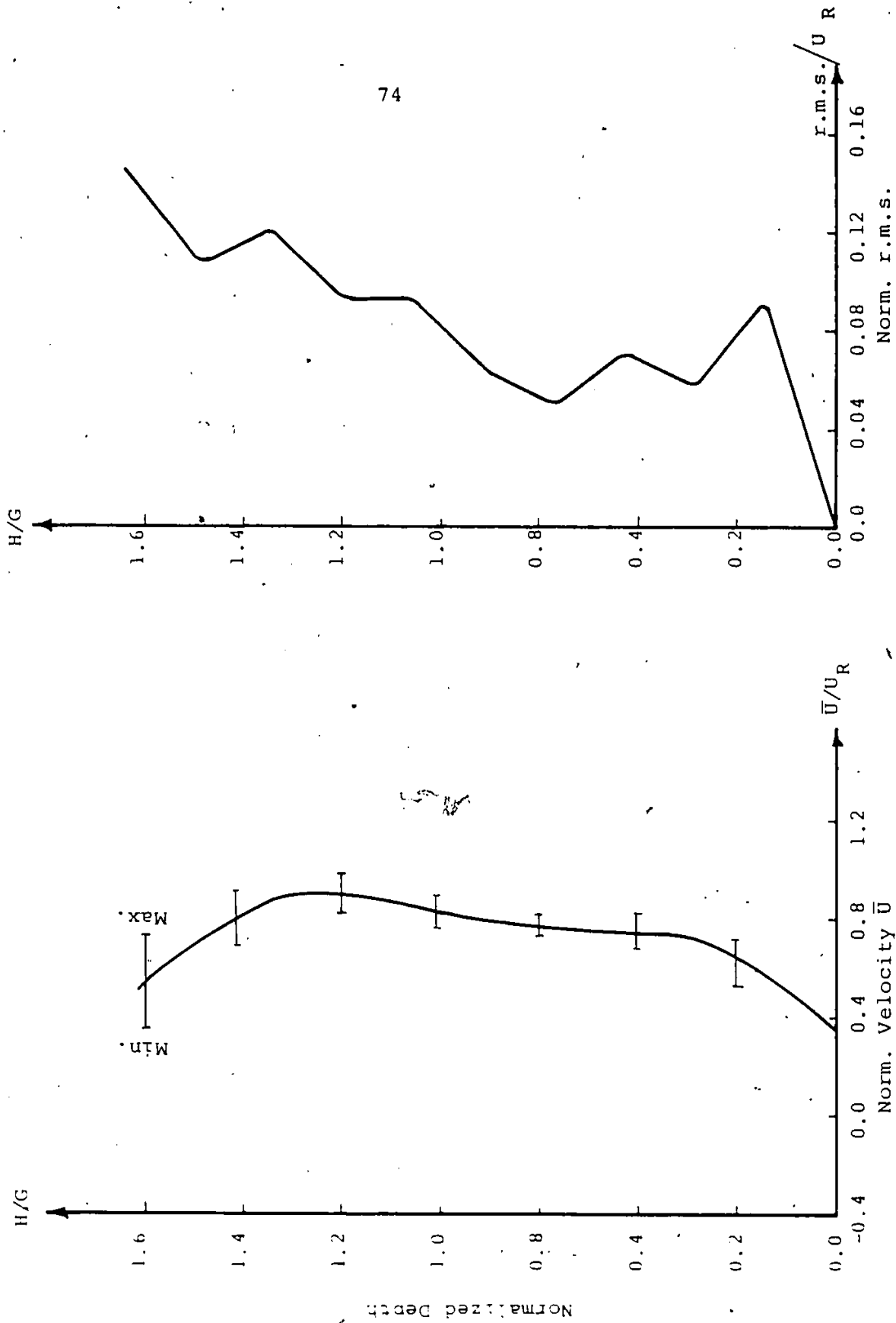


Fig. 4.14 Longitudinal velocity and r.m.s. profiles at $X = 20$ cm, $q = 53.9$ cm³/sec/cm, $L = 30$ cm, $G = 7$ cm).

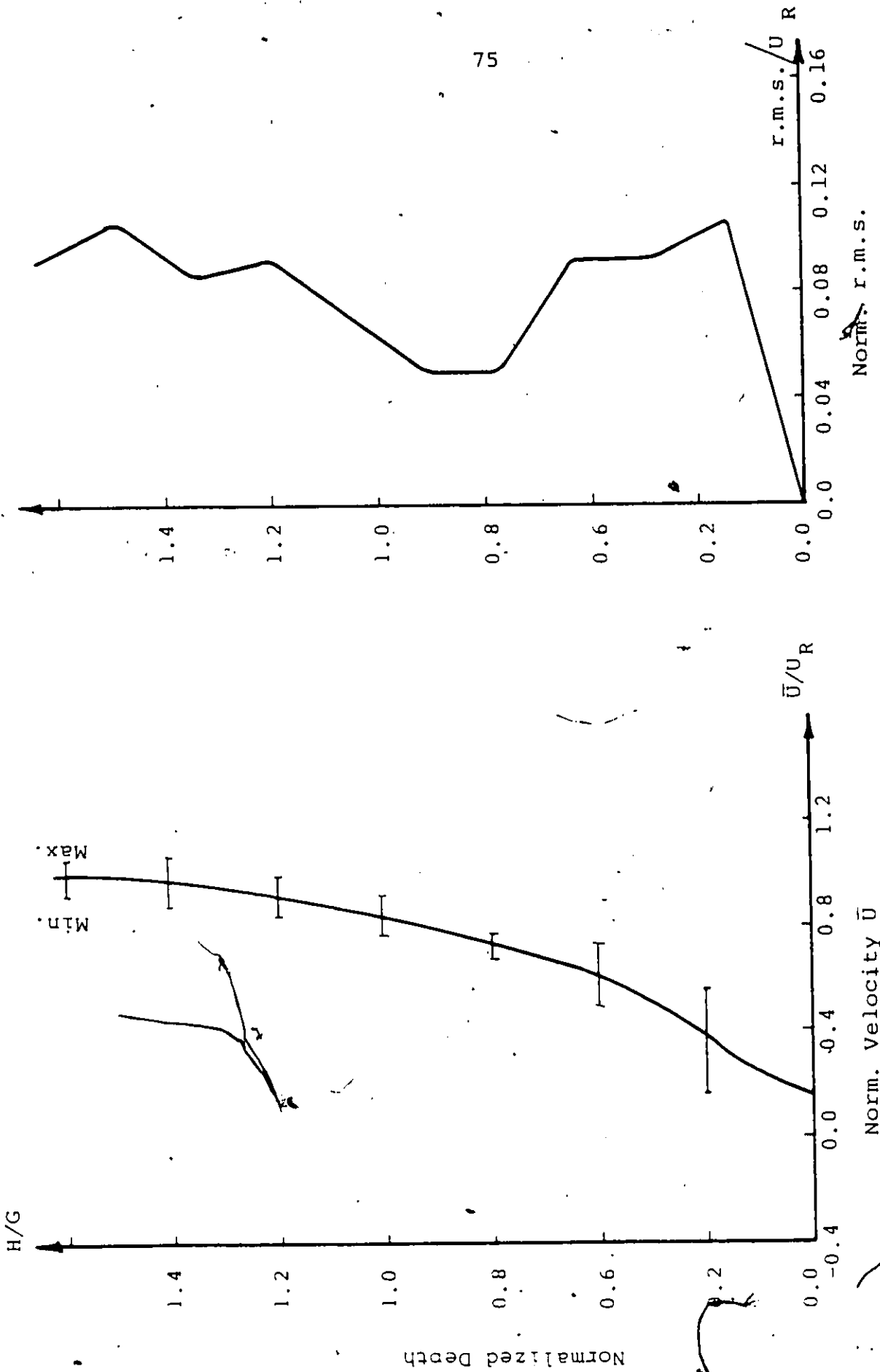
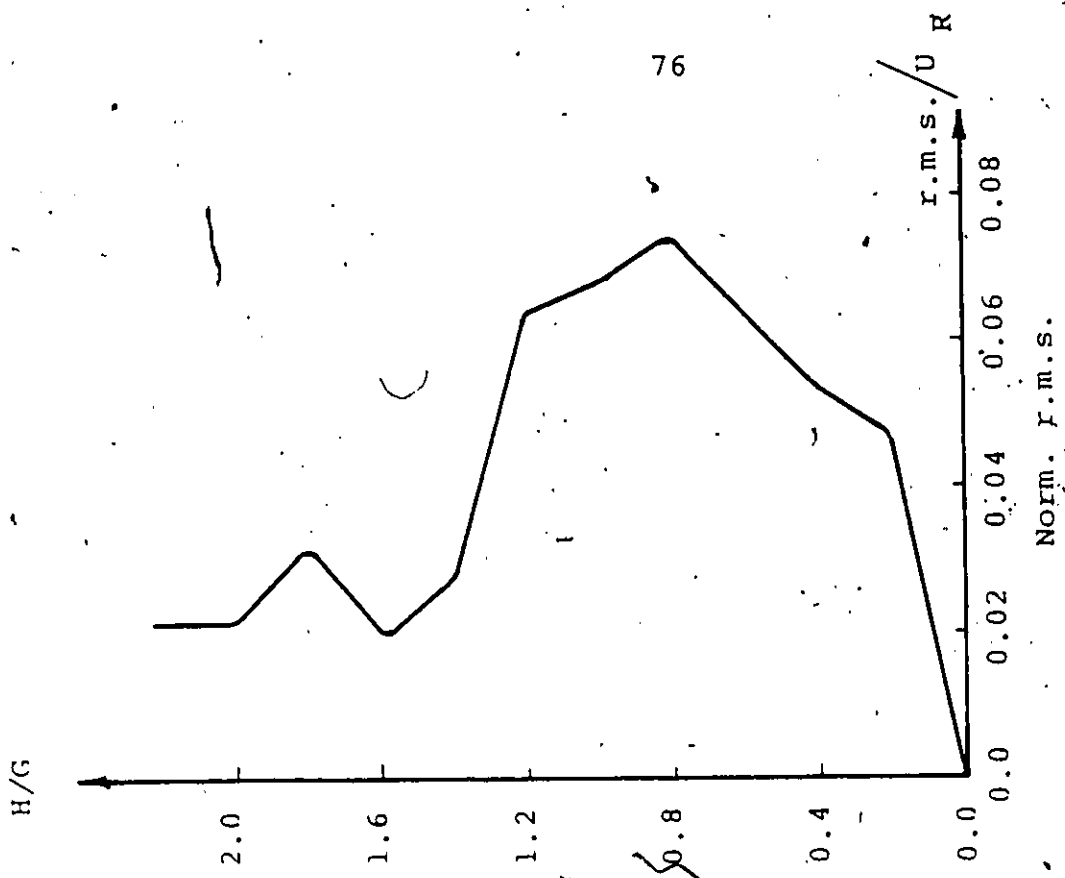


Fig. 4.15 Longitudinal velocity and r.m.s. profiles at $X = 25$ cm, $q = 53.9$ cm³/sec/cm, $L = 30$ cm, $G = 7$ cm).



Norm. r.m.s.

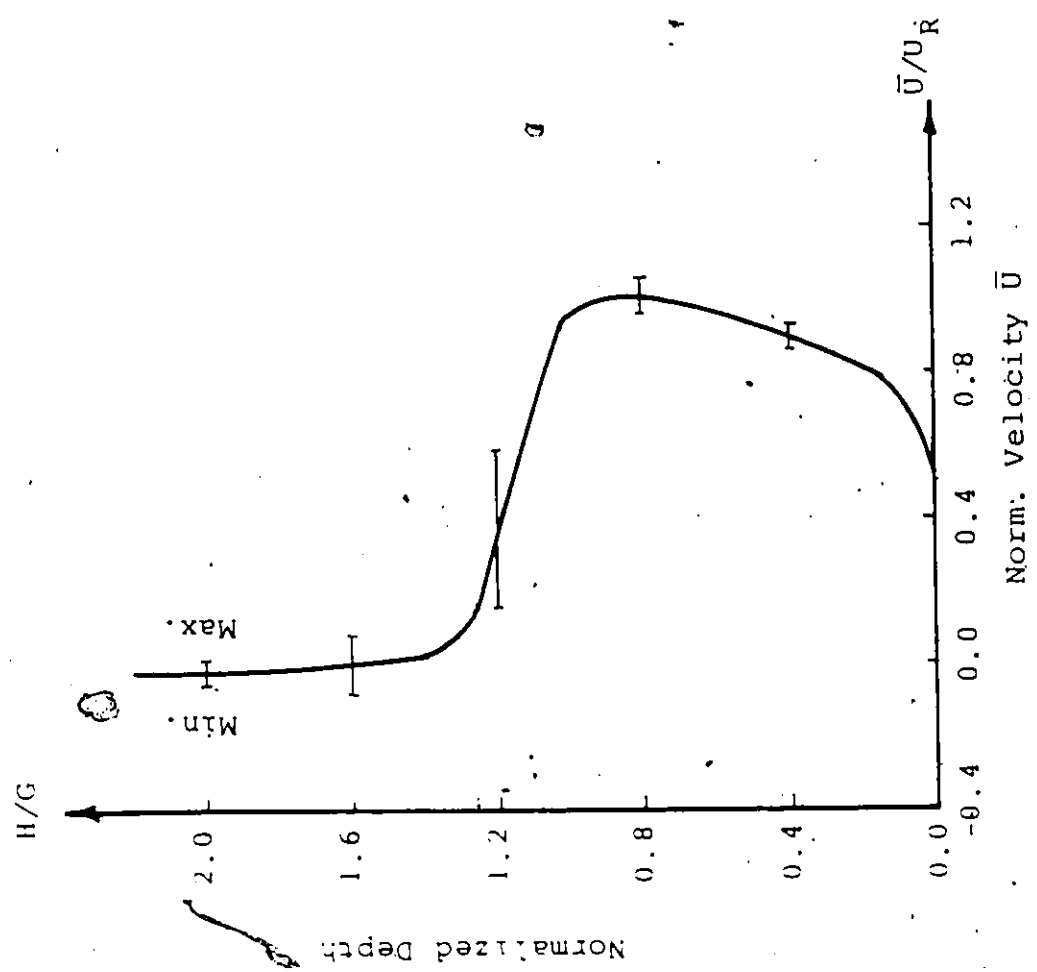


Fig. 4.16 Longitudinal velocity and r.m.s. profiles at $X = 5$ cm, $\alpha = 111$ cm³/sec/cm, $L = 40$ cm, $G = 5$ cm.

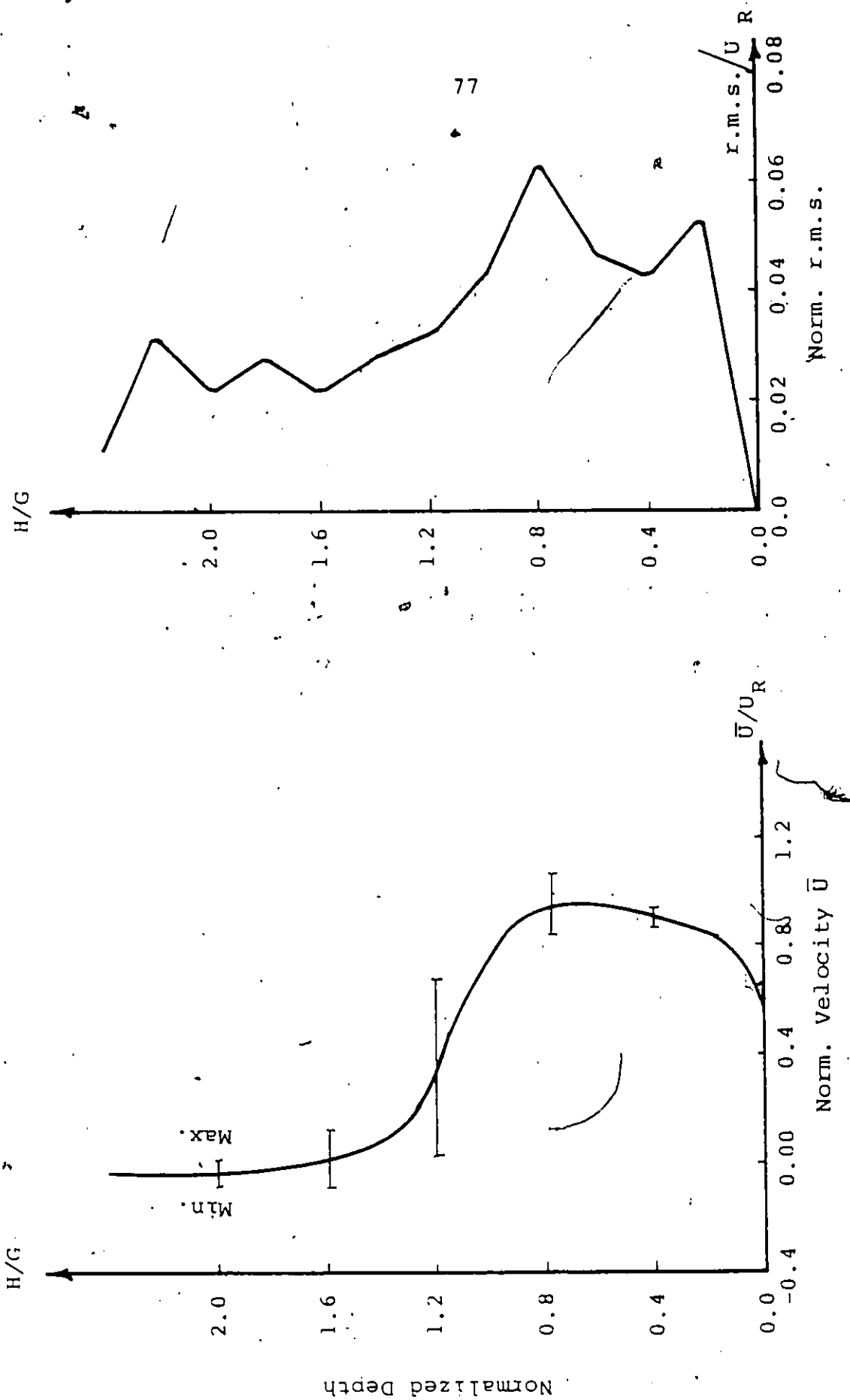


Fig. 4.17 Longitudinal velocity and r.m.s. profiles at $X = 10$ cm, $q = 111 \text{ cm}^3/\text{sec/cm}$, $L = 40$ cm, $G = 5$ cm.

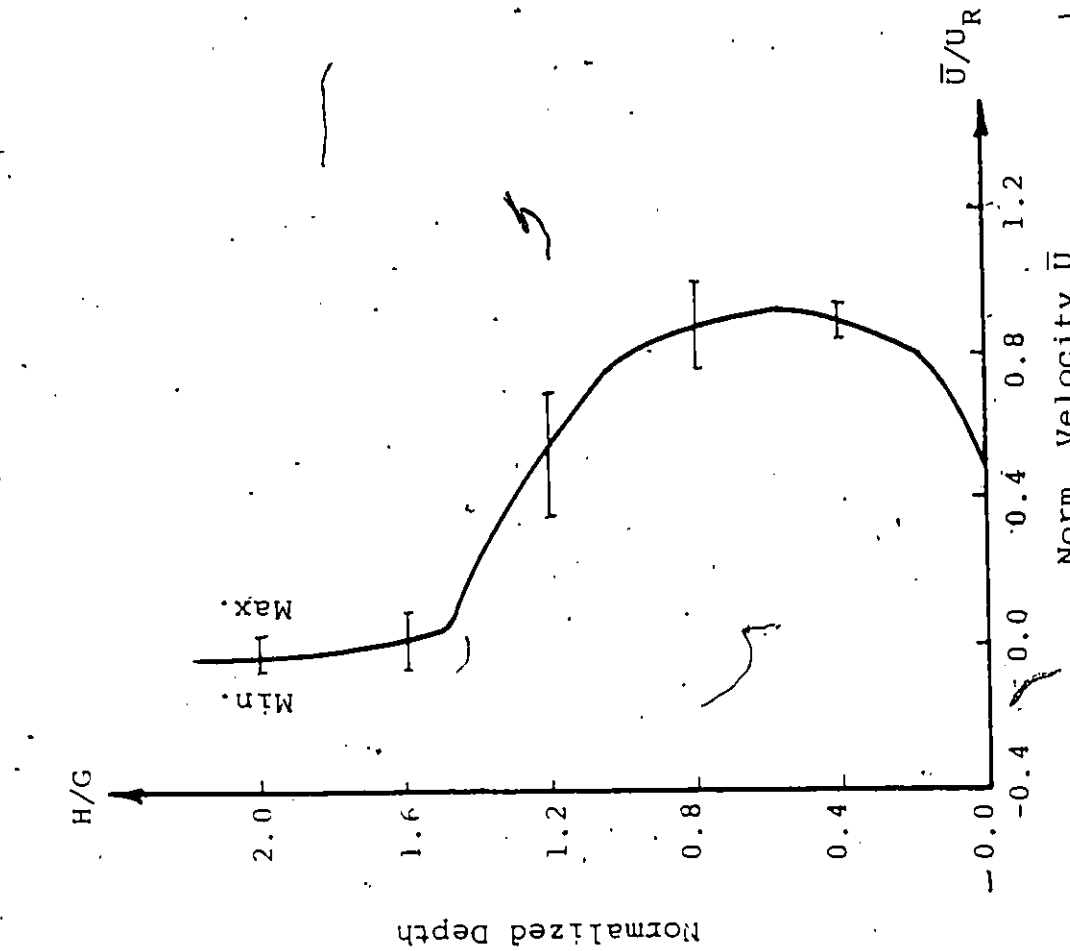
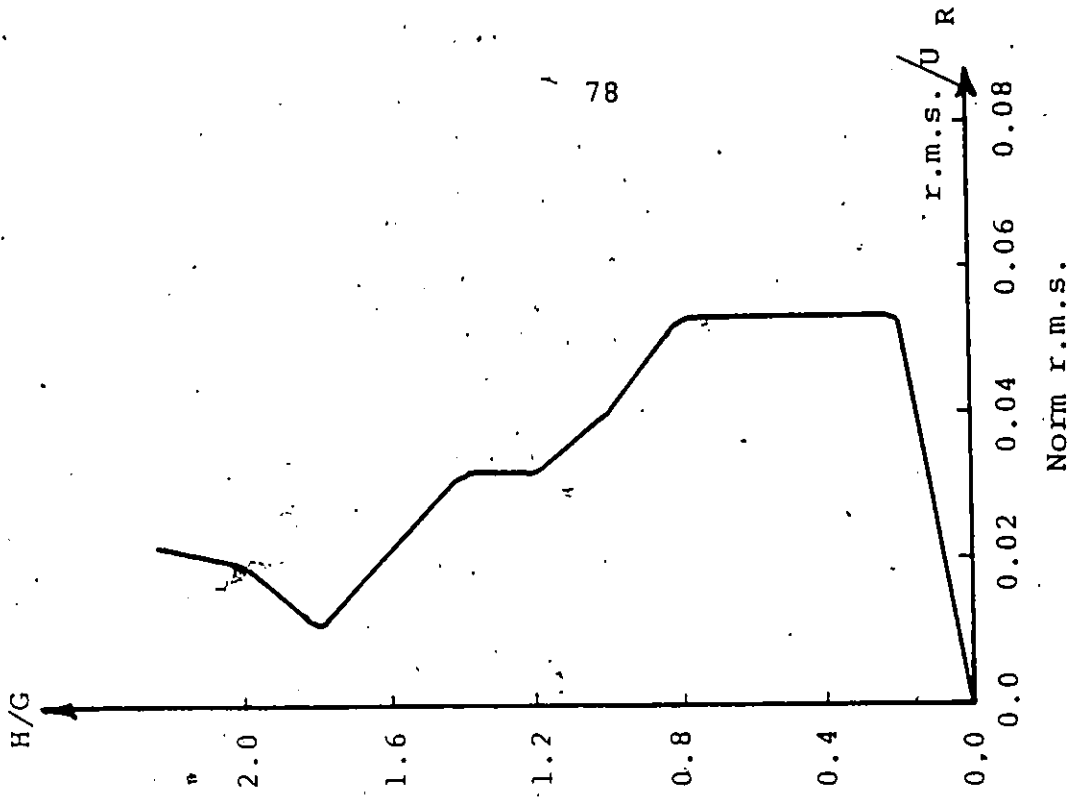


Fig. 4.18 Longitudinal velocity and r.m.s. profiles at $X = 15$ cm, $q = 111$ cm³/sec/cm, $L = 40$ cm, $G = 5$ cm.

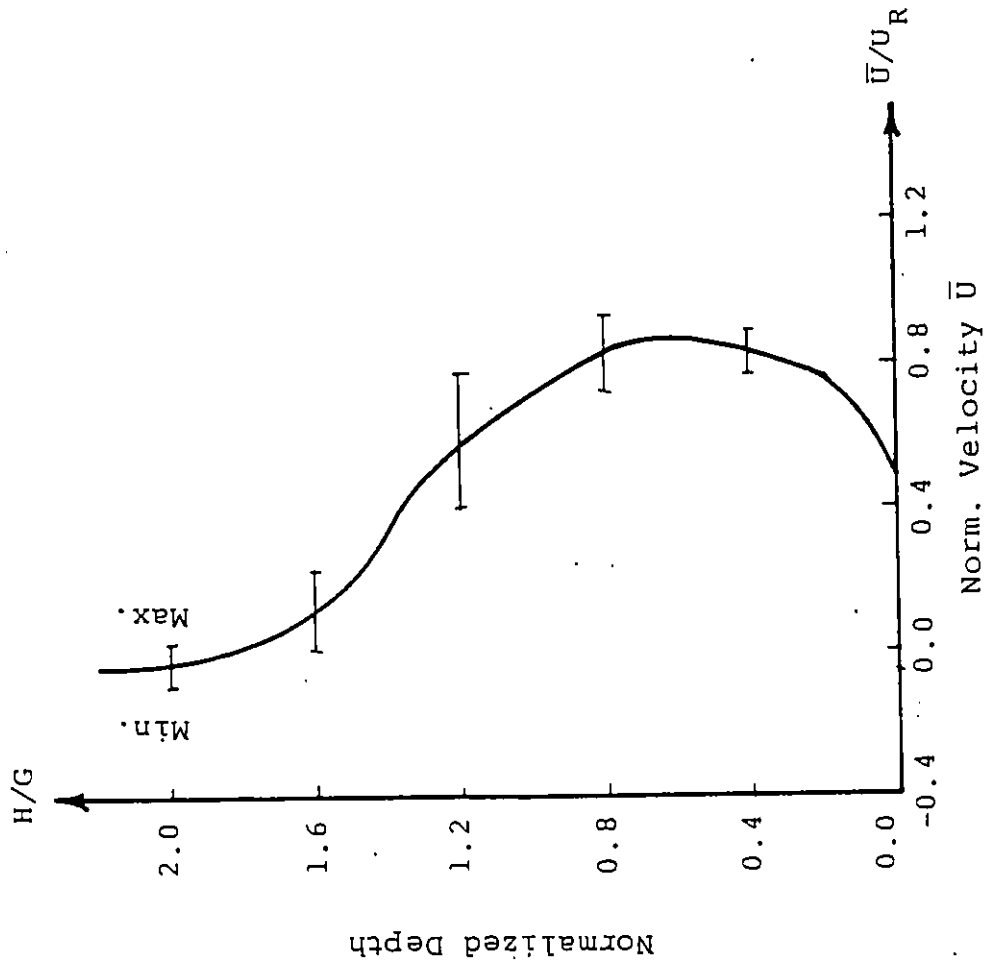
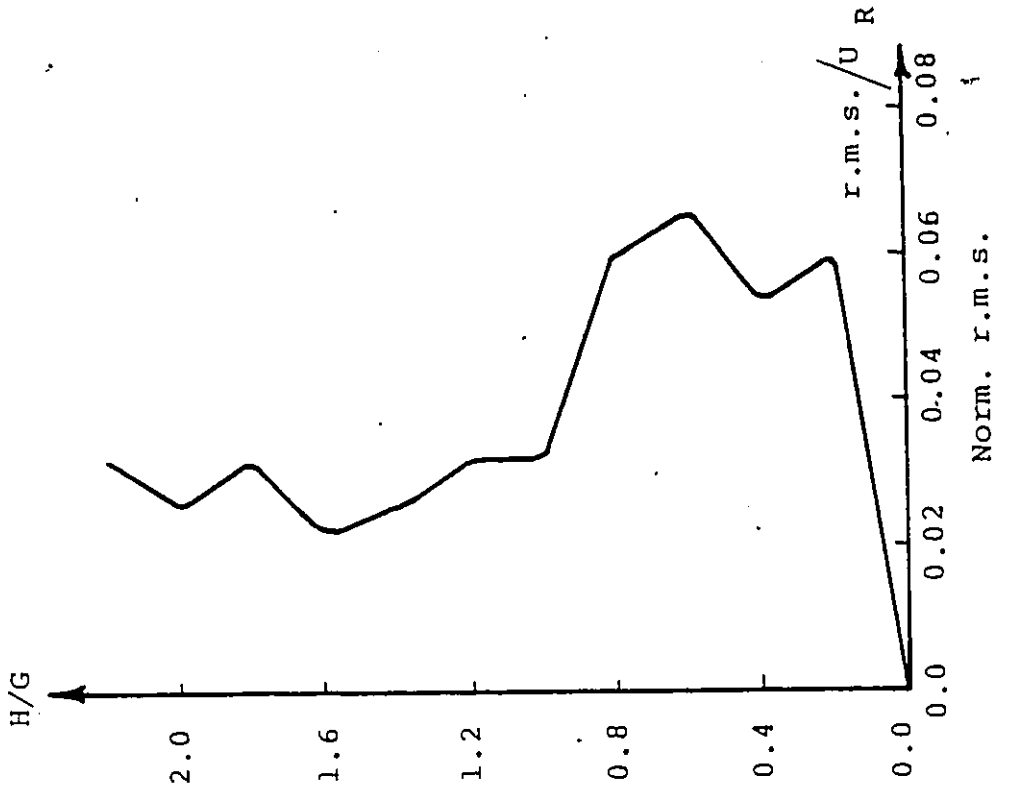


Fig. 4.19 Longitudinal velocity and r.m.s. profiles at $X = 20$ cm, $q = 111 \text{ cm}^3/\text{sec}/\text{cm}$, $L = 40$ cm, $G = 5$ cm.

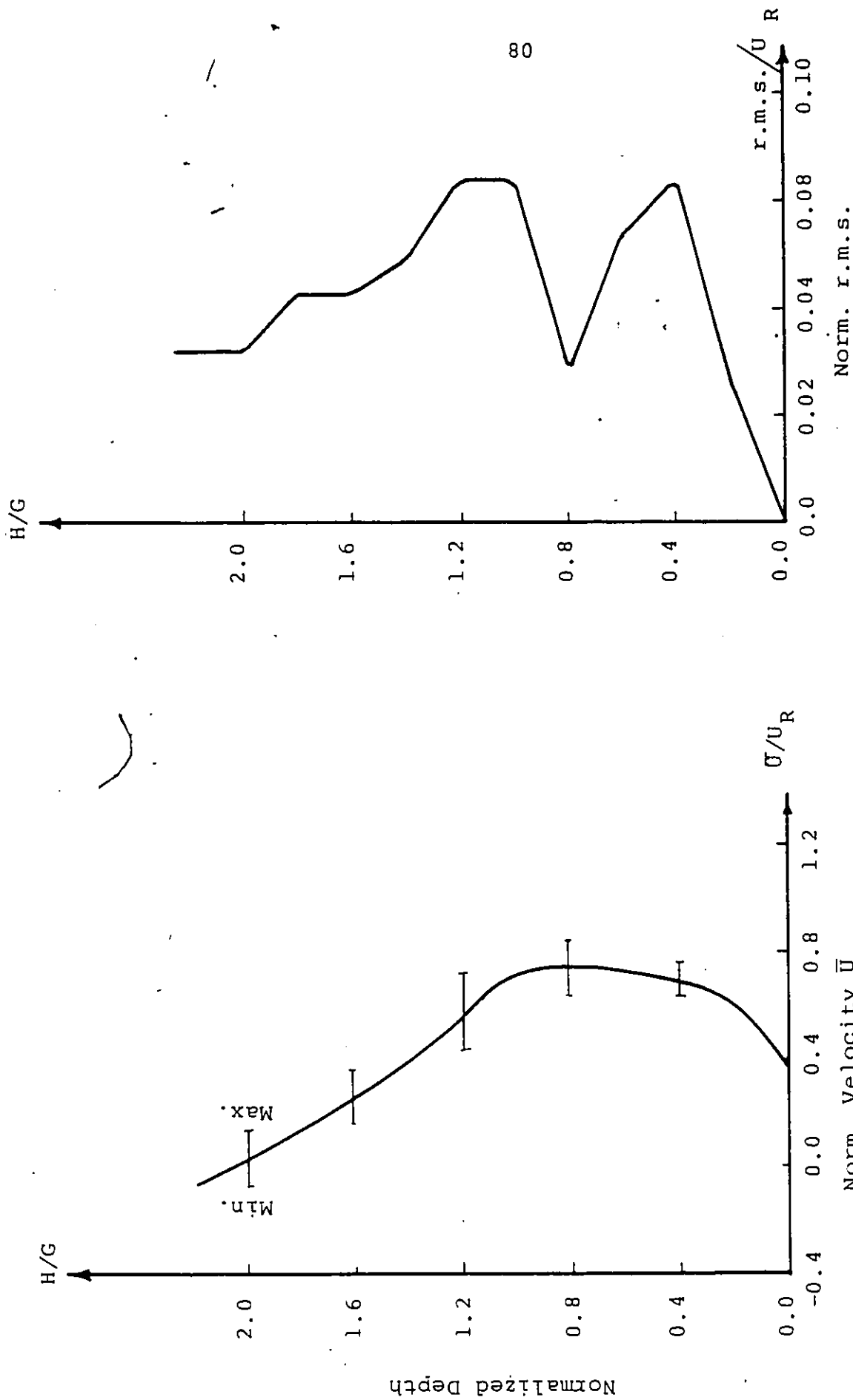


Fig. 4.20 Longitudinal velocity and r.m.s. profiles at $X = 25$ cm, $q = 111 \text{ cm}^3/\text{sec}/\text{cm}$, $L = 40$ cm, $G = 5$ cm).

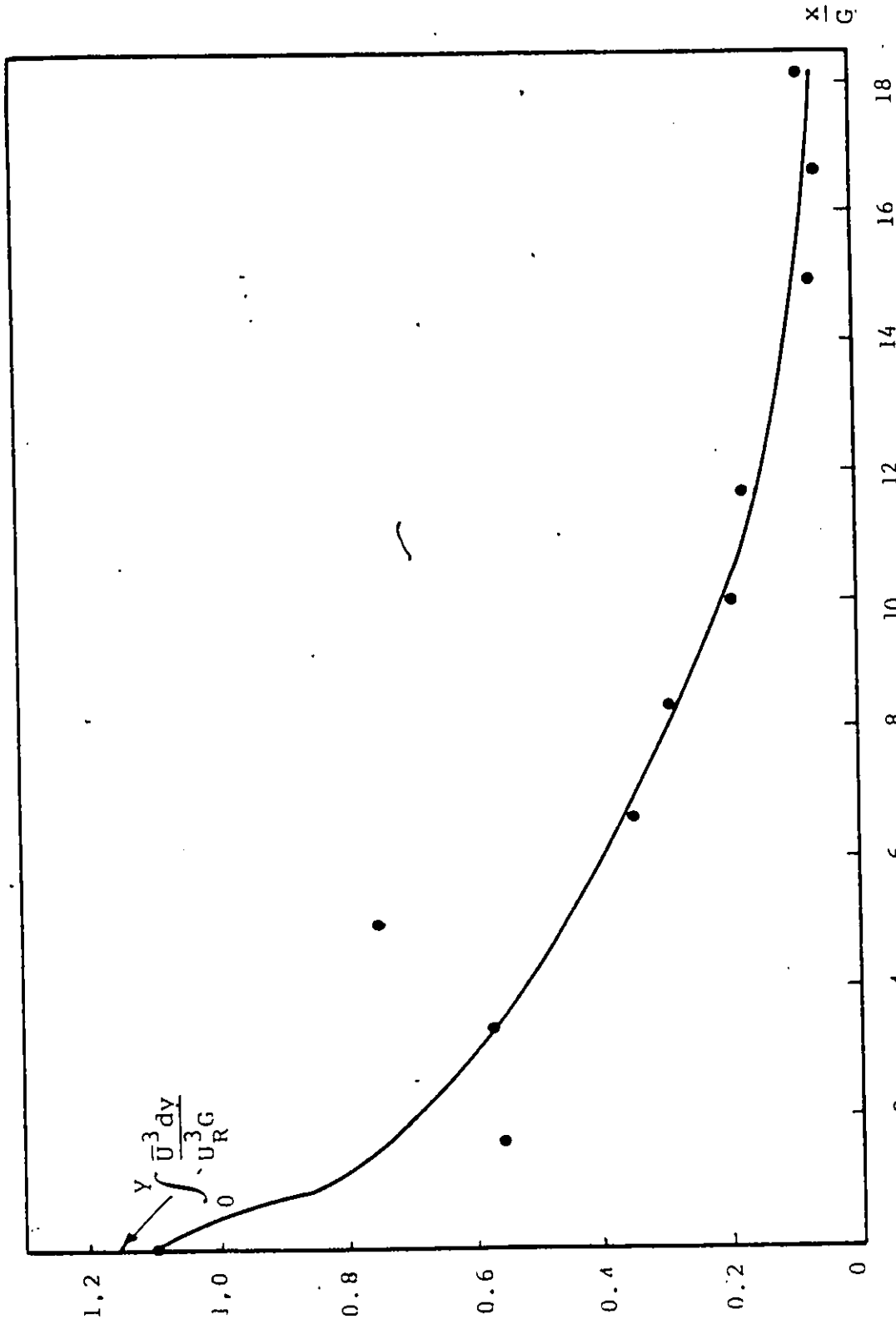


Fig. 4.21. Variation of Dimensionless Mean Kinetic Energy with Distance Along the Tank for ($L = 73$ cm, $G = 3$ cm, $g = 111$ cm³/sec/cm).

C₁₀

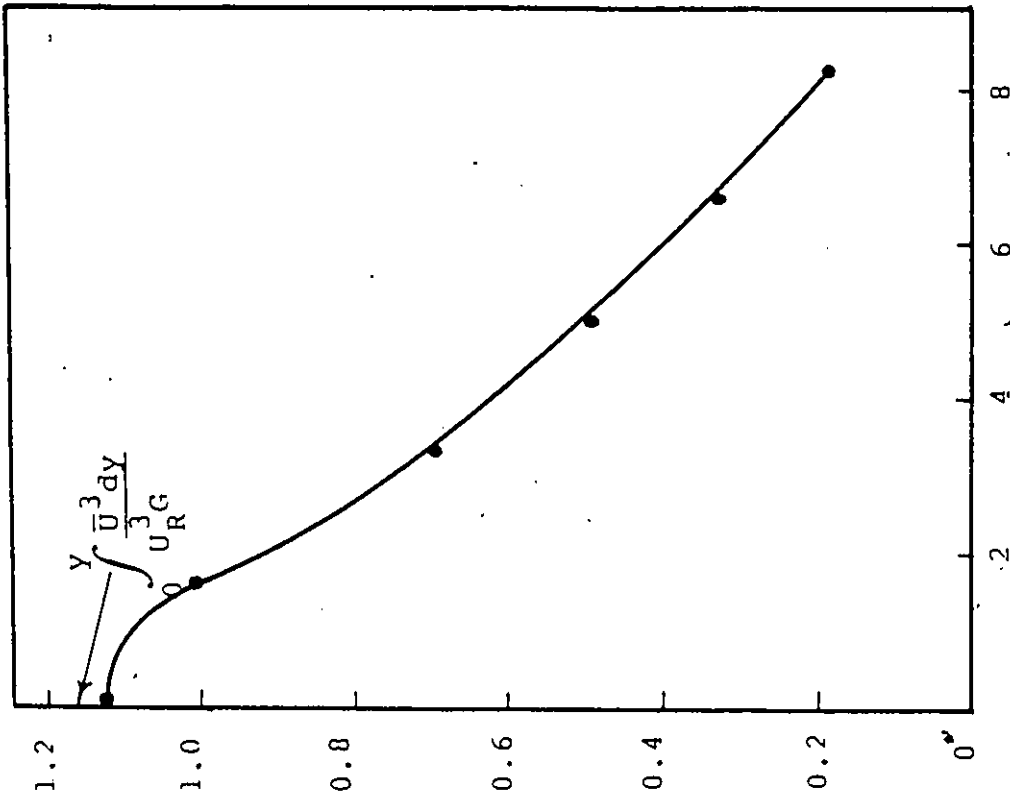


Fig. 4.23 Variation of Dimensionless mean Kinetic Energy with Distance along the Tank for (L=30 cm, G=3 cm, q=53.9 cm³/sec/cm).

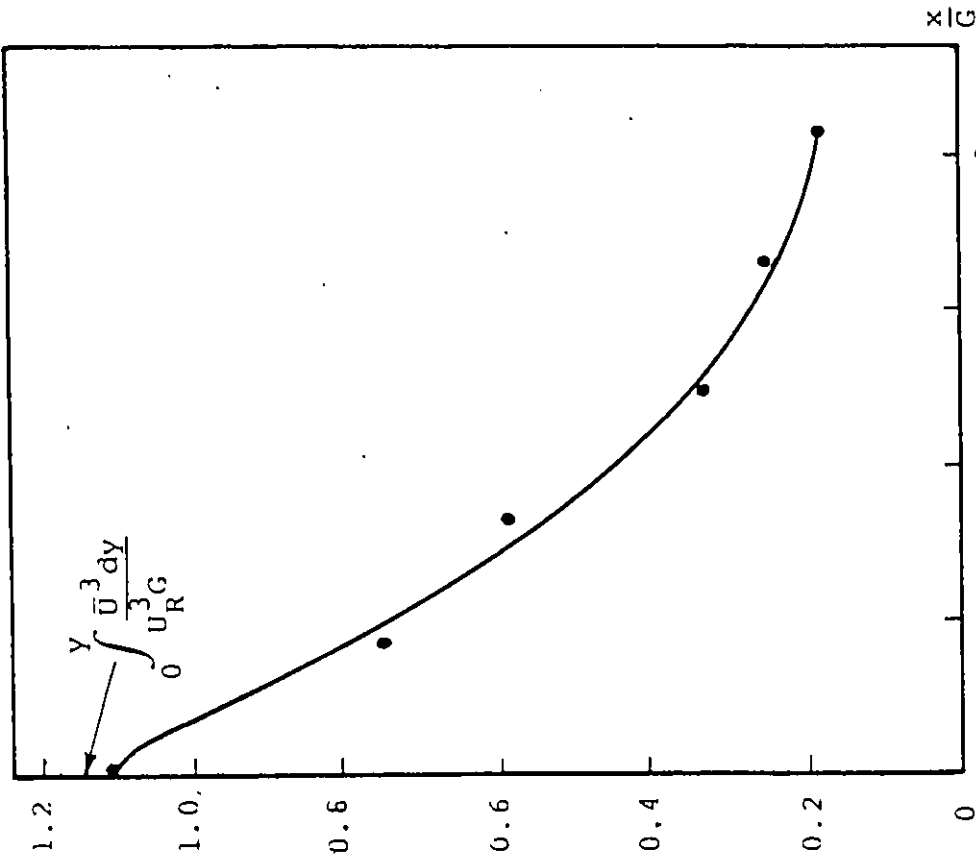


Fig. 4.22 Variation of Dimensionless mean Kinetic Energy with Distance along the Tank for (L=30 cm, G=3 cm, q=87.41 cm³/sec/cm).

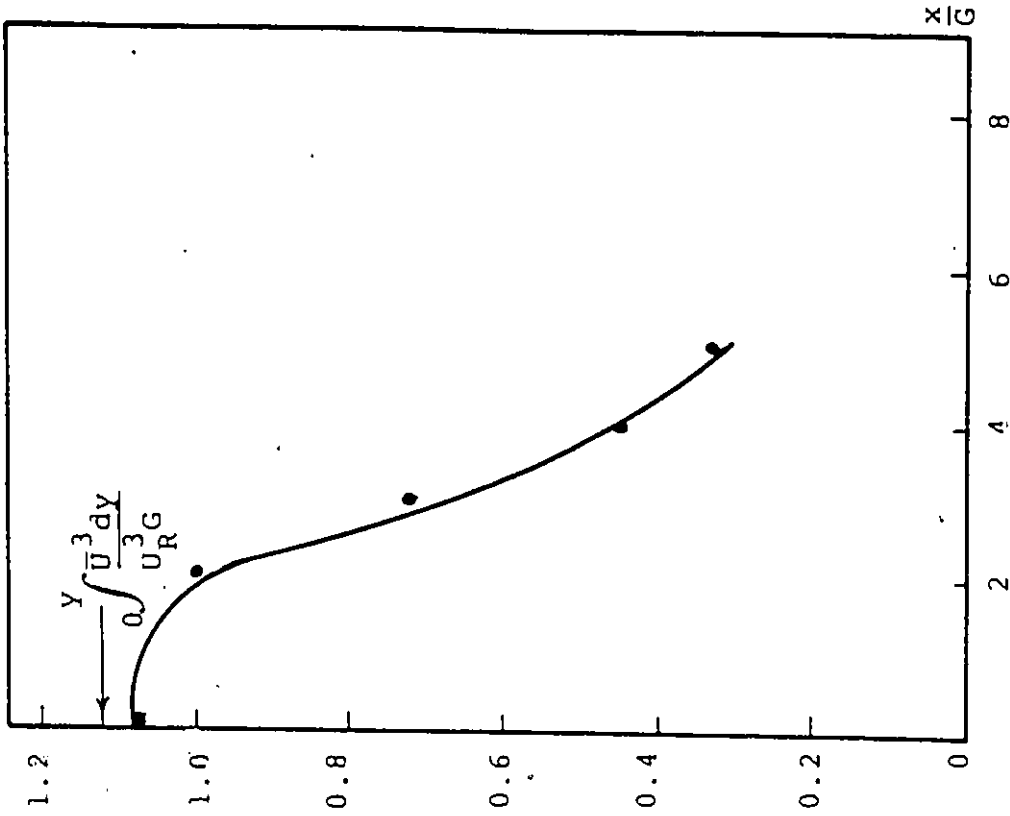


Fig. 4.25 Variation of Dimensionless mean Kinetic Energy with Distance along the Tank for ($L = 30$ cm, $G = 5$ cm, $q = 53.9$ cm³/sec/cm)

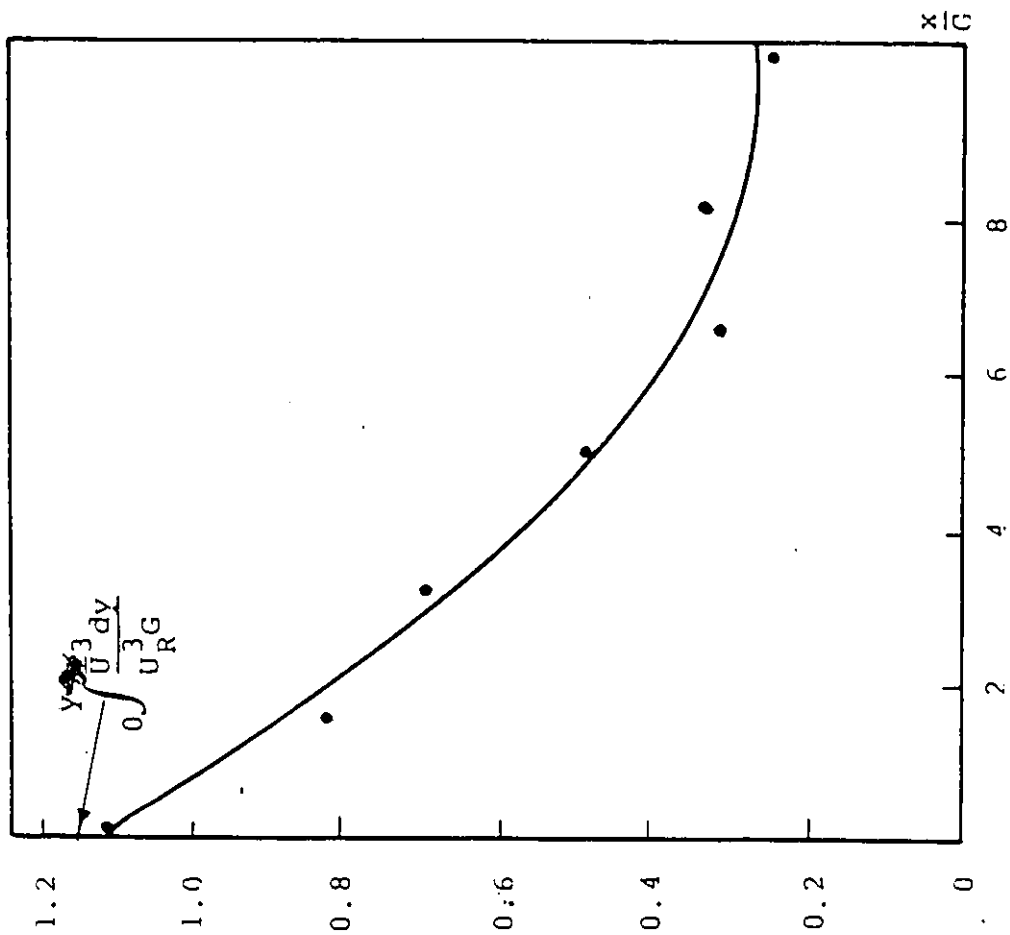


Fig. 4.24 Variation of Dimensionless mean Kinetic Energy with Distance along the Tank for ($L = 40$ cm, $G = 3$ cm, $q = 61.74$ cm³/sec/cm).

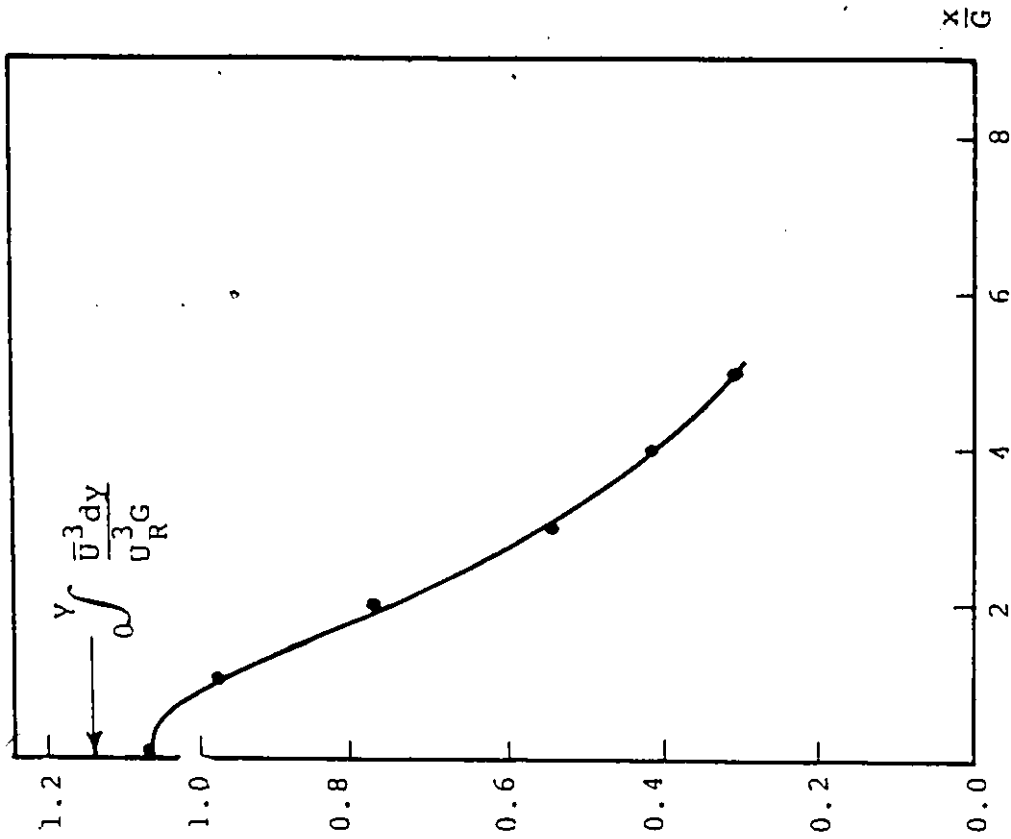


Fig. 4.27 Variation of Dimensionless mean Kinetic Energy with Distance along the Tank for ($L = 30$ cm, $G = 5$ cm, $q = 101.32$ cm³/sec/cm).

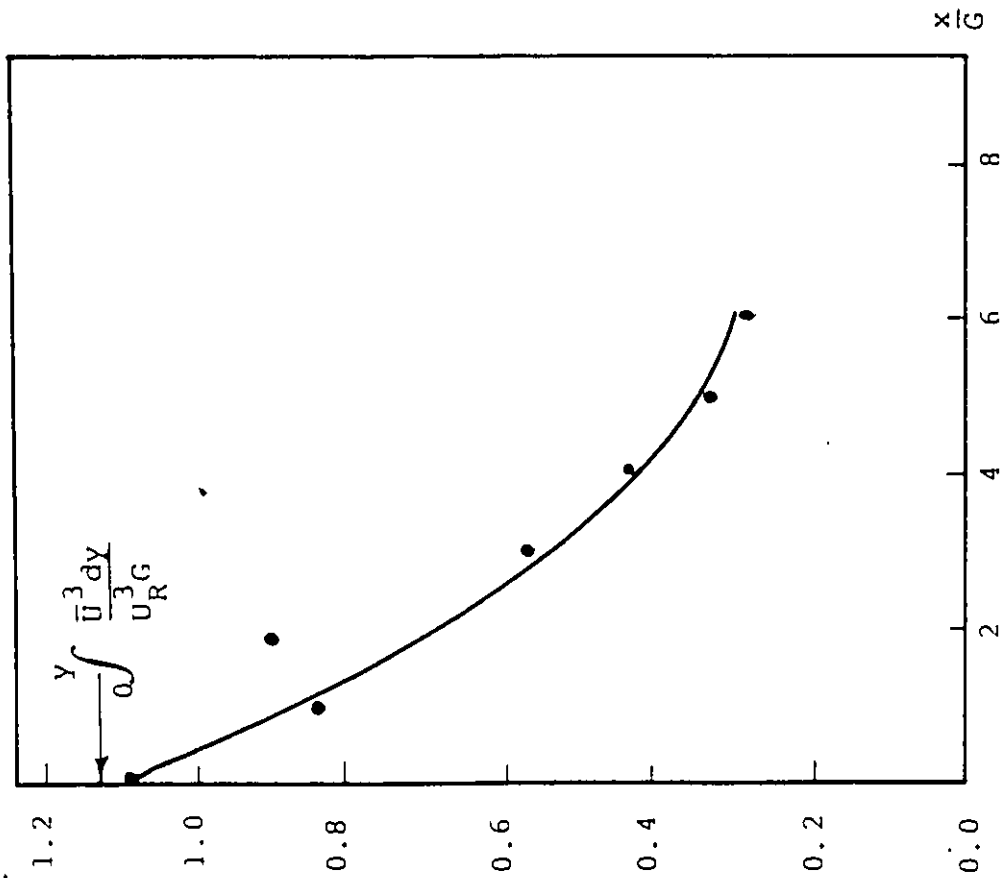


Fig. 4.26 Variation of Dimensionless mean Kinetic Energy with Distance along the Tank for ($L = 40$ cm, $G = 5$ cm, $q = 53.9$ cm³/sec/cm).

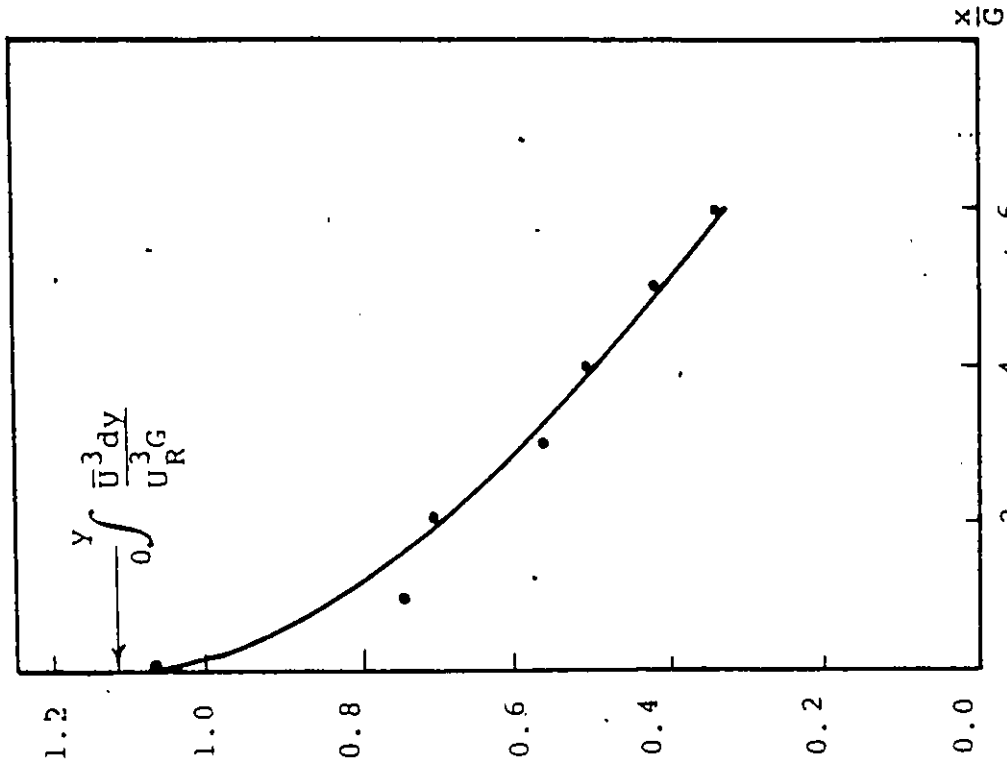


Fig. 4.29 Variation of Dimensionless mean Kinetic Energy with Distance along the Tank for ($L = 40$ cm, $G = 5$ cm, $q = 111$ cm³/sec/cm).

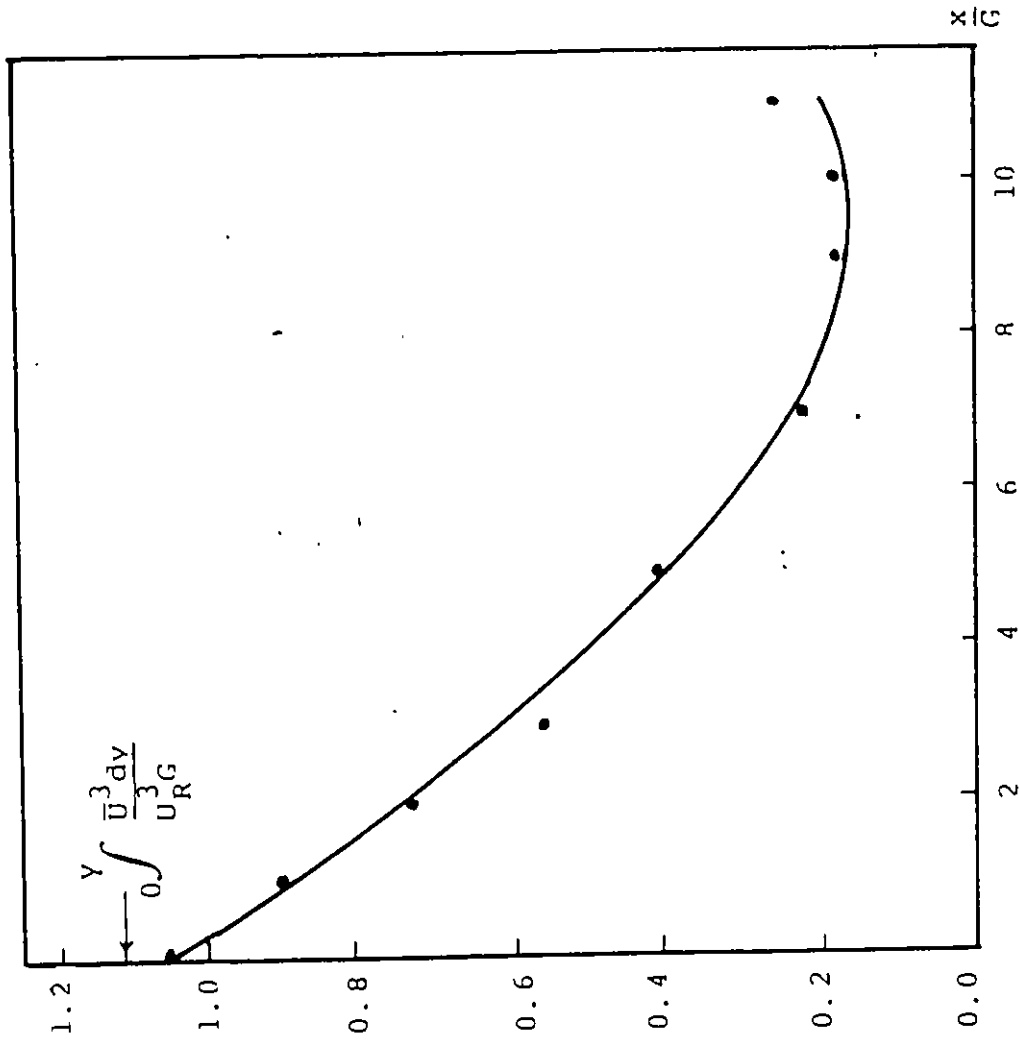


Fig. 4.28 Variation of Dimensionless mean Kinetic Energy with Distance along the Tank for ($L = 73$ cm, $G = 5$ cm, $q = 147$ cm³/sec/cm).

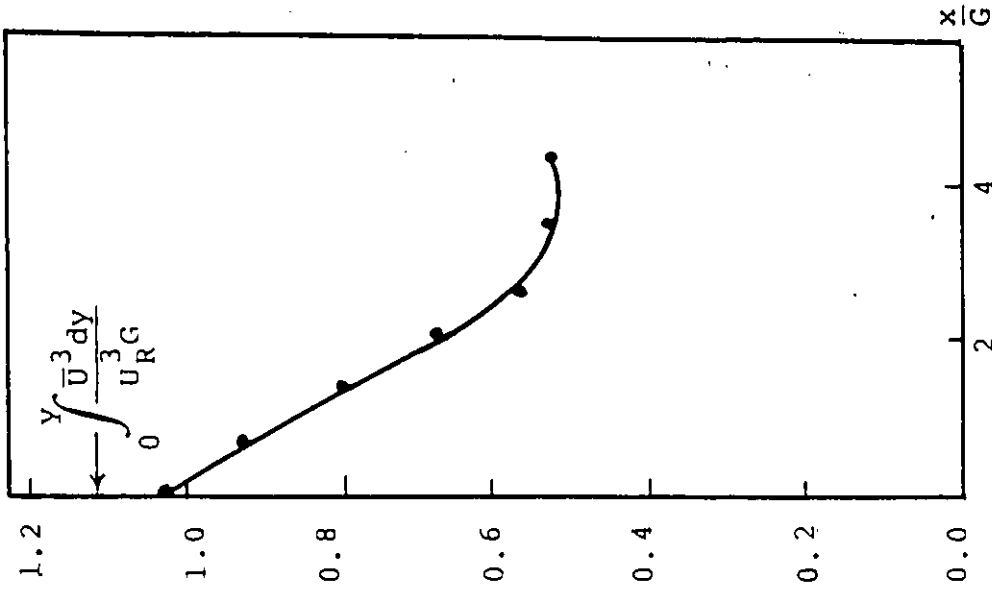


Fig. 4.32

($L = 40$ cm, $G = 7$ cm,
 $q = 53.9$ cm³/sec/cm)

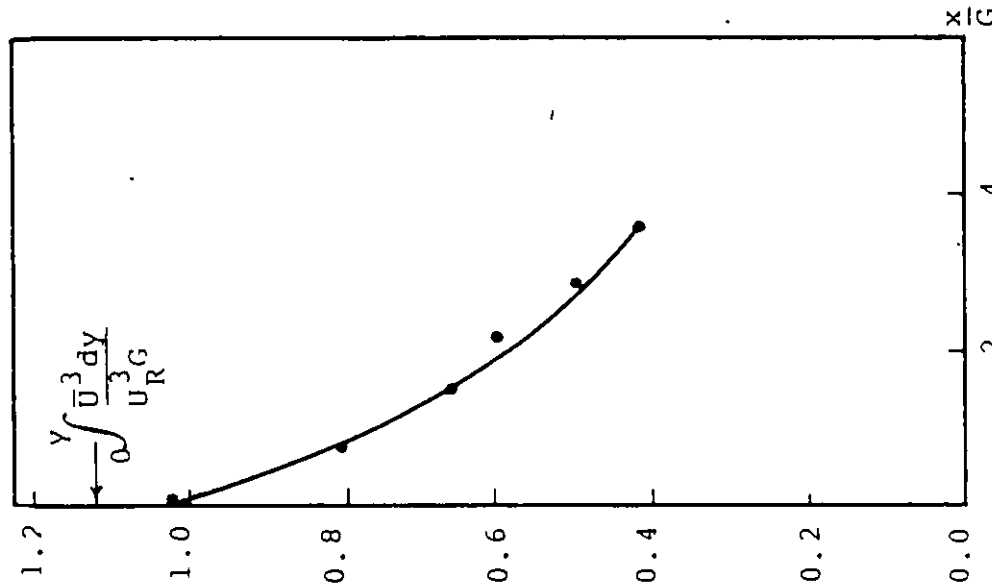


Fig. 4.31

($L = 30$ cm, $G = 7$ cm,
 $q = 106$ cm³/sec/cm)

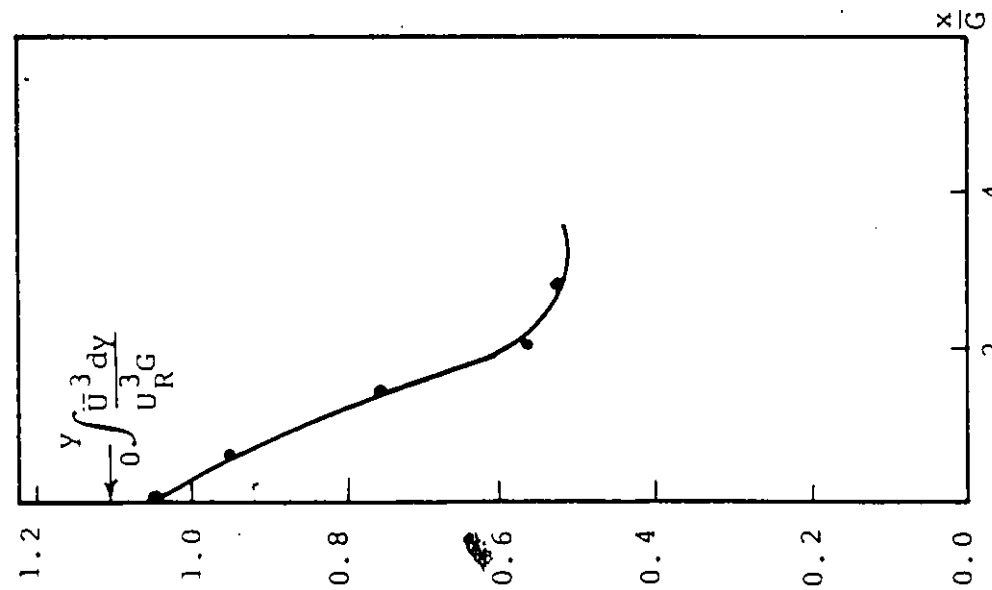


Fig. 4.30

($L = 30$ cm, $G = 7$ cm,
 $q = 53.9$ cm³/sec/cm)

Variation of Dimensionless Mean Kinetic Energy with Distance Along the Tank.

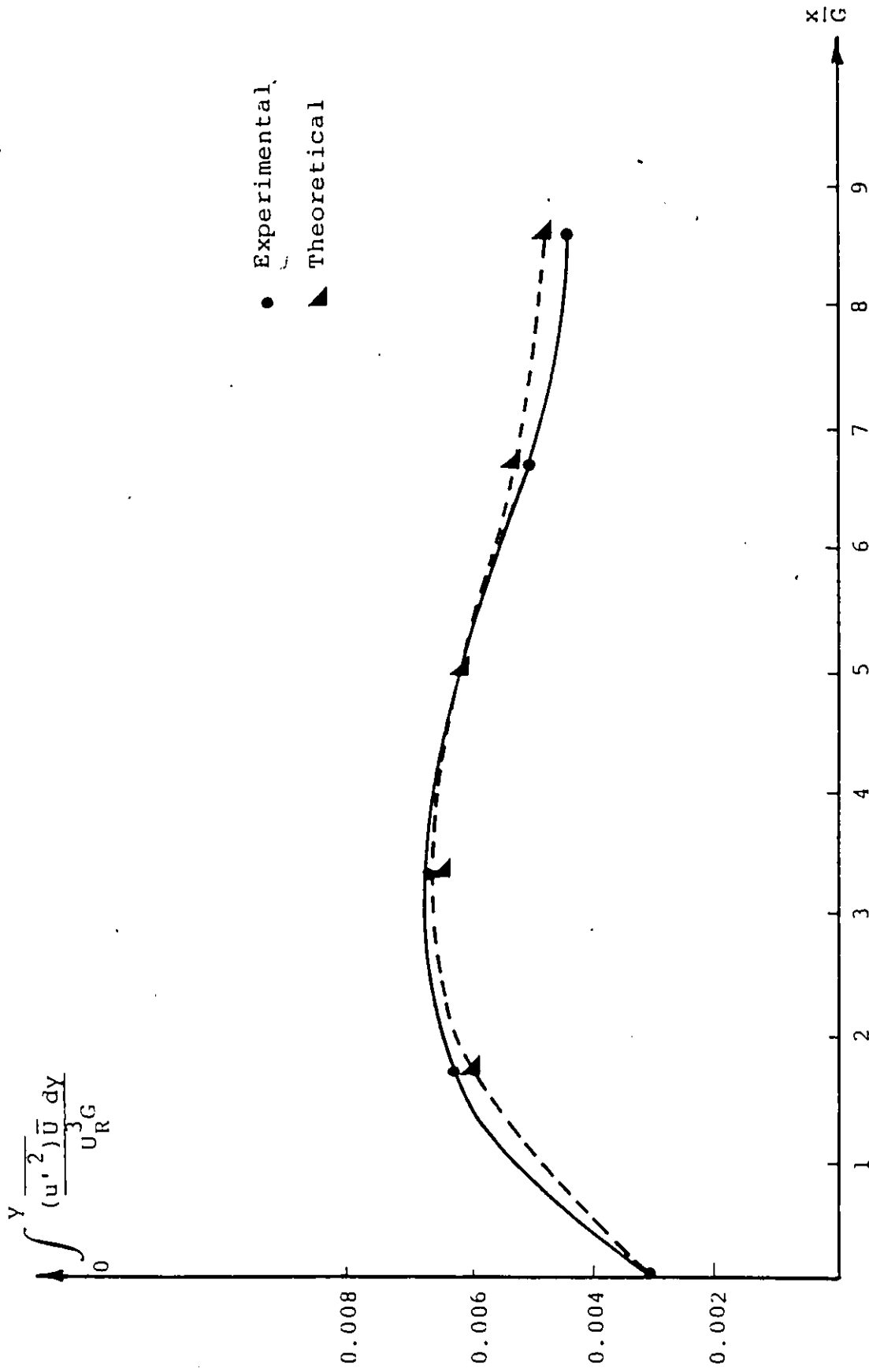


Fig. 4.33 Variation of Dimensionless Turbulent Kinetic Energy with Distance
($L = 30$ cm, $G = 3$ cm, $q = 87.41$ cm³/sec/cm).

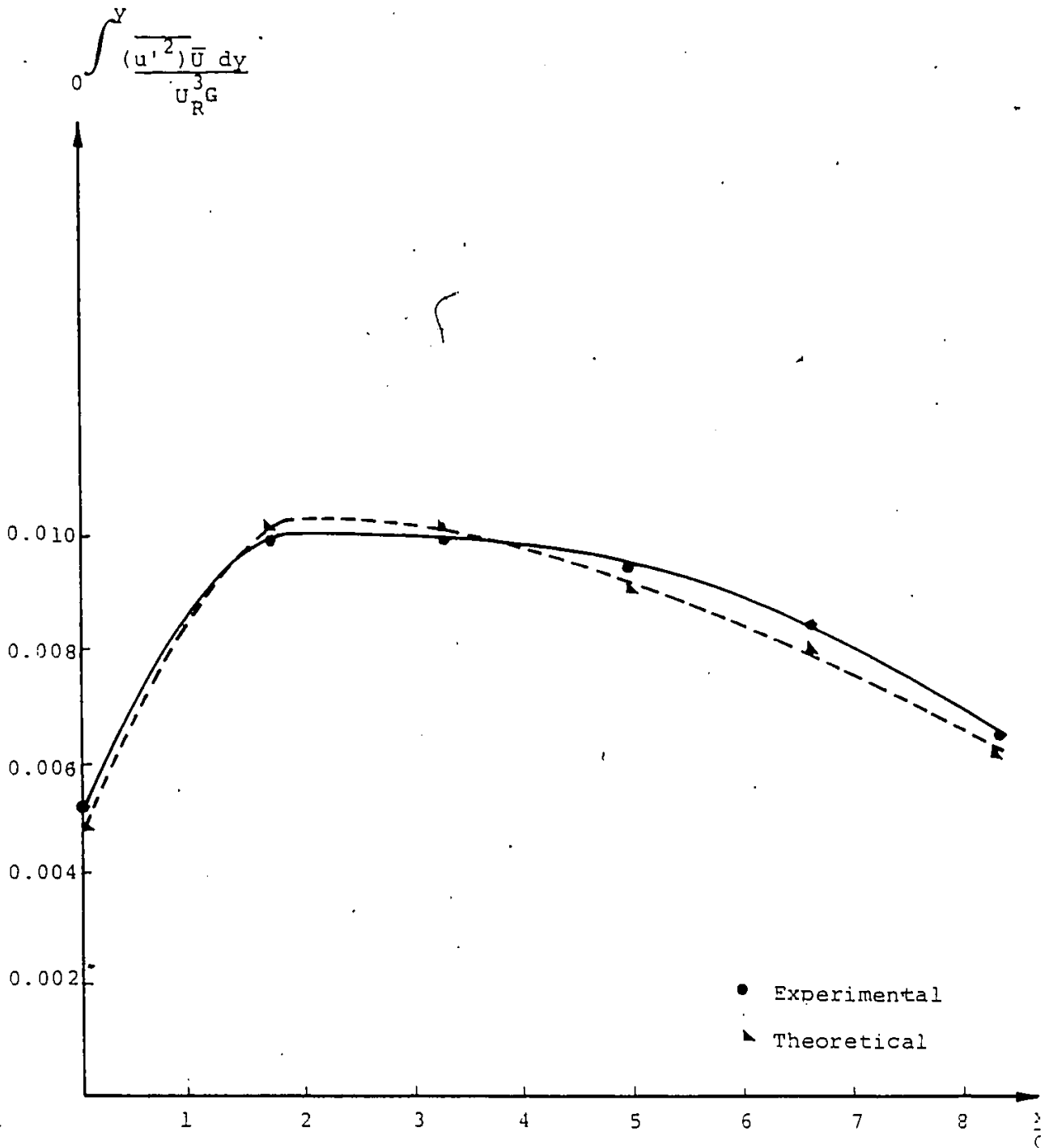


Fig. 4.34 Variation of Dimensionless Turbulent Kinetic Energy with Distance ($L = 30$ cm, $G = 3$ cm, $\alpha = 53.9$ cm³/sec/cm).

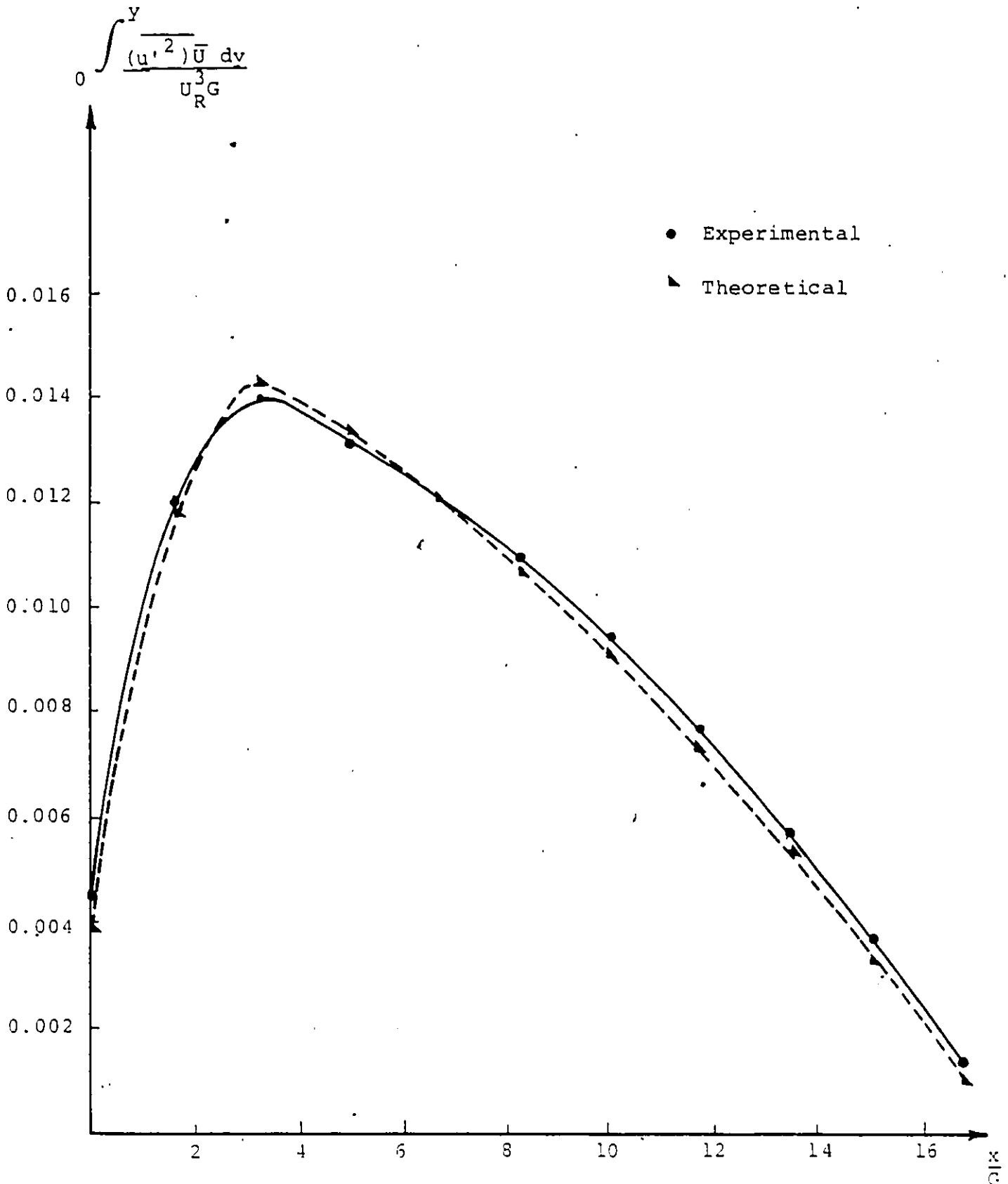


Fig. 4.35 Variation of Dimensionless Turbulent Kinetic Energy with Distance ($L = 73$ cm, $G = 3$ cm, $\alpha = 111$ cm³/sec/cm)

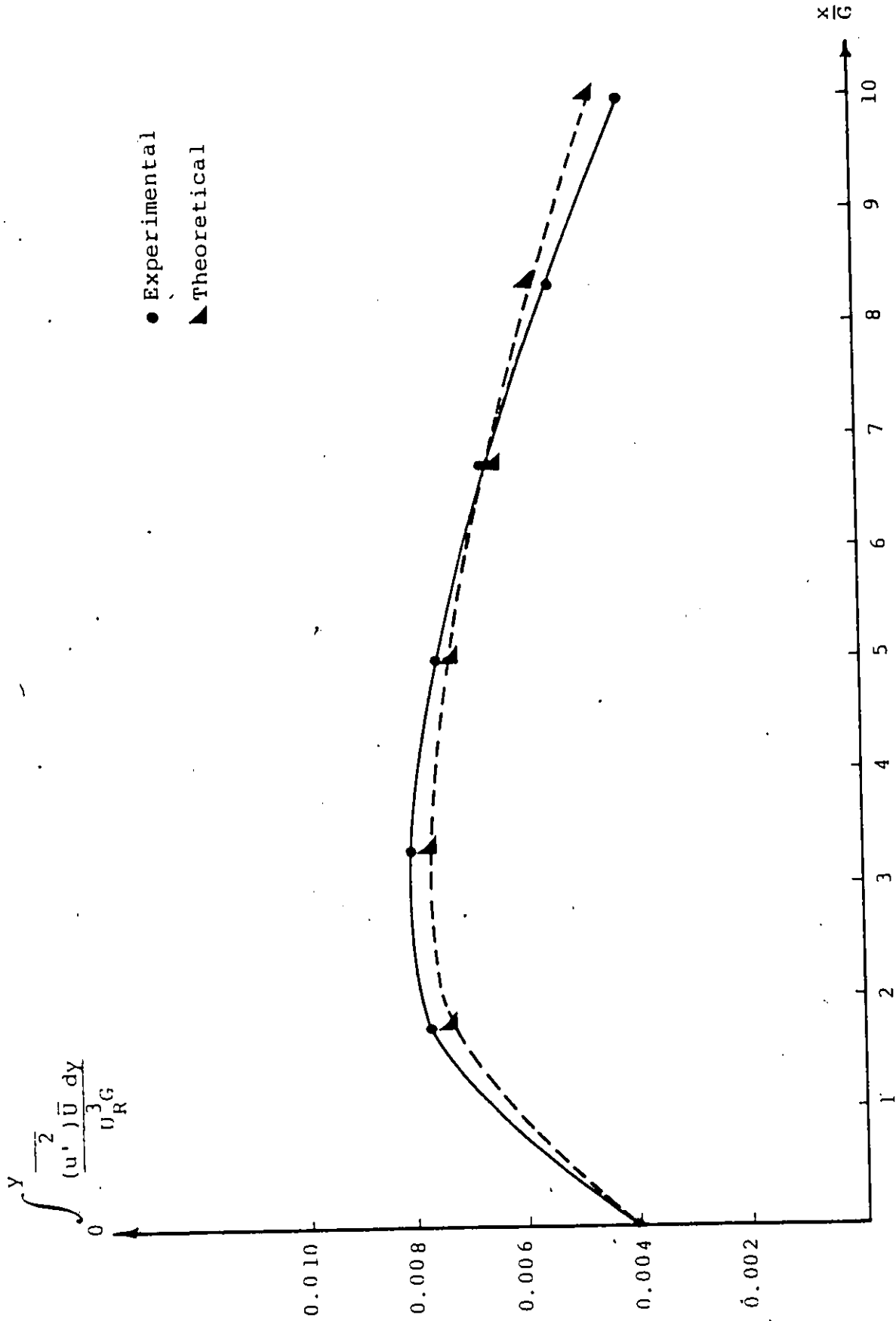


Fig. 4.36 Variation of Dimensionless Turbulent Kinetic Energy with Distance (L = 40 cm, G = 3 cm, q = 61.74 cm³/sec/cm).

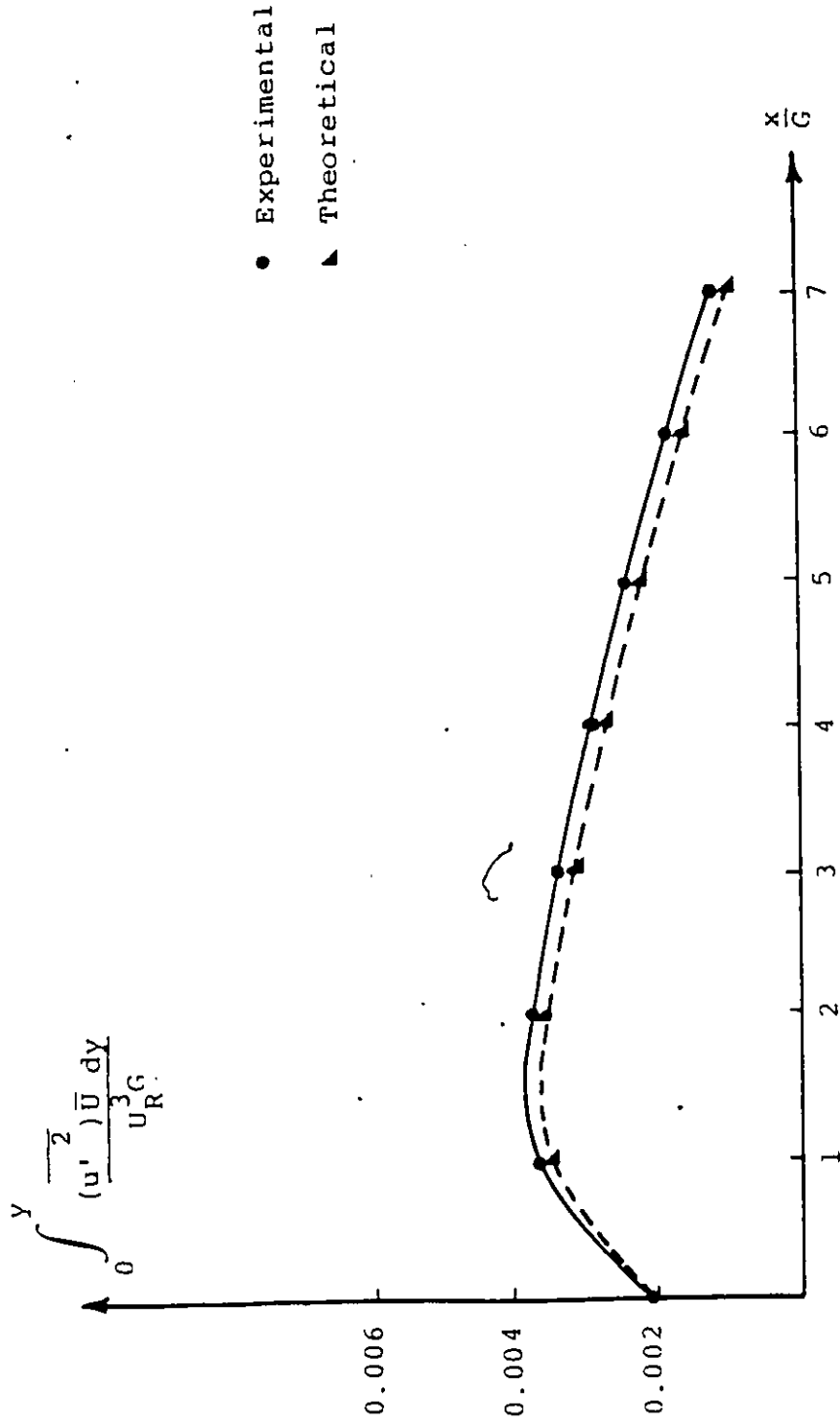


Fig. 4.37 Variation of Dimensionless Turbulent Kinetic Energy with Distance ($L = 40$ cm, $G = 5$ cm, $q = 111$ cm³/sec/cm).

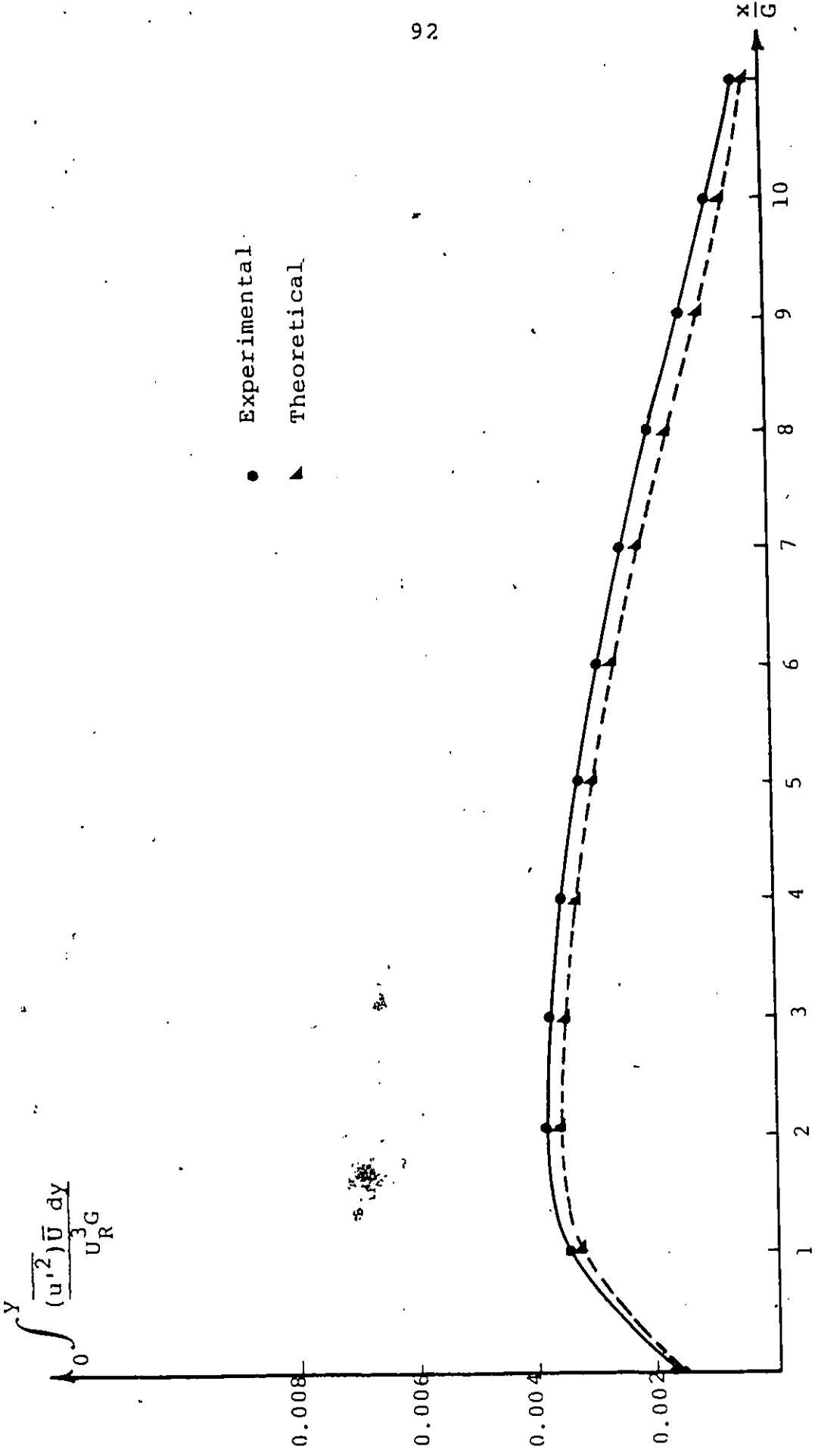


Fig. 4.38 Variation of Dimensionless Turbulent Kinetic Energy with Distance (L = 73 cm, G = 5 cm, q = 147 cm³/sec/cm).

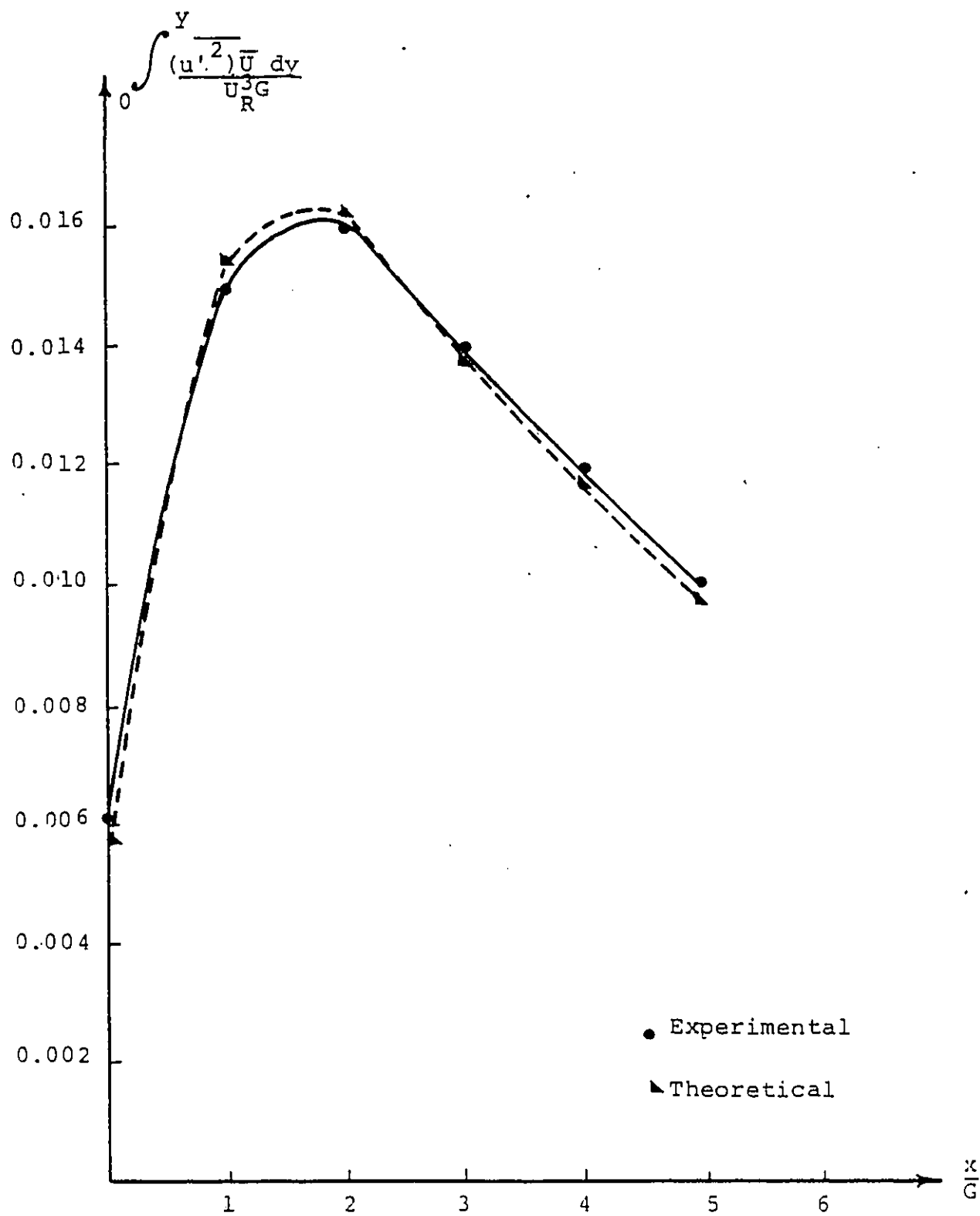


Fig. 4.39 Variation of Dimensionless Turbulent Kinetic Energy with Distance ($L = 30$ cm, $G = 5$ cm, $\alpha = 101.32$ cm³/sec/cm).

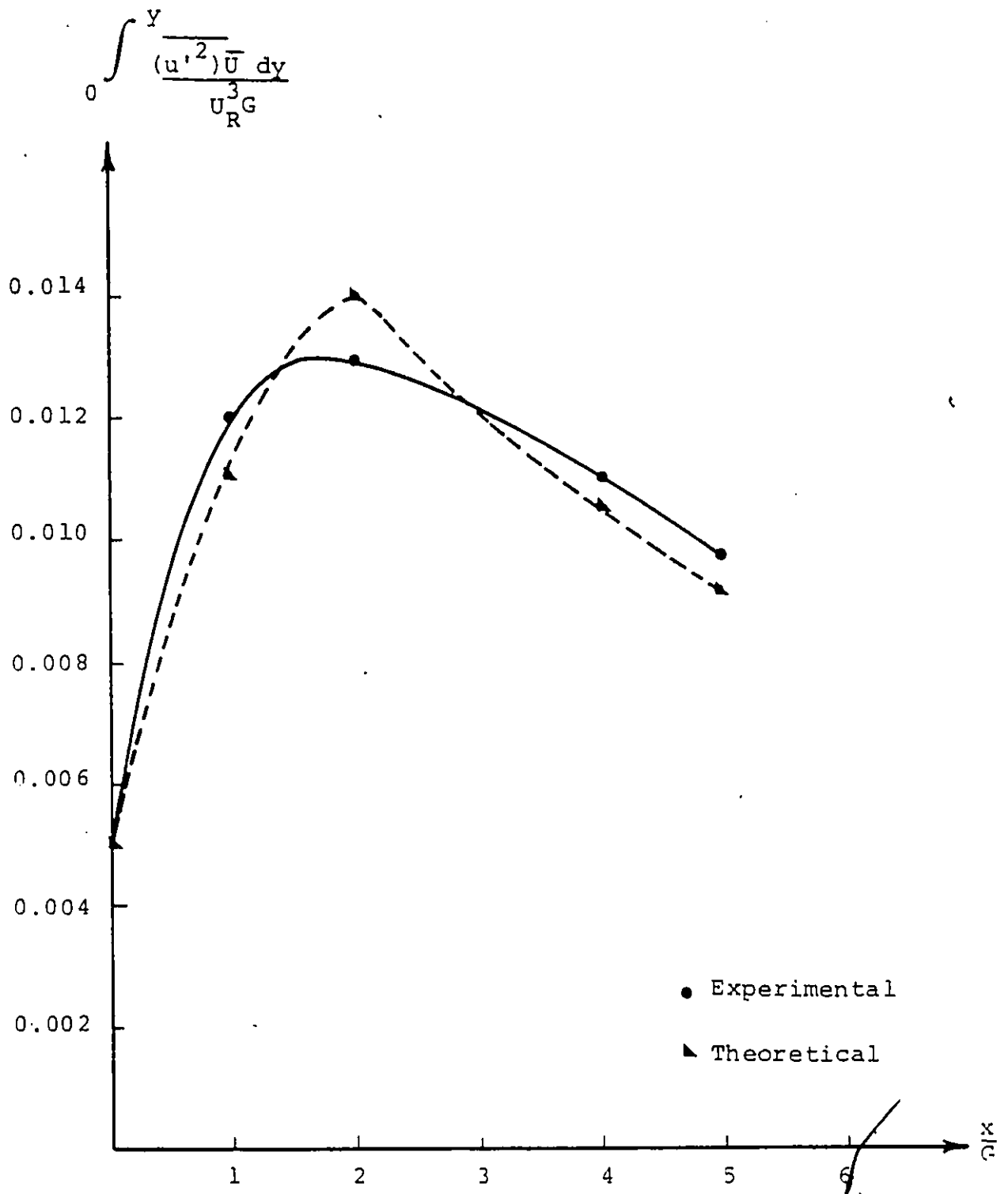


Fig. 4.40 Variation of Dimensionless Turbulent Kinetic Energy with Distance ($L = 30$ cm, $G = 5$ cm, $q = 53.9$ cm³/sec/cm).

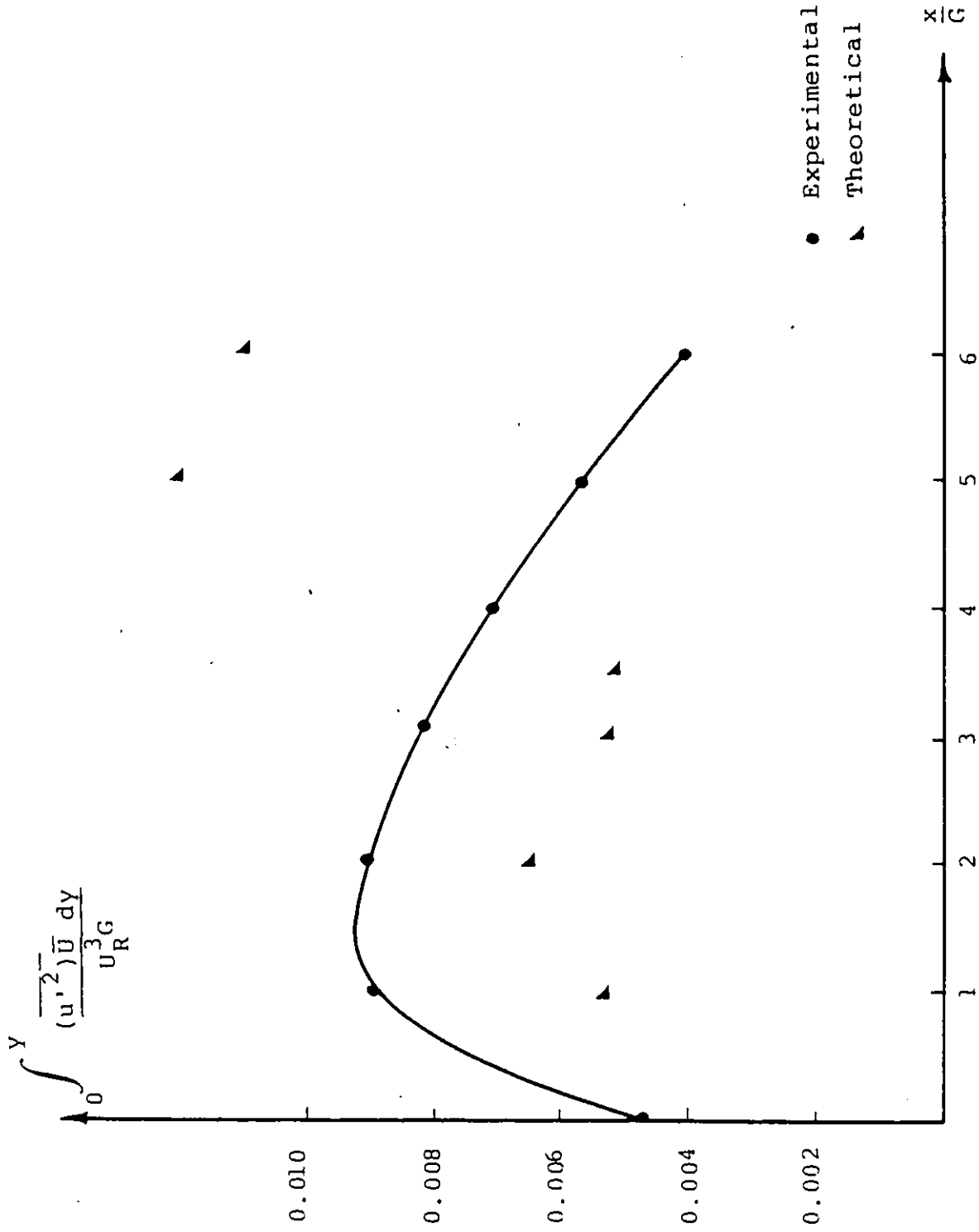


Fig. 4.41 Variation of Dimensionless Turbulent Kinetic Energy with Distance ($L = 40$ cm, $G = 5$ cm, $q = 53.9$ cm³/sec/cm).

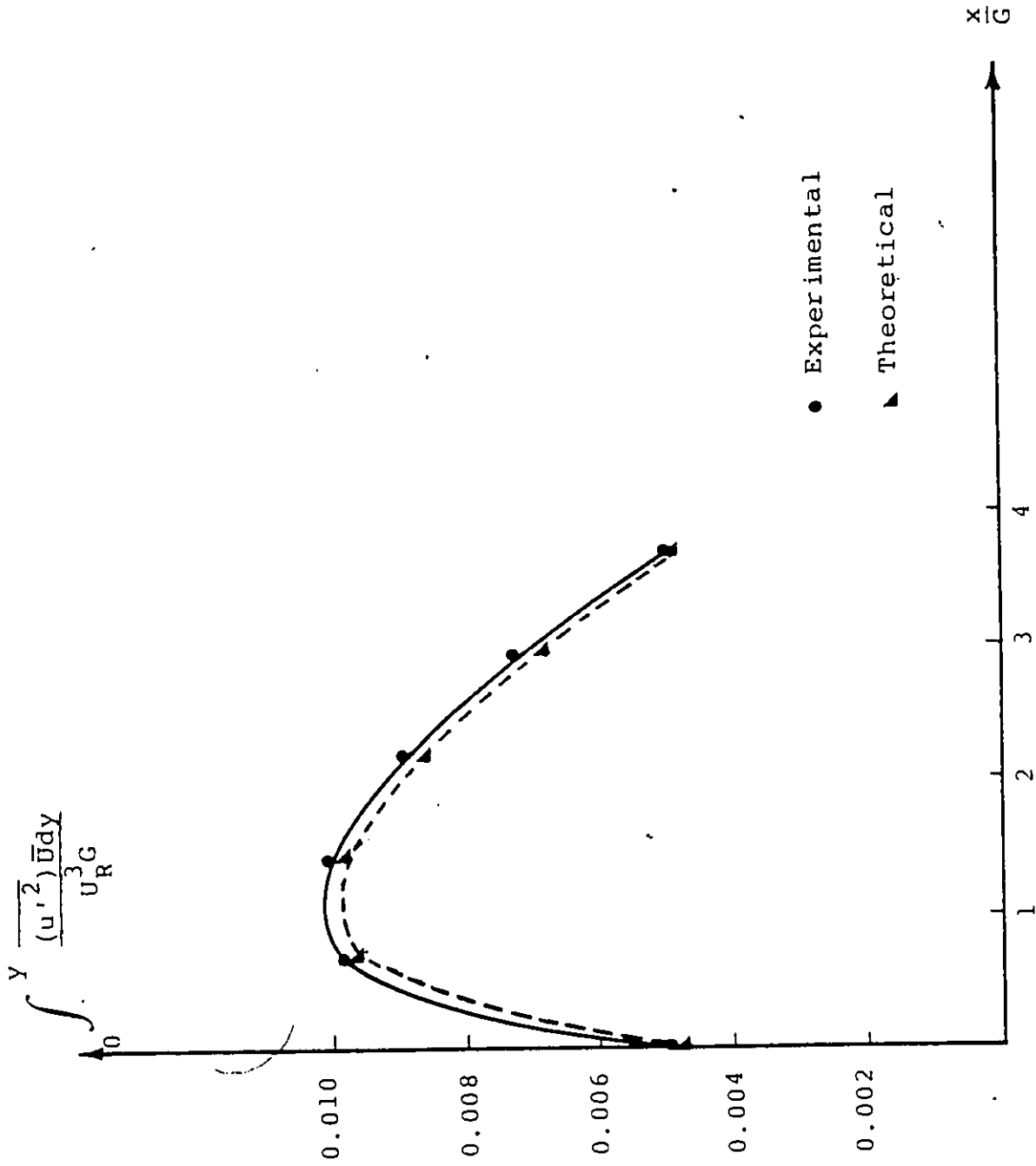


Fig. 4.42 Variation of Dimensionless Turbulent Kinetic Energy with Distance ($L = 30$ cm, $G = 7$ cm, $q = 106$ cm³/sec/cm).

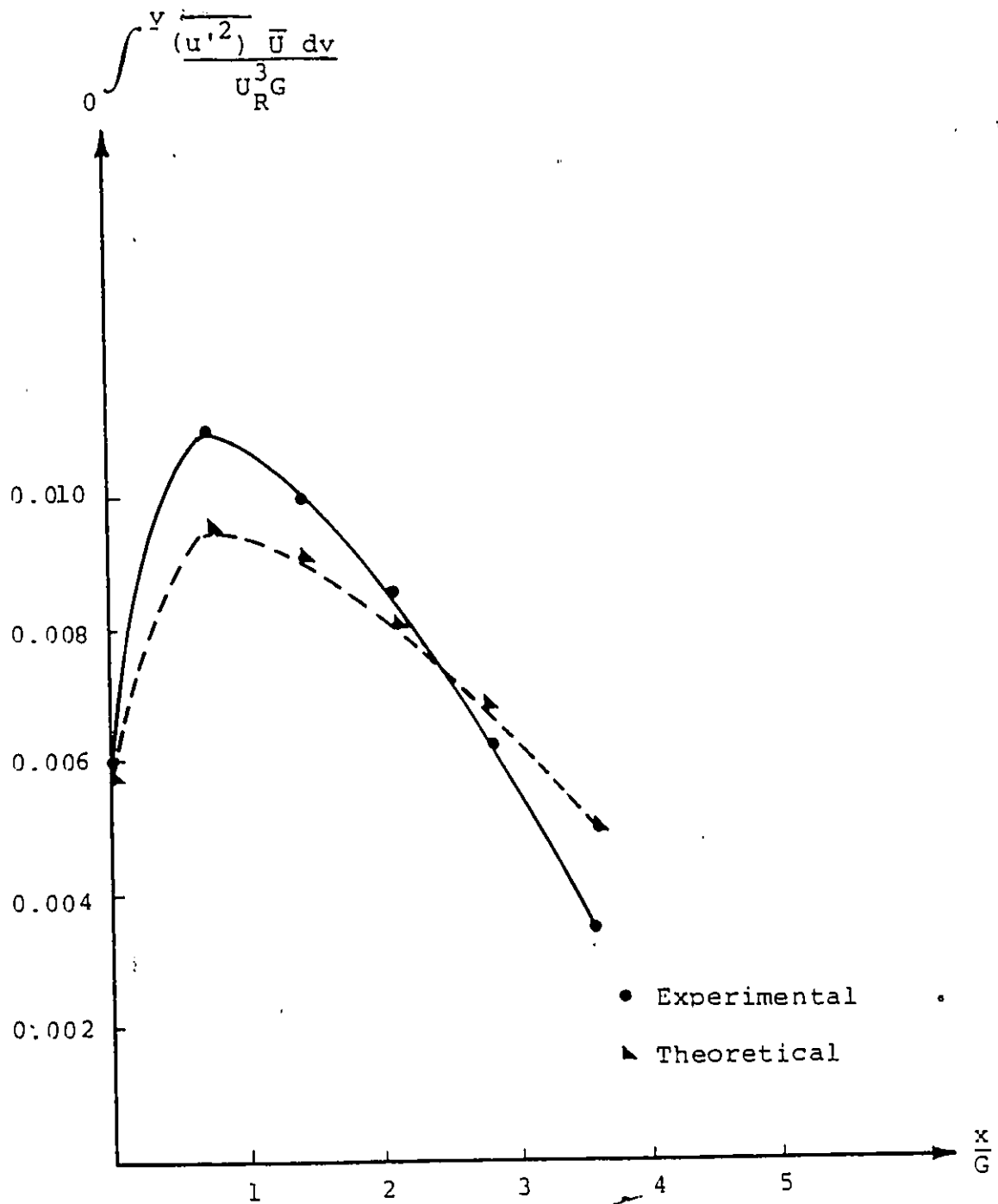


Fig. 4.43 Variation of Dimensionless Turbulent Energy with Distance ($L = 30$ cm, $G = 7$ cm, $q = 53.9$ cm³/sec/cm).

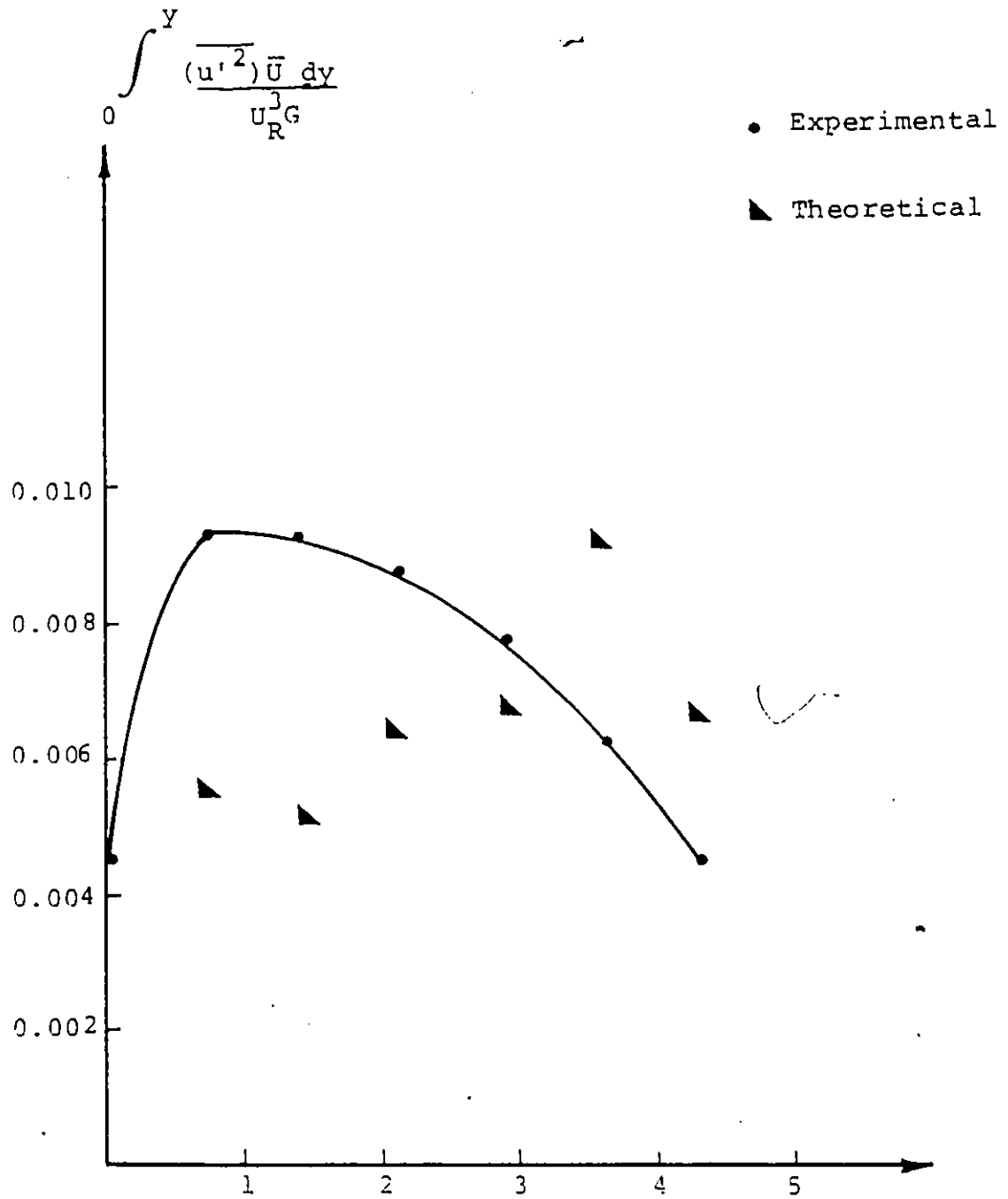


Fig. 4.44 Variation of Dimensionless Turbulent Kinetic Energy with Distance ($L = 40$ cm, $G = 7$ cm, $g = 53.9$ cm³/sec/cm).

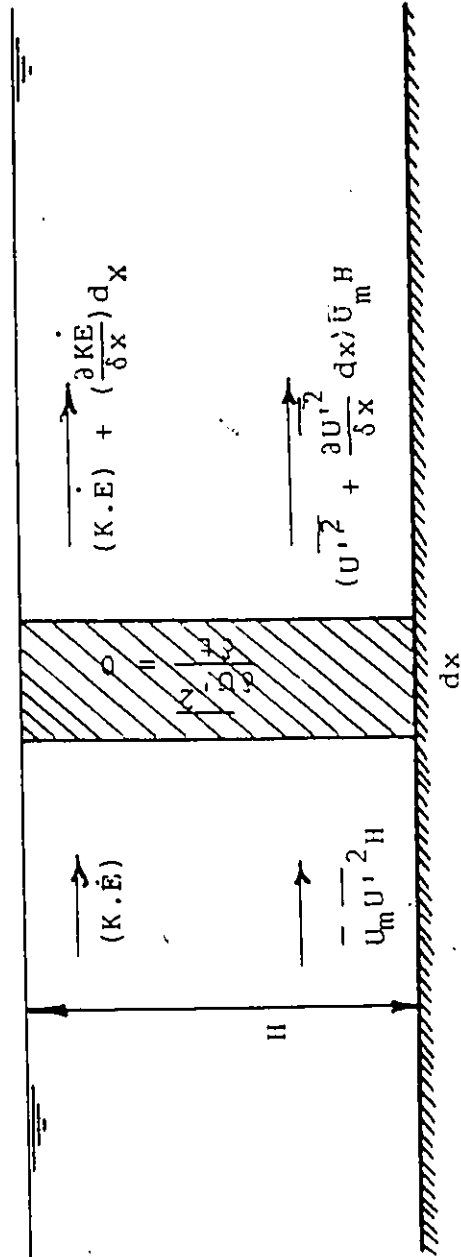


Fig. 4.45 Vertical Strip of Energy Balance in a Settling Basin

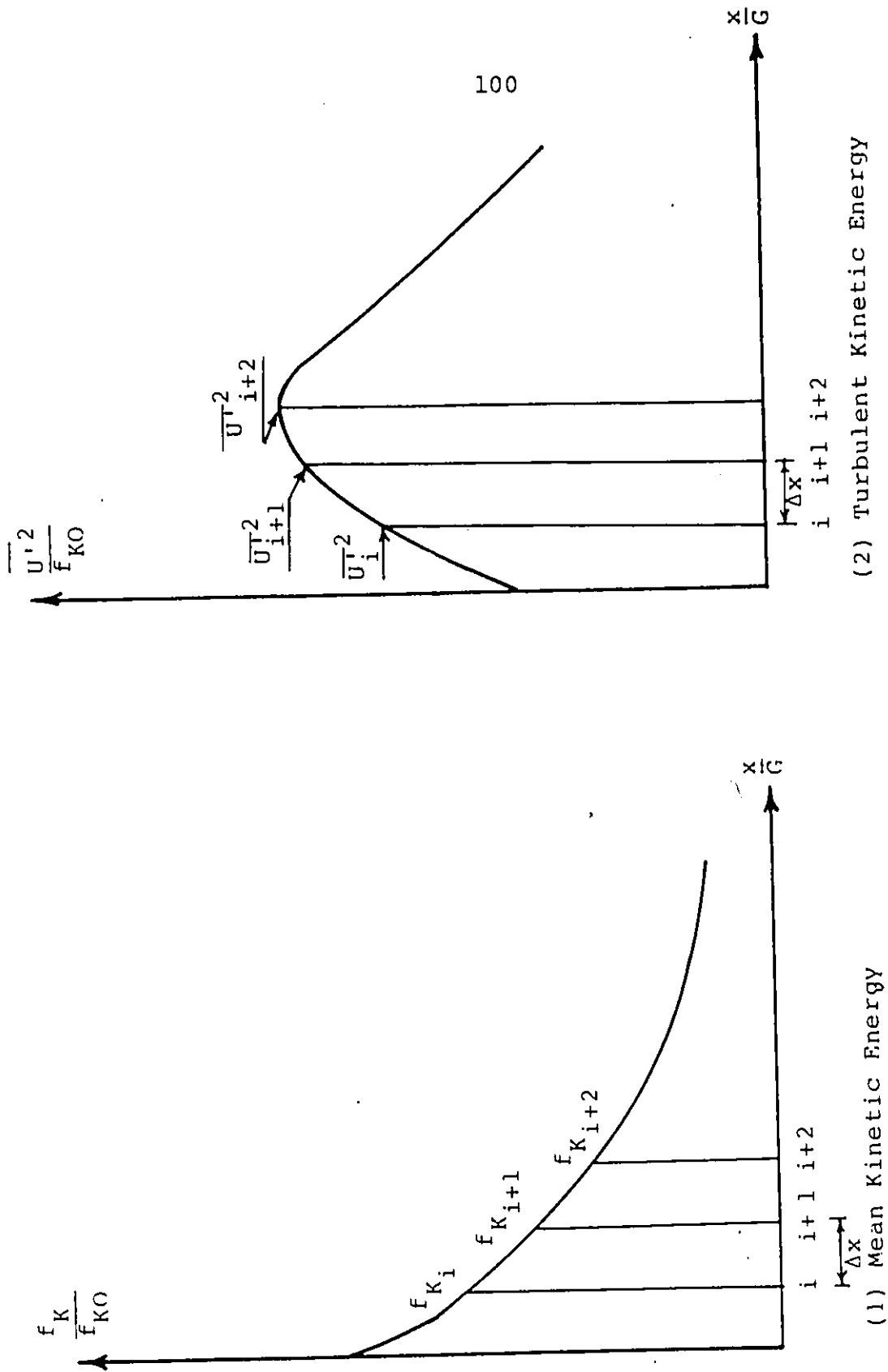


Fig. 4.46 Schematic Representation for Determining the Constants A, B.

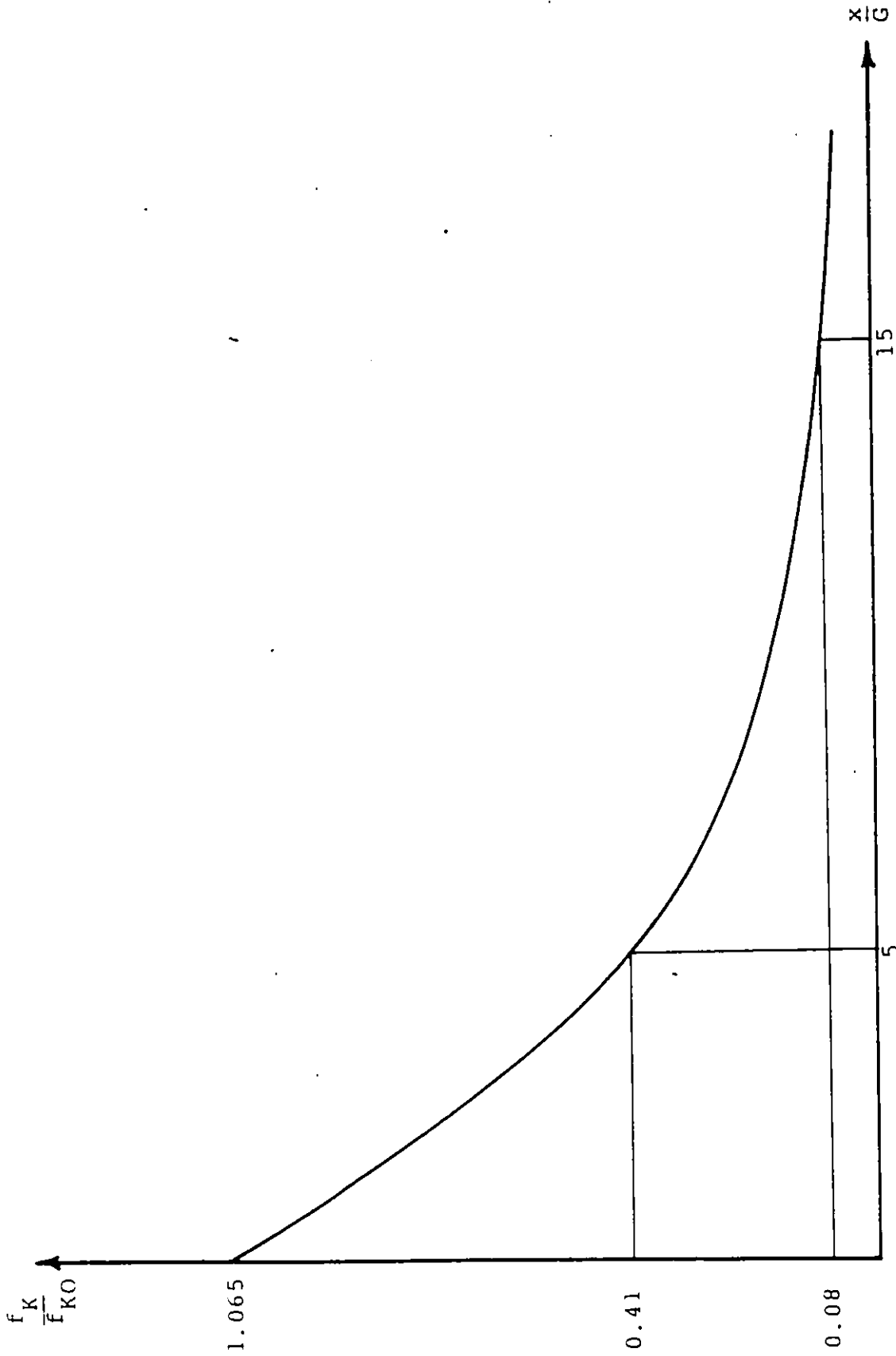


Fig. 4.47 The Best Fitting Curve of Mean Kinetic Energy.

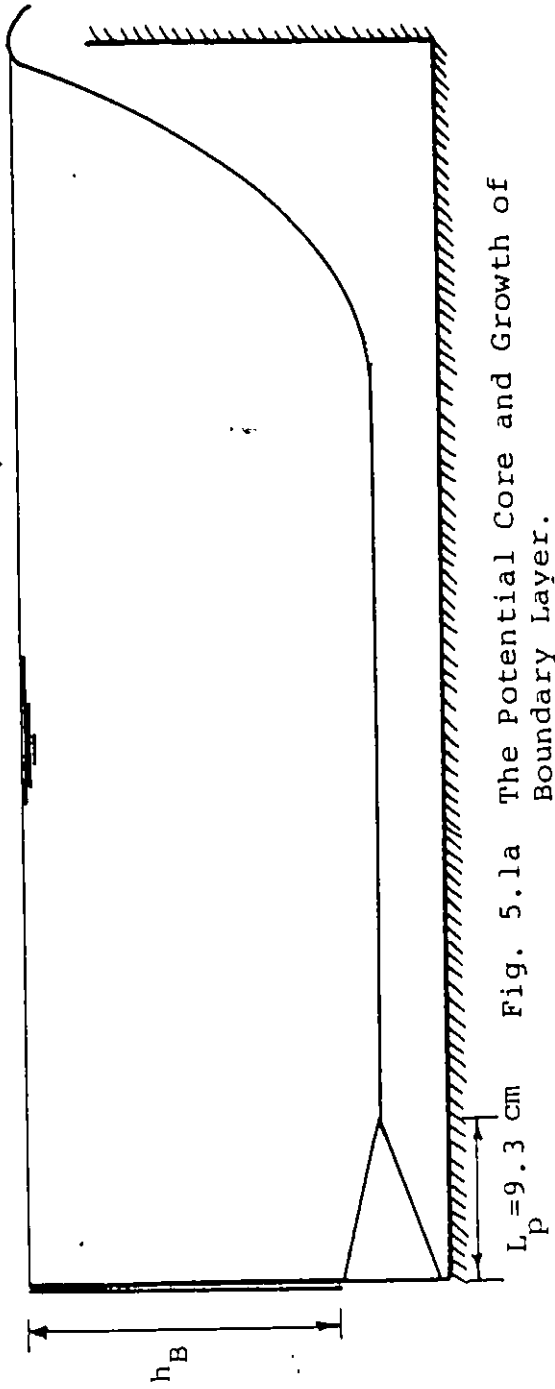


Fig. 5.1a The Potential Core and Growth of Boundary Layer.

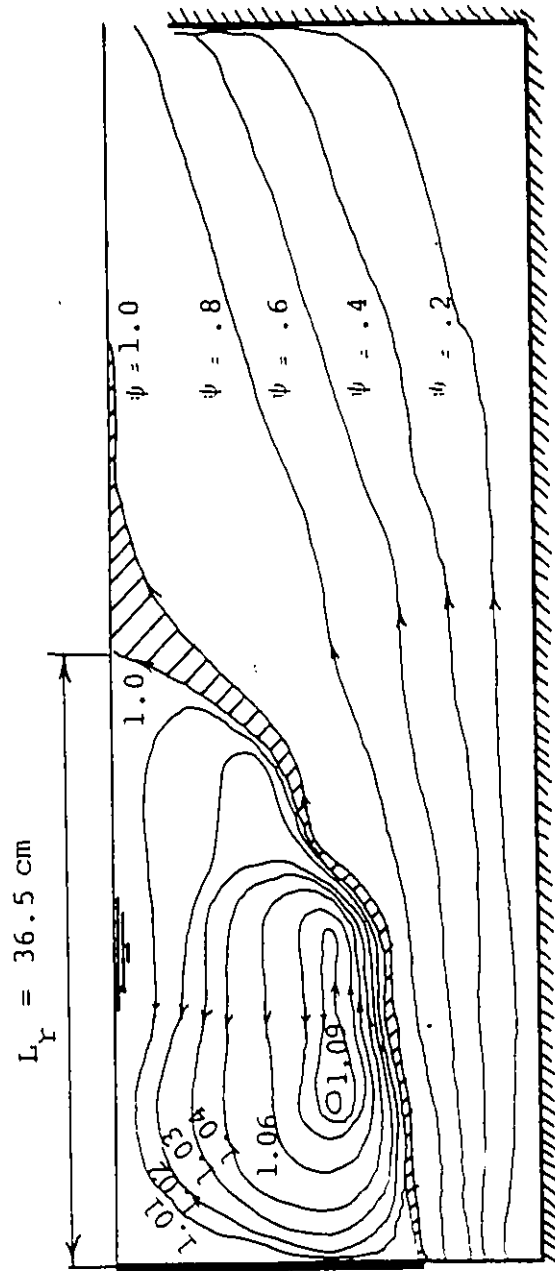


Fig. 5.1b Typical Flow Pattern (normalized)

Flow Characteristics ($L = 73 \text{ cm}$, $G = 3 \text{ cm}$, $q = 111 \text{ cm}^3/\text{sec}/\text{cm}$).

$$L_p = 17 \text{ cm}$$

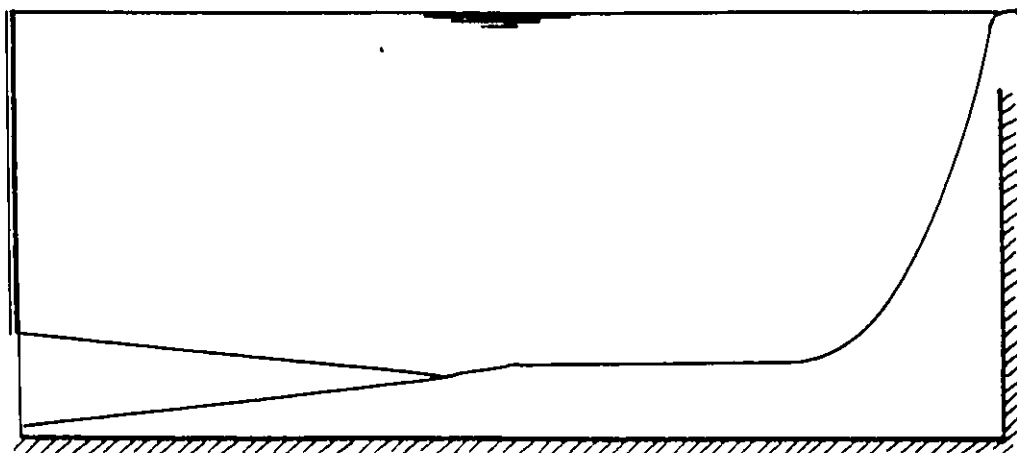


Fig. 5.2a The Potential Core and Growth of Boundary Layer

See Tables 3.2 to 3.28 for water depth (H) and height of the weir

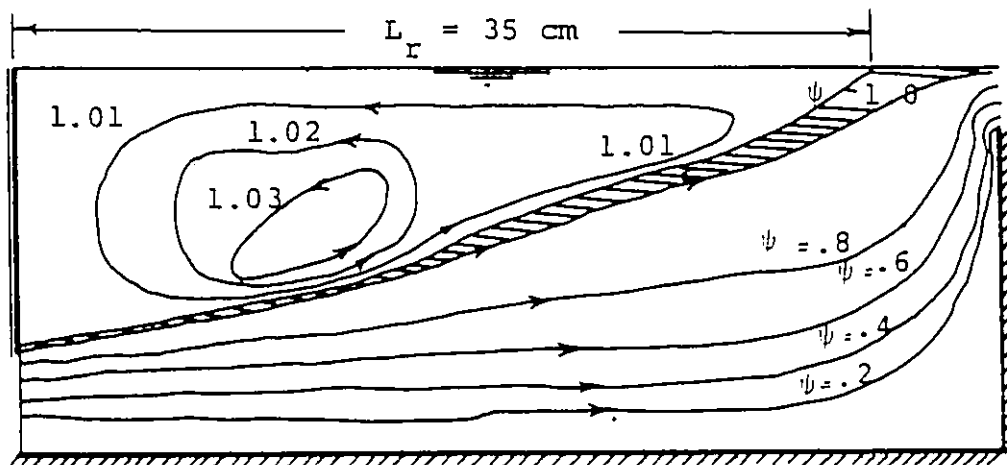


Fig. 5.2b Typical Flow Pattern (normalized)

Flow Characteristics ($G = 3 \text{ cm}$, $L = 40 \text{ cm}$, $q = 61.74 \text{ cm}^3/\text{sec}/\text{cm}$).

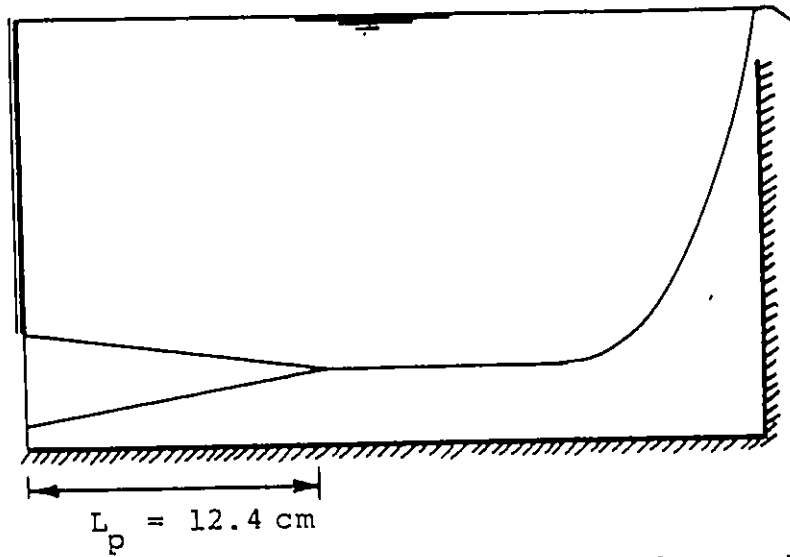


Fig. 5.3a The Potential Core and Growth of Boundary Layer.

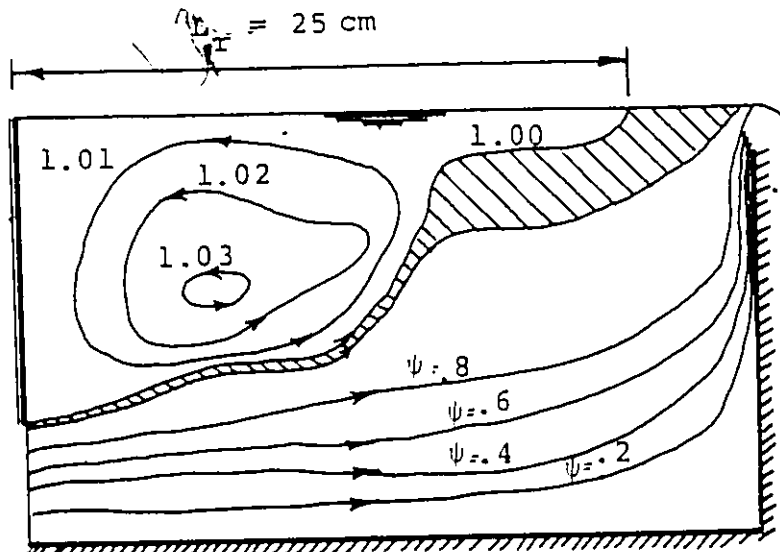


Fig. 5.3b Typical Flow Pattern (normalized).

Flow Characteristics ($G = 3 \text{ cm}$, $L = 30 \text{ cm}$, $q = 87.41 \text{ cm}^3/\text{sec}/\text{cm}$).

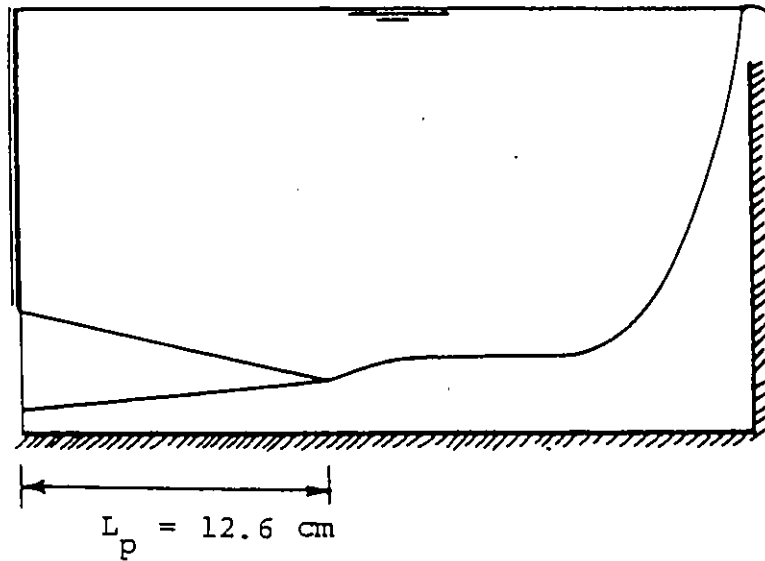


Fig. 5.4a The Potential Core and Growth of Boundary Layer.

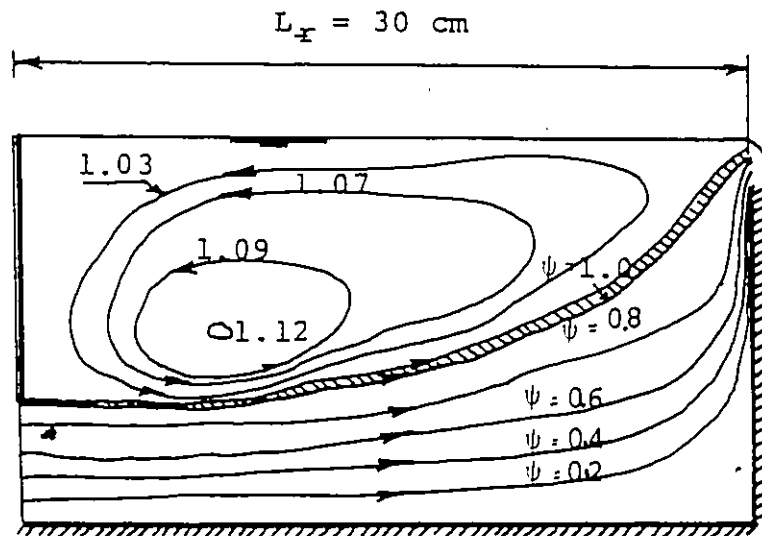


Fig. 5.4b Typical Flow Pattern (normalized)

Flow Characteristics ($G = 3 \text{ cm}$, $L = 30 \text{ cm}$, $q = 53.9 \text{ cm}^3/\text{sec}/\text{cm}$).

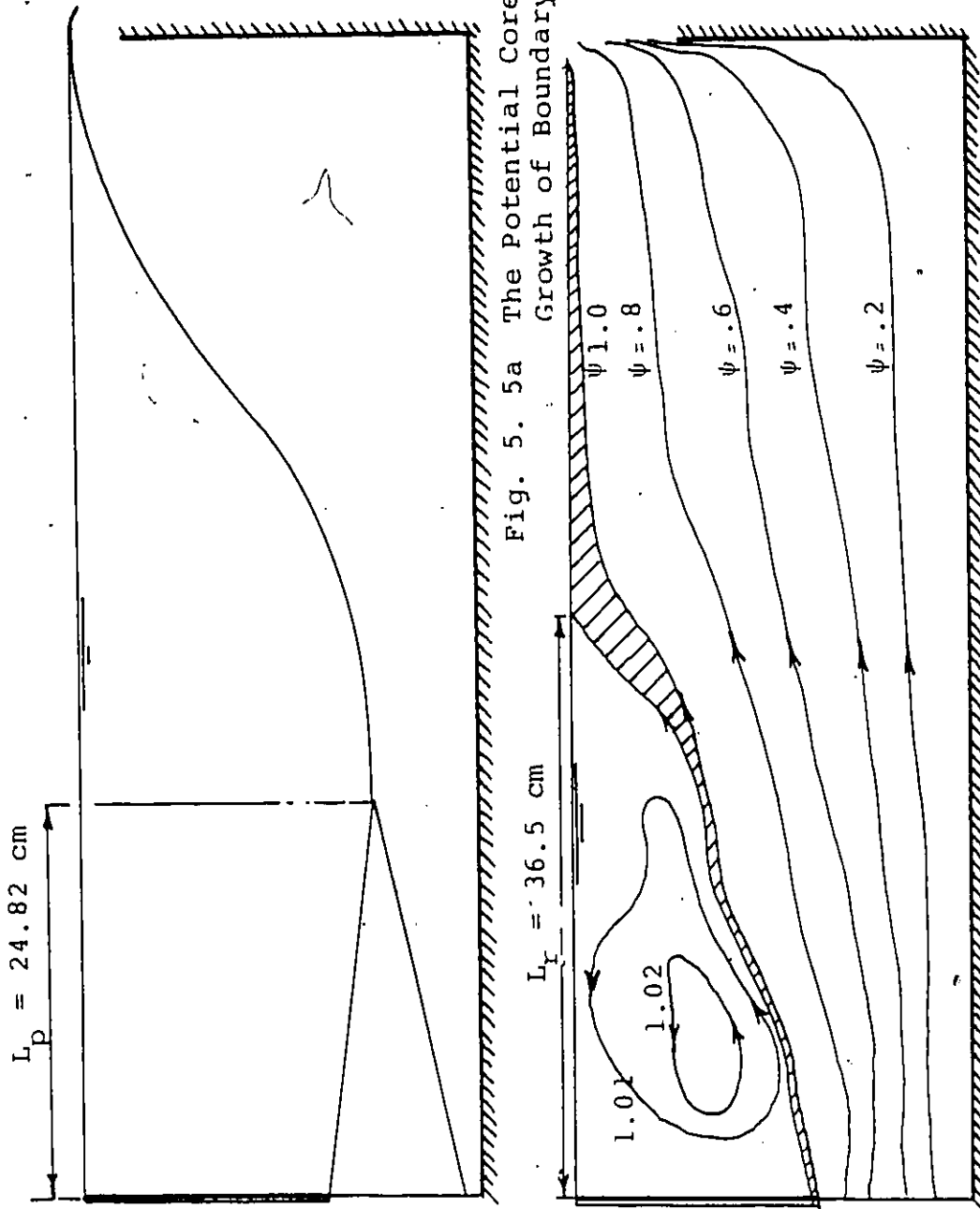


Fig. 5. 5a The Potential Core and Growth of Boundary Layer.

Fig. 5. 5b Typical Flow Pattern (normalized).

Flow Characteristics ($G = 5$ cm, $L = 73$ cm, $q = 147$ cm³/sec/cm).

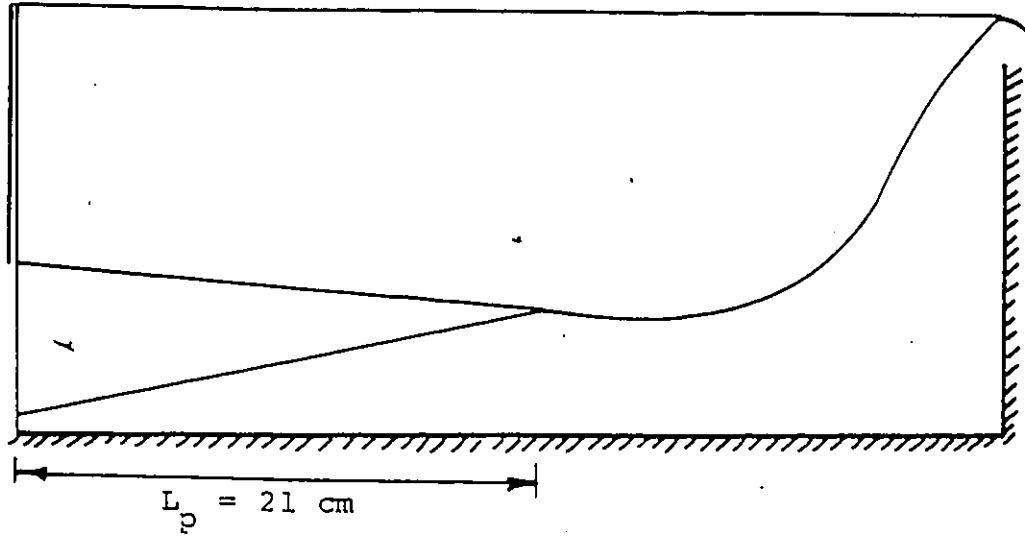


Fig. 5.6a The Potential Core and Growth of Boundary Layer.

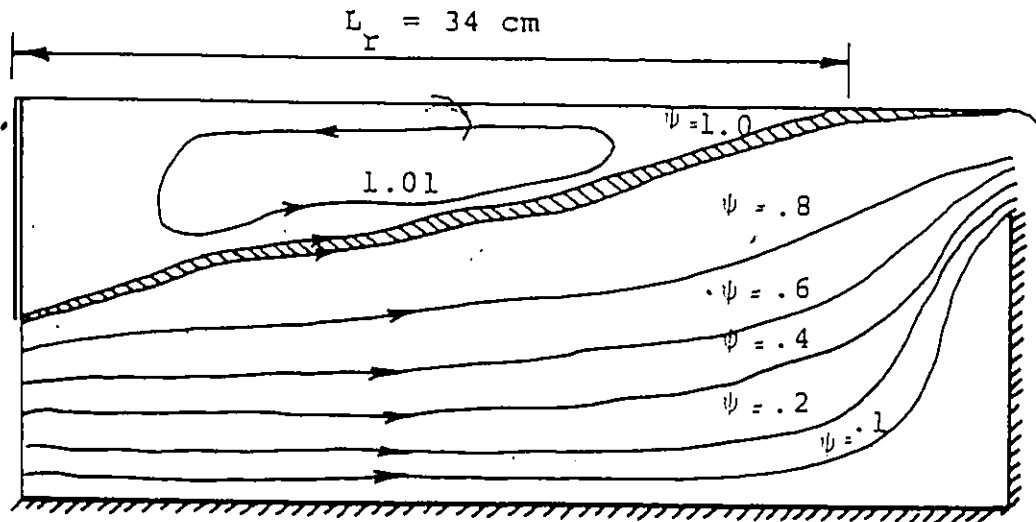


Fig. 5.6b Typical Flow Pattern (normalized)

Flow Characteristics ($G = 5 \text{ cm}$, $L = 40 \text{ cm}$, $\alpha = 111 \text{ cm}^3/\text{sec/cm}$).

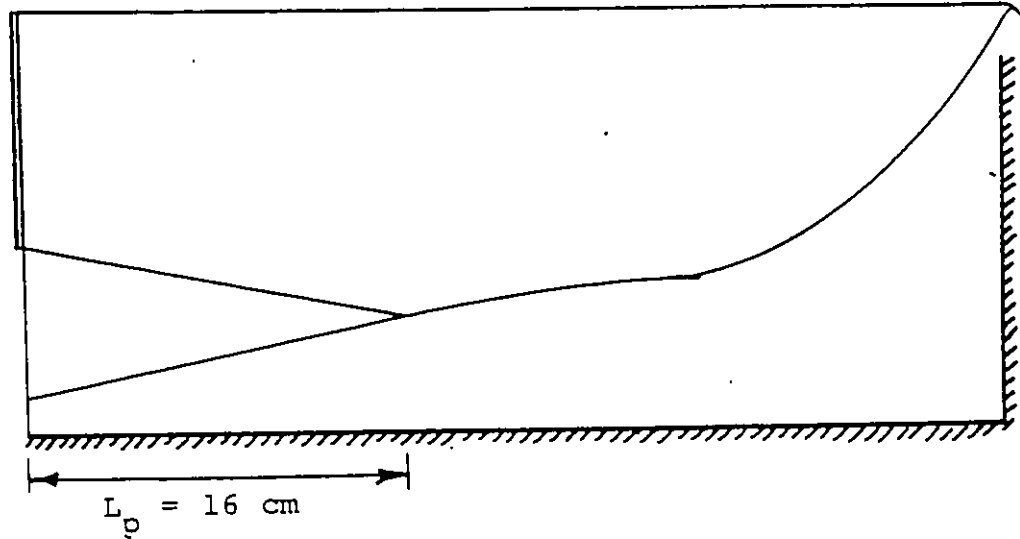


Fig. 5.7a The Potential Core and Growth of Boundary Layer.

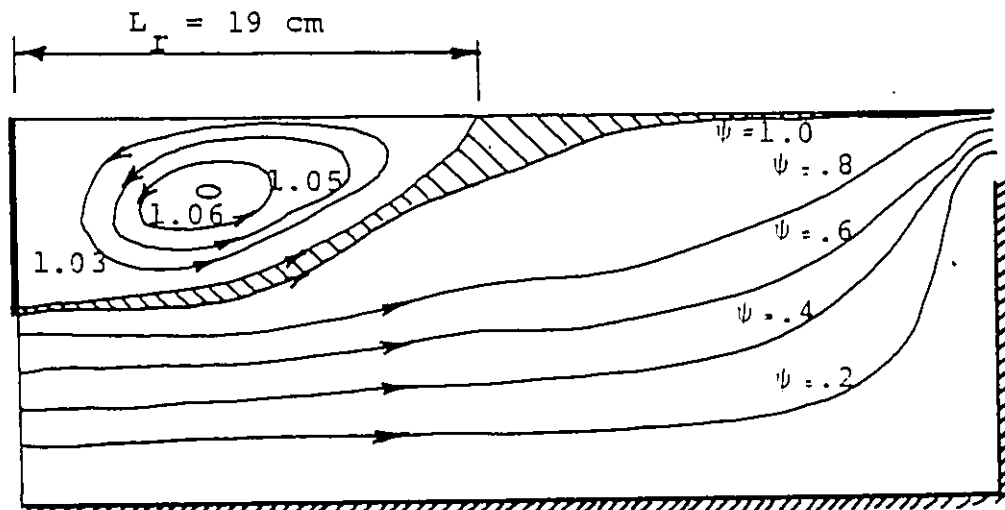


Fig. 5.7b Typical Flow Pattern (normalized).

Flow Characteristics ($G = 5 \text{ cm}$, $L = 40 \text{ cm}$,
 $\alpha = 53.9 \text{ cm}^3/\text{sec}/\text{cm}$).

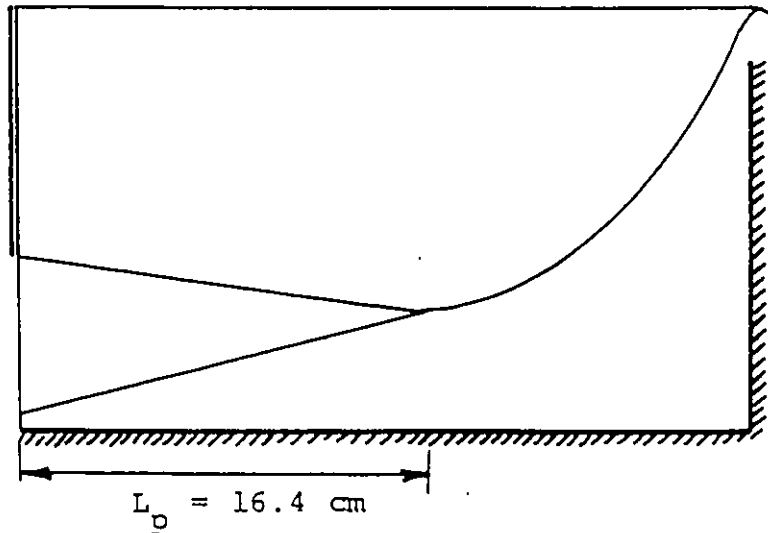


Fig. 5.8a The Potential Core and Growth of Boundary Layer.

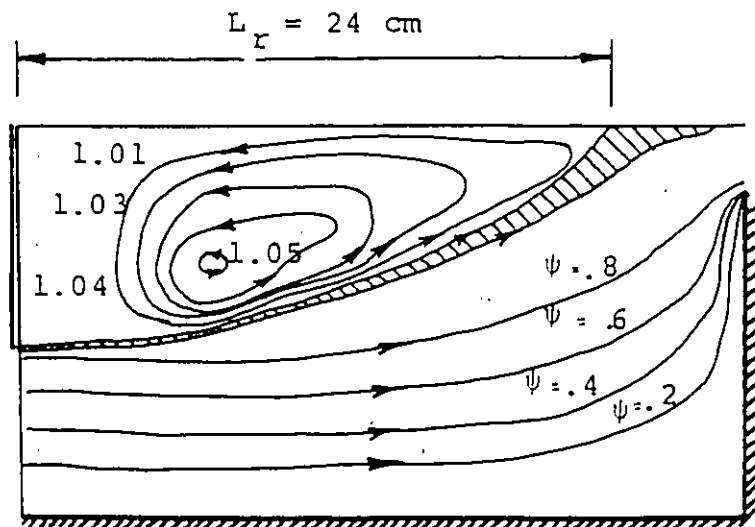


Fig. 5.8b Typical Flow Pattern (normalized).

Flow Characteristics ($G = 5 \text{ cm}$, $L = 30 \text{ cm}$,
 $q = 101.32 \text{ cm}^3/\text{sec}/\text{cm}$).

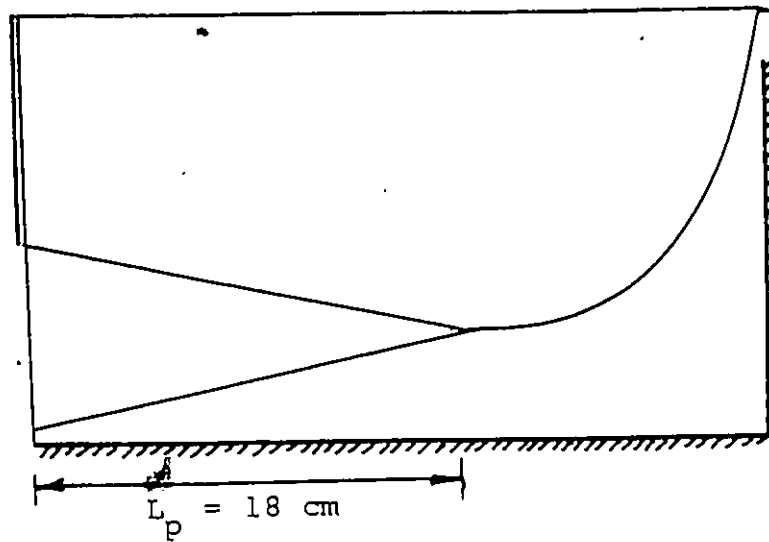


Fig. 5.9a The Potential Core and Growth of Boundary Layer.

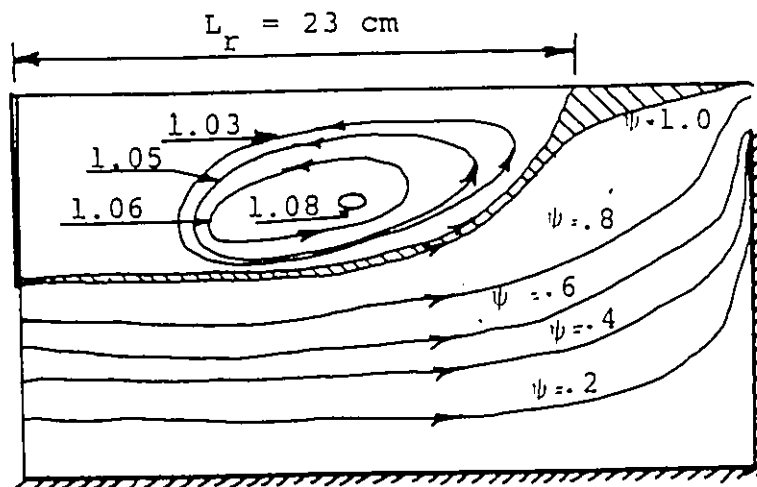


Fig. 5.9b Typical Flow Pattern (normalized)

Flow Characteristics ($G = 5 \text{ cm}$, $L = 30 \text{ cm}$,
 $q = 53.9 \text{ cm}^3/\text{sec}/\text{cm}$).

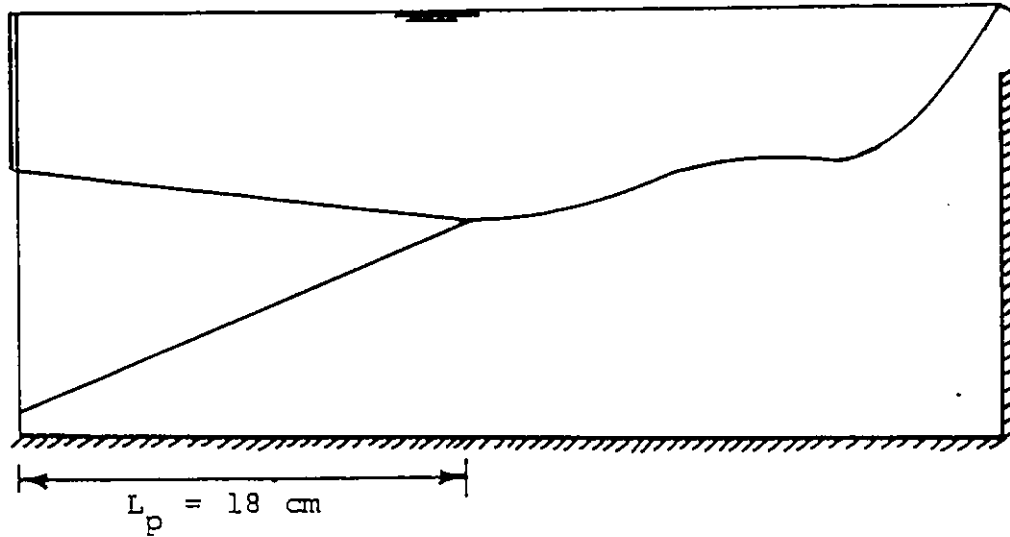
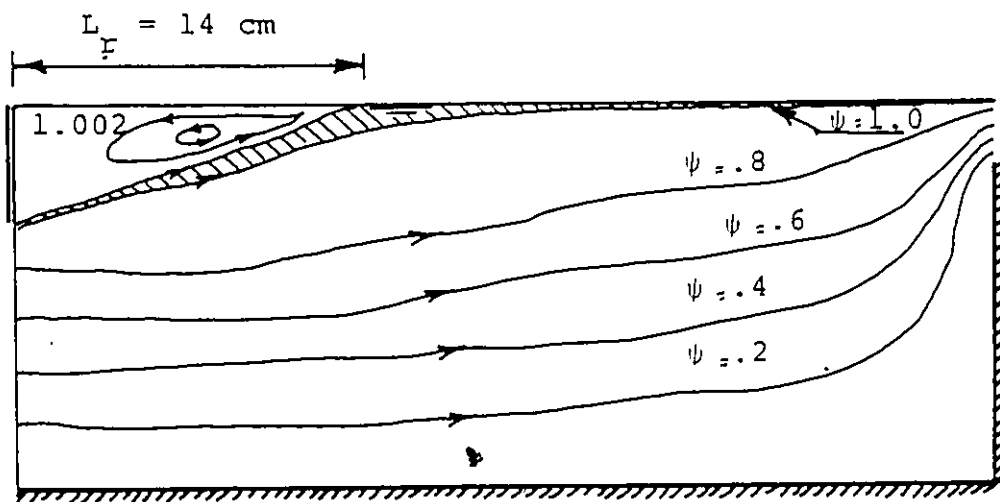


Fig. 5.10a The Potential Core and Growth of Boundary Layer.



5.10b Typical Flow Pattern (normalized).

Flow Characteristics ($G = 7$ cm, $L = 40$ cm, $q = 53.9$ cm³/sec/cm).

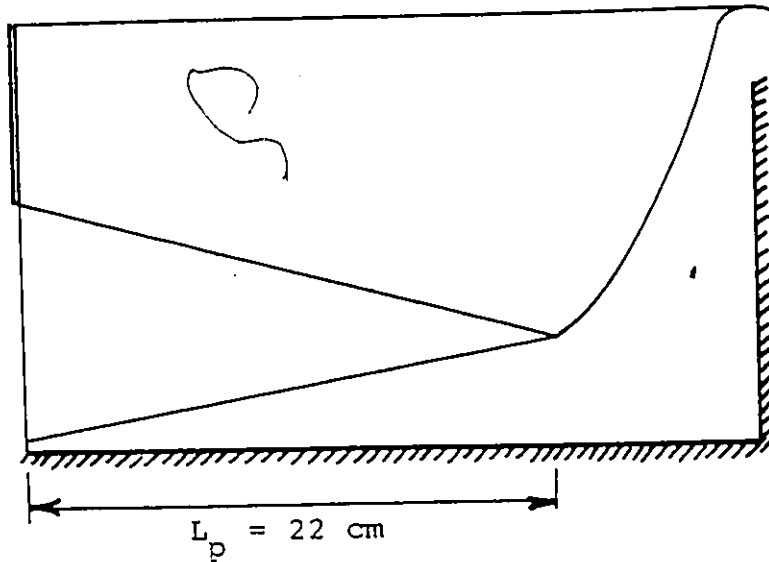


Fig. 5.11a The Potential Core and Growth of Boundary Layer.

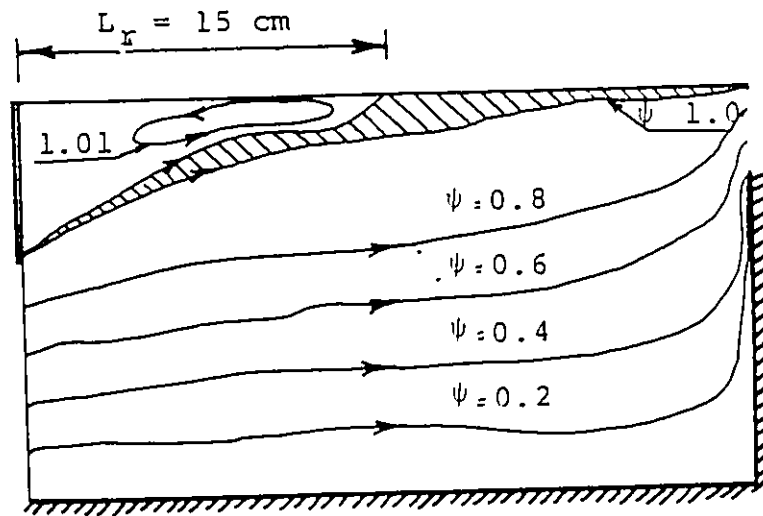


Fig. 5.11b Typical Flow Pattern (normalized).

Flow Characteristics ($G = 7 \text{ cm}$, $L = 30 \text{ cm}$,
 $q = 106 \text{ cm}^3/\text{sec}/\text{cm}$).

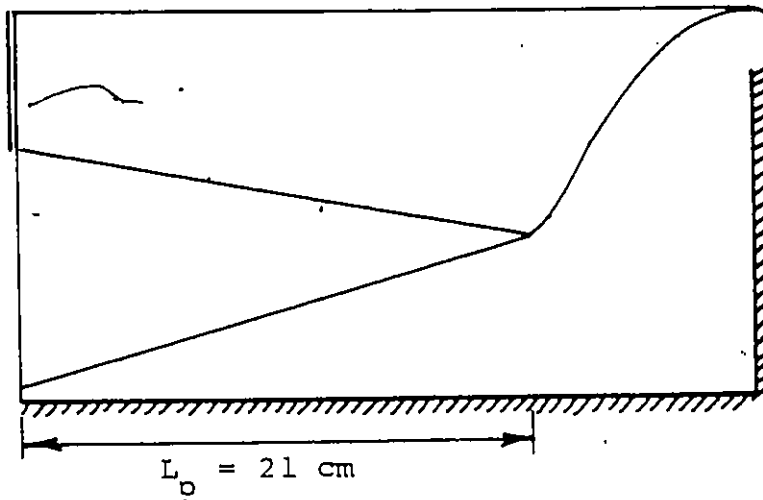


Fig. 5.12a The Potential Core and Growth of Boundary Layer.

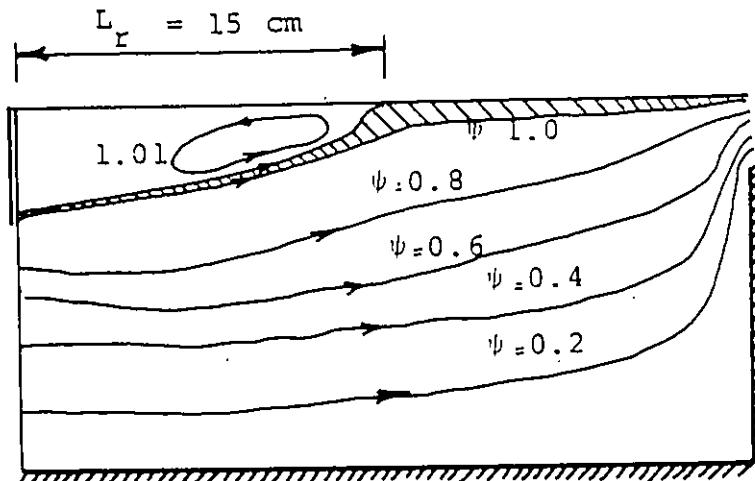


Fig. 5.12b Typical Flow Pattern (normalized).

Flow Characteristics ($G = 7 \text{ cm}$, $L = 30 \text{ cm}$,
 $q = 53.9 \text{ cm}^3/\text{sec}/\text{cm}$).

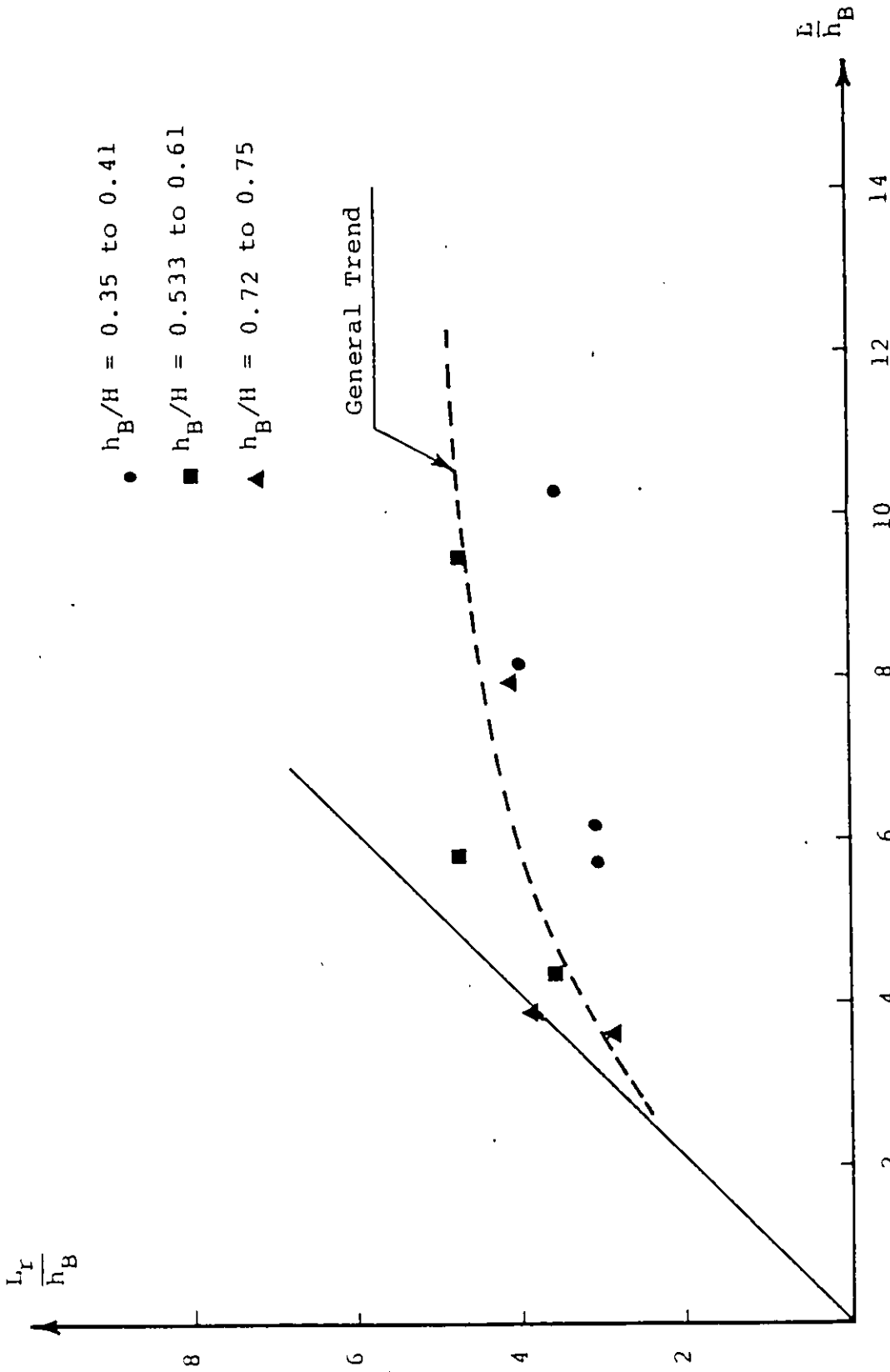


Fig. 5.13 Effect of tank Length on Roller Length.

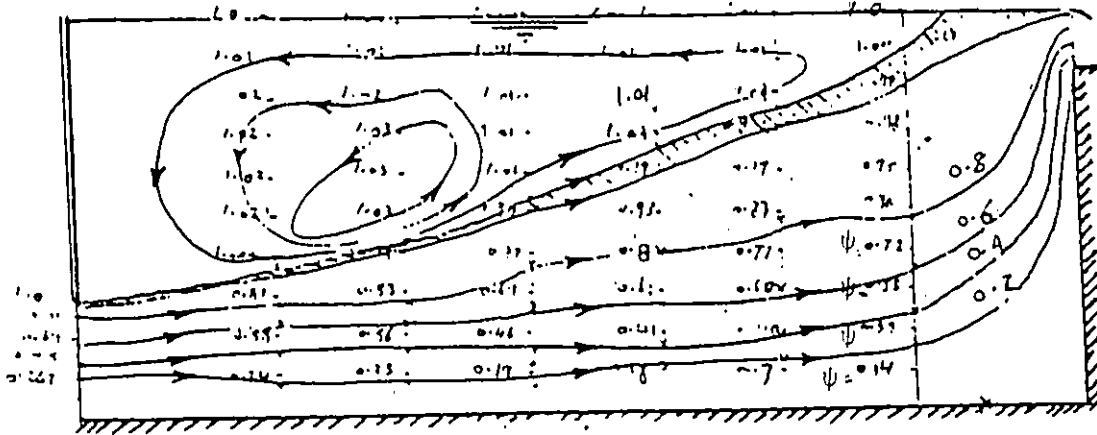


Fig. 5.14a

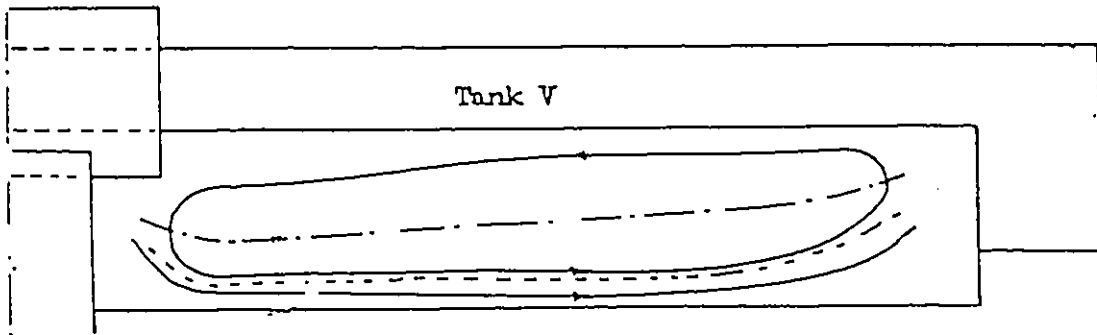


Fig. 5.14b

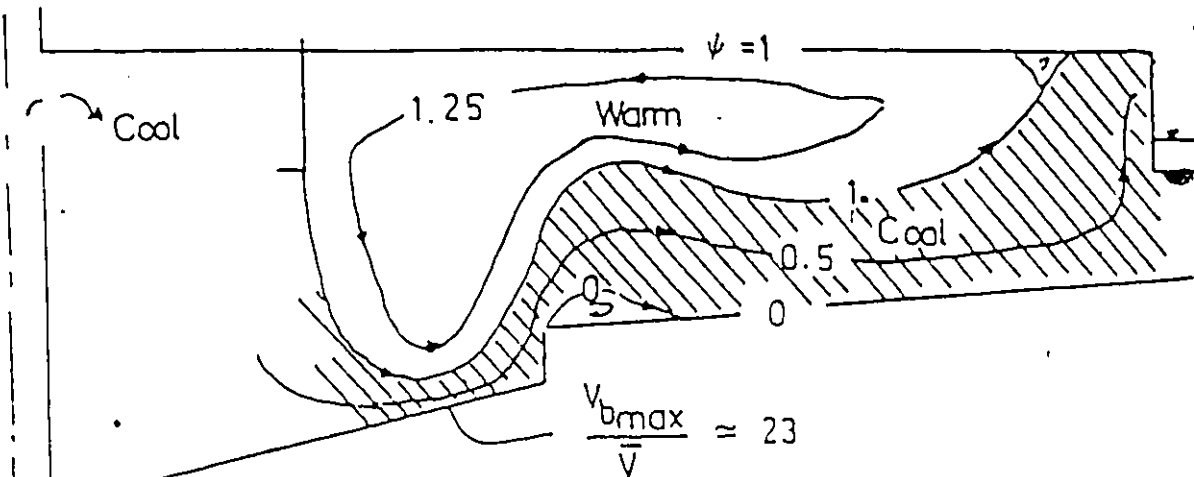


Fig. 5.14c

Comparison of the General Features of Settling Tank Flow for (a) the present Study, (b) Khattab, (c) McCorquodale.

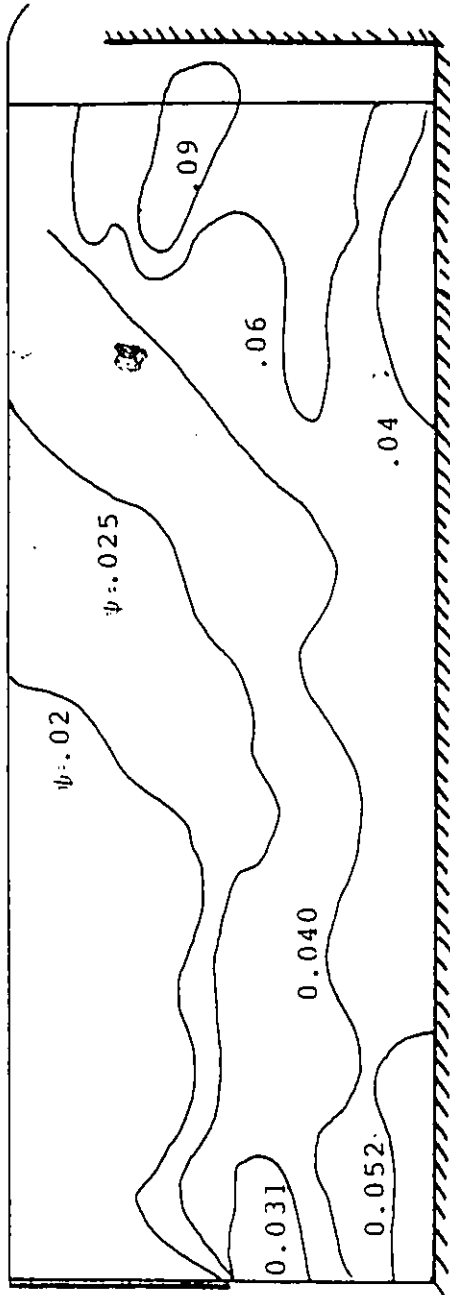


Fig. 5.15 Distribution of (r.m.s.) values for Flow Characteristics
 ($L = 73$ cm, $G = 5$ cm, $q = 147$ cm³/sec/cm).

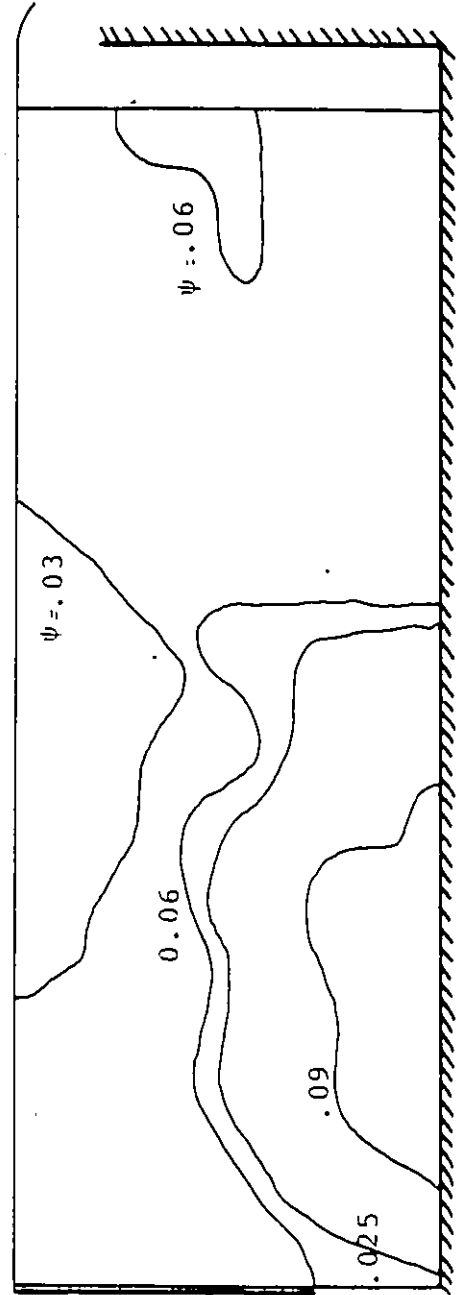


Fig. 5.16 Distribution of (r.m.s.) values for Flow Characteristics
 ($L = 73$ cm, $G = 3$ cm, $q = 111$ cm³/sec/cm).

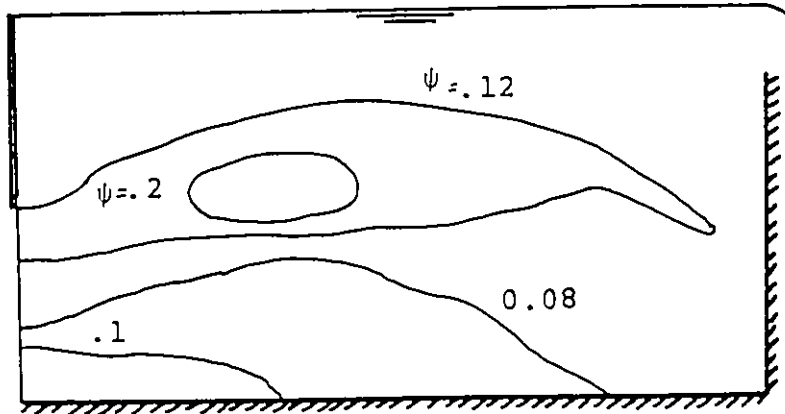


Fig. 5.17 Distribution of (r.m.s.) values for Flow Characteristics ($L = 30$ cm, $G = 5$ cm, $q = 101.32$ cm³/sec/cm).

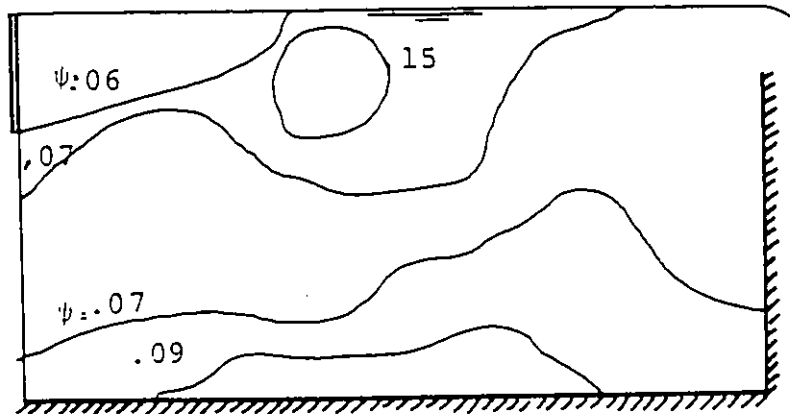


Fig. 5.18 Distribution of (r.m.s.) values for Flow Characteristics ($L = 30$ cm, $G = 7$ cm, $q = 106$ cm³/sec/cm).

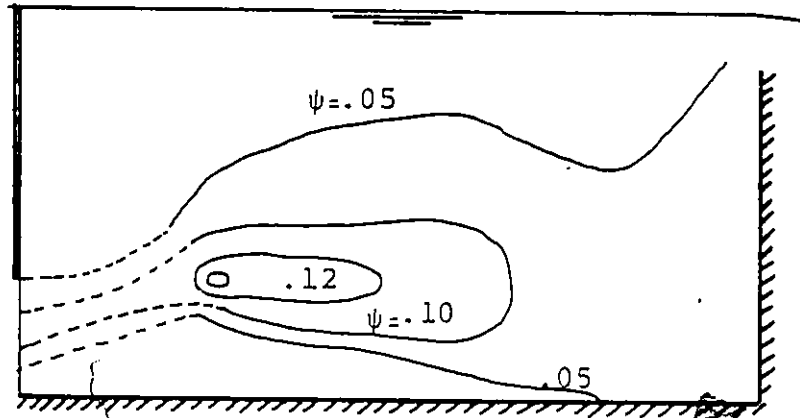


Fig. 5.19 Distribution of (r.m.s.) values for Flow Characteristics
($L = 30$ cm, $G = 3$ cm, $\alpha = 53.9$ cm³/sec/cm).

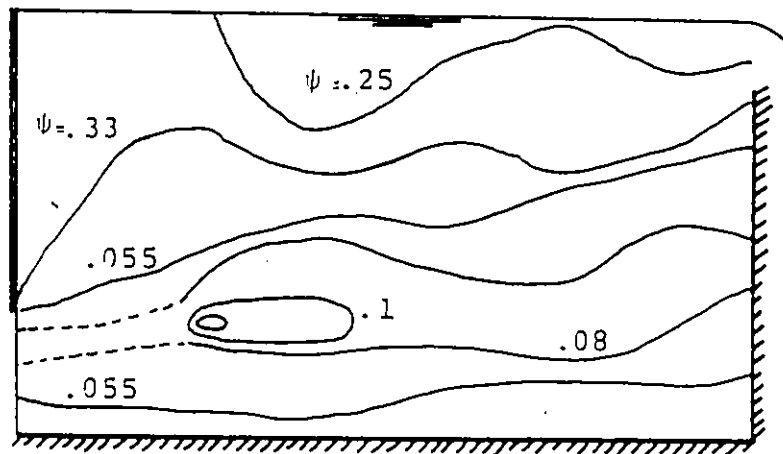


Fig. 5.20 Distribution of (r.m.s.) values for Flow Characteristics
($L = 30$ cm, $G = 3$ cm, $\alpha = 87.41$ cm³/sec/cm).

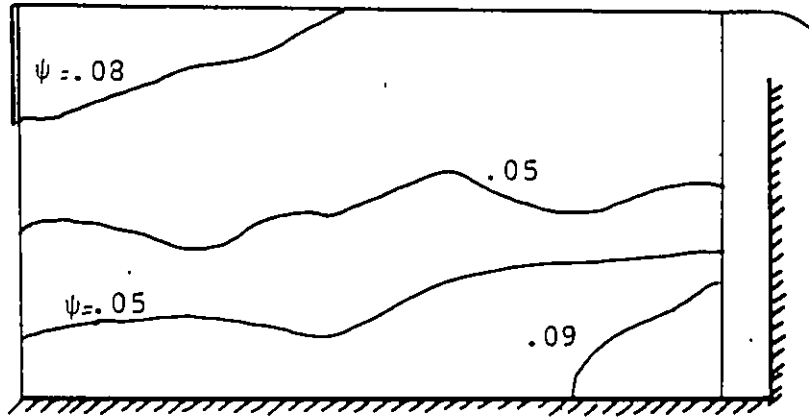


Fig. 5.21 Distribution of (r.m.s.) values for Flow Characteristics ($L = 30$ cm, $G = 7$ cm, $\alpha = 53.9$ cm³/sec/cm).

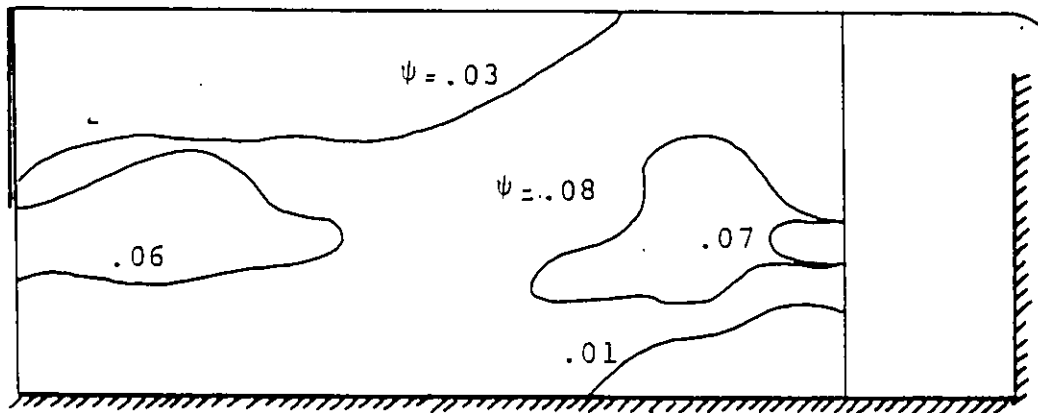


Fig. 5.22 Distribution of (r.m.s.) values for Flow Characteristics ($L = 40$ cm, $G = \text{cm}$, $\alpha = 111$ cm³/sec/cm).

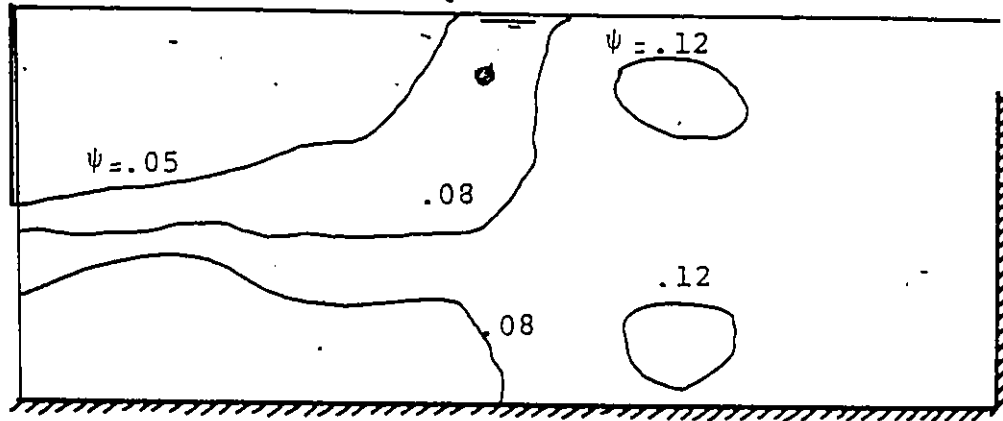


Fig. 5.23 Distribution of (r.m.s.) values for Flow Characteristics ($L = 40$ cm, $G = 5$ cm, $q = 53.9$ cm³/sec/cm).

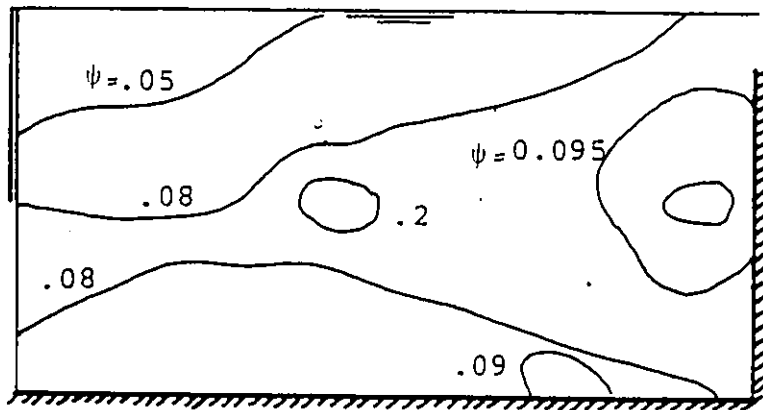


Fig. 5.24 Distribution of (r.m.s.) values for Flow Characteristics ($L = 30$ cm, $G = 5$ cm, $q = 53.9$ cm³/sec/cm).



Fig. 5.25 Distribution of (r.m.s.) values for Flow
Characteristic ($L = 40$ cm, $G = 3$ cm,
 $\alpha = 61.74$ cm³/sec/cm).

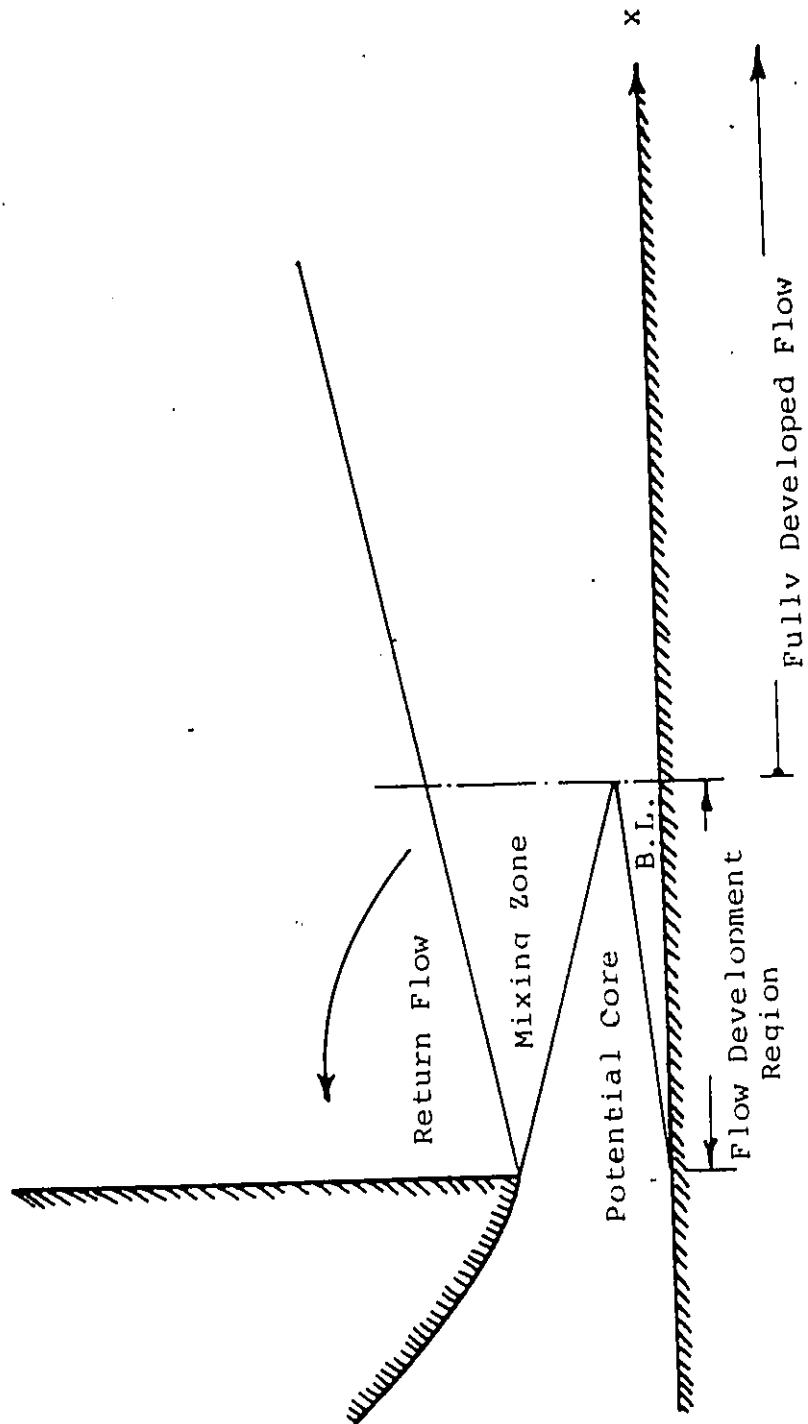


Fig. 5.26 Definition Sketch of Plane Turbulent Wall Jets

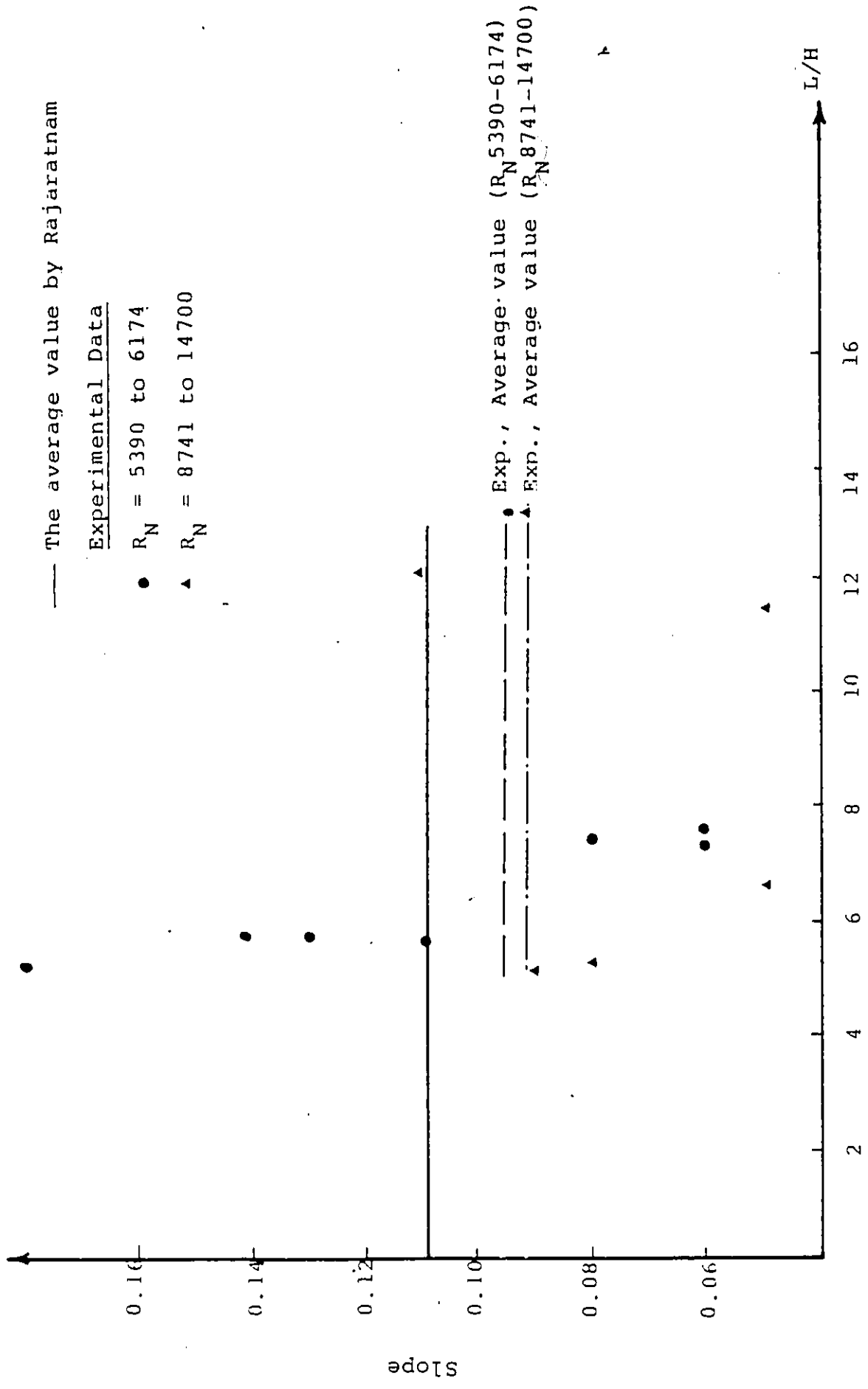


Fig. 5.27 Comparison of the Slope of Potential Core.

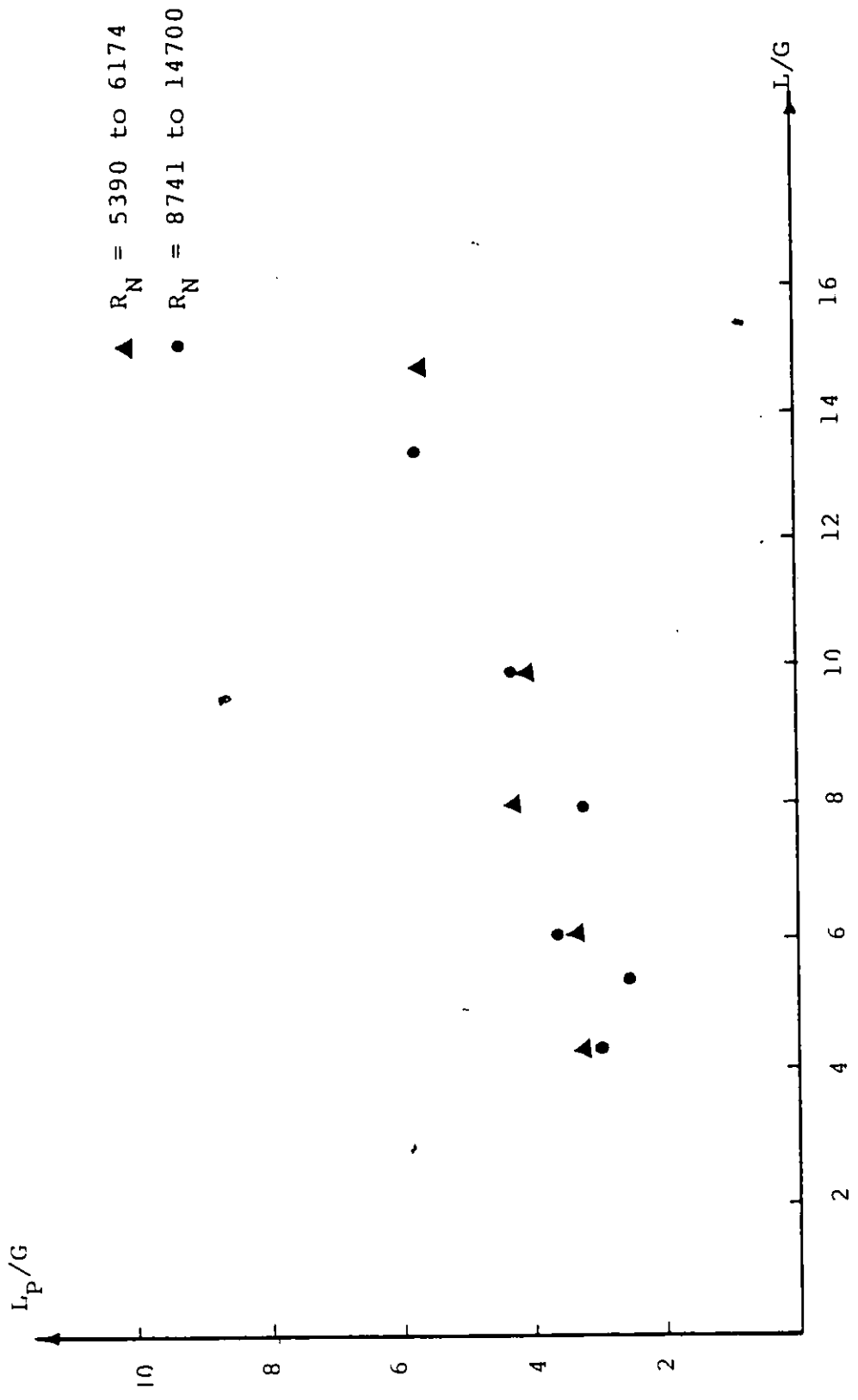


Fig. 5.28 The Effect of Tank Length on the Length of the Potential Core.

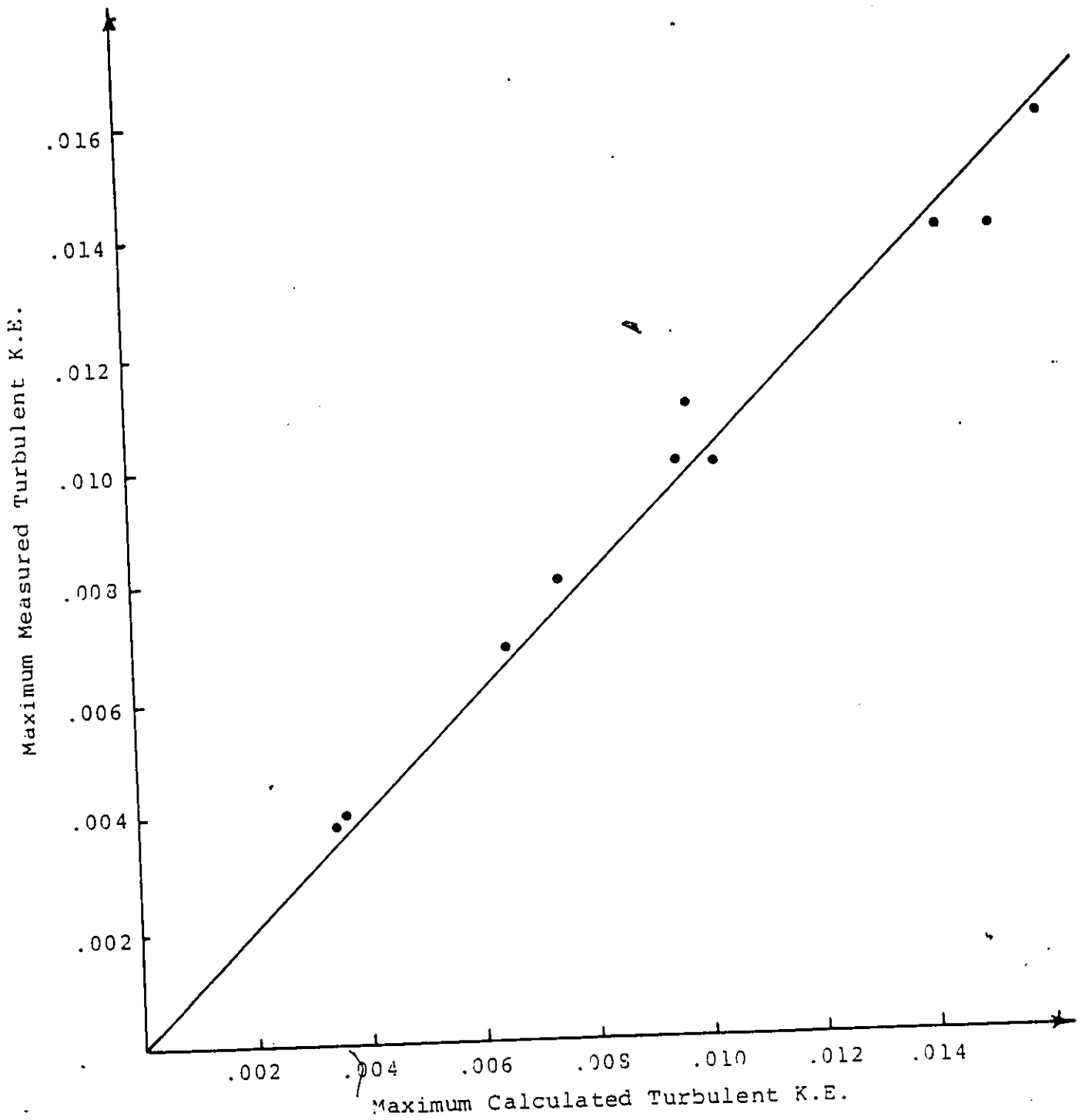


Fig. 5.29 Maximum calculated and measured values of turbulent kinetic energy.

APPENDIX A

Tables

TABLE 3.1
Equipment Details

Equipment	Model/ Type	Range and/or Comments	Manufacturer/ Supplier
* 15 mW He-Ne Laser	124A	= 6328 nm	Thermo-Systems Inc.
* Polarization Rotator	9101-2	-	(Specifications and operations procedures are found in litera- ture supplied by the manufacturer, 2500 North Cleveland Ave. St. Paul, Minnesota, 55113, U.S.A.)
* Beam Splitter	915	W = 50 mm	
* Acousto-optic Cell and Frequency Shifter	985	-	
* Focusing Lens	9117	f = 102.1 mm	"
* Photo Multi- plier System	962	-	"
* Frequency Tracker	1051-2	2KHZ-50 MHZ	"
* High Pass Filter	10095	0-10 MHZ	"
* Photodetector Aperature	9161-11	Aperature Diam.=0.28 mm	"
* Oscilloscope	5103N	-	Tectronics Inc.

TABLE 3.2

Measured Longitudinal Mean Velocity and (r.m.s.)
Profiles for, $q = 61.74 \text{ cm}^3/\text{sec}/\text{cm}$ at $X = 0.0 \text{ cm}$

Water Depth (H) = 11 cm Gate Opening (G) = 3 cm
Length of Tank (L) = 40 cm Head Over
Height of Weir = 8.5 cm the Weir = 2.3 cm

Elev. (cm)	VELOCITY (volts)		r.m.s. (volt) Average
	\bar{U}_{max}	\bar{U}_{min}	
1	4.91	4.80	0.1
1.5	4.91	4.80	0.1
2	5.00	4.87	0.15
2.5	5.00	4.80	0.18
3	5.00	4.8	0.15

Average Reference Velocity $U_R = 4.9$ volts

$$E = \bar{U}_{\text{max}} \text{ or } \bar{U}_{\text{min}}$$

From Table 3.2 to Table 3.28 the proportional voltage is related to the fluid velocity at the measuring point by,

$$\bar{U} = 6.651 [E - E_s]$$

where \bar{U} is the longitudinal velocity in cm/sec, E is the output to be read from the frequency. The frequency shifter was set such that E_s was observed to be 1.0.

TABLE 3.3

Measured Longitudinal Mean Velocity and (r.m.s.)
Profiles for, $q = 61.74 \text{ cm}^3/\text{sec}/\text{cm}$ at $X = 13 \text{ cm}$

Water Depth (H) = 11 cm Gate Opening (G) = 3 cm
Length of Tank (L) = 40 cm Head over
Height of Weir = 8.5 cm the Weir = 2.3 cm

Elev. (cm)	VELOCITY (volts)		r.m.s. (volt) Average
	\bar{U}_{max}	\bar{U}_{min}	
1	4.75	4.58	0.20
2	4.91	4.59	0.35
3	4.29	2.85	0.35
4	3.05	1.10	0.40
5	1.15	0.97	0.15
6	1.09	0.85	0.10
7	1.07	0.85	0.13
8	1.05	0.75	0.15
9	1.05	0.75	0.15
10	1.03	0.65	0.15

TABLE 3.4

Measured Longitudinal Mean Velocity and (r.m.s.)
Profiles for, $q = 61.74 \text{ cm}^3/\text{sec}/\text{cm}$ at $X = 23 \text{ cm}$

Water Depth (H) : = 11 cm Gate Opening (G) = 3 cm
Length of Tank (L) = 40 cm Head over
Height of Weir = 8.5 cm the Weir = 2.3 cm

Elev. (cm)	VELOCITY (volts)		r.m.s. (volt) Average
	\bar{U}_{max}	\bar{U}_{min}	
1	4.65	4.25	0.25
2	4.67	3.95	0.50
3	4.35	3.20	0.50
4	4.05	2.55	0.30
5	3.70	1.40	0.30
6	2.57	1.15	0.30
7	1.35	0.98	0.15
8	1.15	0.90	0.15
9	1.05	0.85	0.15
10	1.02	0.80	0.15

TABLE 3.5

Measured Longitudinal Mean Velocity and (r.m.s.)
Profiles for, $q = 61.74 \text{ cm}^3/\text{sec}/\text{cm}$ at $X = 33 \text{ cm}$

Water Depth (H): - 11 cm Gate Opening (G) = 3 cm
Length of Tank (L): = 40 cm Head over
Height of Weir = 8.5 cm the Weir = 2.3 cm

Elev. (cm)	VELOCITY (volts)		r.m.s. (volt) Average
	\bar{U}_{max}	\bar{U}_{min}	
1	3.70	3.30	0.35
2	4.05	3.45	0.35
3	4.00	3.19	0.50
4	3.45	2.65	0.55
5	2.90	1.75	0.45
6	2.70	1.59	0.45
7	1.85	0.98	0.45
8	1.25	0.85	0.30
9	1.09	0.55	0.25
10	0.75	0.55	0.22

TABLE 3.6

Measured Longitudinal Mean Velocity and (r.m.s.)
Profiles for, $q = 87.41 \text{ cm}^3/\text{sec}/\text{cm}$ at $X = 0.0 \text{ cm}$

Water Depth (H) = 11.5 cm Gate Opening (G) = 3 cm
Length of Tank (L) = 30 cm Head Over
Height of Weir = 8.5 cm the Weir = 2.9 cm

Elev. (cm)	VELOCITY (volts)		r.m.s. (volt) Average
	\bar{U}_{max}	\bar{U}_{min}	
1	6.91	6.81	0.30
1.5	6.98	6.97	0.15
2	7.03	6.98	0.25
2.5	7.10	7.04	0.30
3	6.98	6.96	0.30

Average Reference Velocity, $U_R = 6.97$

TABLE 3.7

Measured Longitudinal Mean Velocity and (r.m.s.)
Profiles for, $q = 87.41 \text{ cm}^3/\text{sec}/\text{cm}$ at $X = 13 \text{ cm}$

Water Depth (H) = 11.5 cm Gate Opening (G) = 3 cm
Length of Tank (L) = 30 cm Head over the
Height of Weir = 8.5 cm weir = 2.9 cm

Elev. (cm)	VELOCITY (volts)		r.m.s. (volt) Average
	\bar{U}_{max}	\bar{U}_{min}	
1	6.75	6.49	0.38
2	7.15	6.65	0.50
3	6.15	5.20	0.75
4	4.60	2.40	0.65
5	2.09	1.19	0.55
6	1.05	0.75	0.28
7	1.05	0.75	0.20
8	1.05	0.75	0.15
9	1.08	0.70	0.15
10	1.05	0.70	0.15
11	1.05	0.60	0.18

TABLE 3.8

Measured Longitudinal Mean Velocity and (r.m.s.)
Profiles for, $q = 87.41 \text{ cm}^3/\text{sec}/\text{cm}$ at $X = 28 \text{ cm}$

Water Depth (H) = 11.5 cm Gate Opening = 3 cm
Length of Tank (L) = 30 cm Head over the weir = 2.9 cm
Height of weir = 8.5 cm

Elev. (cm)	VELOCITY (volts)		r.m.s. (volt) Average
	\bar{U}_{\max}	\bar{U}_{\min}	
1	1.13	1.04	0.10
2	4.50	3.60	0.40
3	4.85	4.05	0.50
4	4.65	4.05	0.65
5	4.50	3.95	0.75
6	4.50	3.65	0.50
7	3.40	2.85	0.45
8	3.05	2.15	0.25
9	2.50	1.25	0.22
10	1.15	1.08	0.10
11	1.15	1.08	0.10

TABLE 3.9

Measured Longitudinal Mean Velocity and (r.m.s.)
Profiles for, $q = 111 \text{ cm}^3/\text{sec}/\text{cm}$ at $X = 0.0$

Water Depth (H) = 12 cm Gate Opening (G) = 3 cm
Length of Tank (L) = 73 cm Head over the weir = 3.4 cm
Height of Weir = 8.5 cm

Elev. (cm)	VELOCITY (volts)		r.m.s. (volt) Average
	\bar{U}_{max}	\bar{U}_{min}	
1	6.26	5.95	0.25
1.5	6.30	6.00	0.18
2	6.35	6.25	0.20
2.5	6.45	6.29	0.20
3	6.60	6.35	0.30

Average Reference Velocity, $U_R = 6.28$

TABLE 3.10

Measured Longitudinal Mean Velocity and (r.m.s.)
Profiles for, $q = 111 \text{ cm}^3/\text{sec}/\text{cm}$, $X = 13 \text{ cm}$

Water Depth (H) = 12 cm Gate Opening (G) = 3 cm
Length of Tank (L) = 73 cm Head over the weir = 3.4
Height of Weir = 8.5

Elev. (cm)	VELOCITY (volts)		r.m.s. (volt Average)
	\bar{U}_{max}	\bar{U}_{min}	
1	5.86	5.52	0.42
2	6.23	5.80	0.50
3	5.80	4.30	1.00
4	4.20	2.20	1.00
5	3.40	1.10	0.75
6	1.62	0.60	0.40
7	0.92	0.50	0.20
8	0.92	0.50	0.25
9	0.92	0.50	0.20
10	0.82	0.48	0.20
11	0.82	0.45	0.20
12	0.82	0.45	

TABLE 3.11

Measured Longitudinal Mean Velocity and (r.m.s.)
Profiles for, $q = 111 \text{ cm}^3/\text{sec}/\text{cm}$ at $X = 28. \text{ cm}$

Water Depth (H) = 12 c.m. Gate Opening (G) = 3 cm
Length of Tank (L) = 73 cm Head over the
Height of Weir = 8.5 cm weir = 3.4 cm

Elev. (cm)	VELOCITY (volts)		r.m.s. (volt) Average
	\bar{U}_{max}	\bar{U}_{min}	
1	6.10	4.65	0.40
2	6.15	4.85	0.75
3	5.95	4.60	0.78
4	5.30	2.50	1.00
5	3.90	2.10	0.75
6	3.30	1.30	0.45
7	2.50	0.85	0.30
8	1.30	0.85	0.20
9	1.09	0.75	0.30
10	1.03	0.65	0.20
11	1.03	0.75	0.20
12	1.03	0.75	0.15

TABLE 3.12 .

Measured Longitudinal Mean Velocity and (r.m.s.)
Profiles for, $q = 111 \text{ cm}^3/\text{sec}/\text{cm}$ at $X = 43 \text{ cm}$

Water Depth (H) = 12 cm Gate Opening (G) = 3 cm
Length of Tank (L) = 73 cm Head over the
Height of Weir = 8.5 cm weir = 3.4 cm

Elev. (cm)	VELOCITY (volts)		r.m.s. (volt) Average
	\bar{U}_{max}	\bar{U}_{min}	
1	5.09	4.08	0.15
2	5.60	4.09	0.15
3	5.12	3.95	0.22
4	4.70	3.65	0.20
5	4.70	3.20	0.22
6	4.50	2.85	0.20
7	2.90	1.15	0.10
8	2.90	1.15	0.22
9	2.90	1.15	0.28
10	2.65	1.09	0.25
11	2.55	1.09	0.20
12	2.30	1.09	0.25

TABLE 3.13

Measured Longitudinal Mean Velocity and (r.m.s.)
Profiles for, $q = 111 \text{ cm}^3/\text{sec}/\text{cm}$ at $X = 63 \text{ cm}$

Water Depth (H) = 12 cm Gate Opening (G) = 3 cm
Length of Tank (L) = 73 cm Head Over the
Height of Weir = 8.5 cm weir = 3.4 cm
+

Elev. (cm)	VELOCITY (volts)		r.m.s. (volt) Average
	\bar{U}_{max}	\bar{U}_{min}	
1	3.45	1.65	0.40
2	3.70	1.65	0.40
3	3.70	1.79	0.45
4	3.70	1.95	0.42
5	4.30	2.10	0.50
6	4.04	2.14	0.40
7	3.90	2.10	0.42
8	3.85	2.20	0.42
9	3.75	2.60	0.40
10	3.65	2.60	0.35
11	3.60	2.60	0.30
12	3.50	2.60	0.30

TABLE 3.14

Measured Longitudinal Mean Velocity and (r.m.s.)
Profiles for, $q = 101.32 \text{ cm}^3/\text{sec}/\text{cm}$ at $X = 0.0 \text{ cm}$

Water Depth (H) = 11.8 cm Gate Opening (G) = 5 cm
Length of Tank (L) = 30 cm Head Over the
Height of Weir = 8.5 cm weir = 3.2 cm

Elev. (cm)	VELOCITY (volts)		r.m.s. (volt) Average
	\bar{U}_{max}	\bar{U}_{min}	
1	4.55	4.35	0.40
1.5	4.79	4.70	0.20
2	4.79	4.70	0.15
2.5	4.79	4.70	0.15
3	4.79	4.70	0.15
3.5	4.85	4.78	0.25
4	4.91	4.80	0.30
4.5	5.05	4.90	0.30
5	4.80	4.72	0.30

Average Reference Velocity, $U_R = 3.76$

TABLE 3.15

Measured Longitudinal Mean Velocity and (r.m.s.)
Profiles for, $q = 101.32 \text{ cm}^3/\text{sec}/\text{cm}$ at $X = 13 \text{ cm}$

Water Depth (H) = 11.8 cm Gate Opening (G) = 5 cm
Length of Tank (L) = 30 cm Head Over the
Height of Weir = 8.5 cm Weir = 3.2 cm

Elev. (cm)	VELOCITY (Volts)		r.m.s. (volt) Average
	\bar{U}_{max}	\bar{U}_{min}	
1	4.30	4.18	0.25
2	4.58	4.40	0.25
3	4.82	4.70	0.30
4	4.85	4.42	0.60
5	4.09	3.15	0.75
6	2.85	1.85	0.75
7	2.20	0.99	0.40
8	1.10	0.65	0.25
9	0.85	0.55	0.20
10	0.85	0.55	0.20
11	0.85	0.55	0.20

TABLE 3.16

Measured Longitudinal Mean Velocity and (r.m.s.)
Profiles for, $q = 101.32 \text{ cm}^3/\text{sec}/\text{cm}$ at $X = 28 \text{ cm}$

Water Depth (H) = 11.8 cm Gate Opening (G) = 5. cm
Length of Tank (L) = 30 cm Head Over the
Height of Weir = 8.5 cm Weir = 3.2 cm

Elev. (cm)	VELOCITY (volts)		r.m.s. (volt) Average
	\bar{U}_{max}	\bar{U}_{min}	
1	1.48	1.19	0.15
2	2.56	1.65	0.45
3	2.96	2.09	0.40
4	3.29	2.70	0.42
5	3.43	3.18	0.30
6	3.60	3.18	0.25
7	3.47	3.09	0.30
8	3.35	2.85	0.35
9	2.87	2.45	0.40
10	2.45	2.23	0.30
11	2.19	1.45	0.30

TABLE 3.17

Measured Longitudinal Mean Velocity and (r.m.s.)
Profiles for, $q = 111 \text{ cm}^3/\text{sec}/\text{cm}$ at $X = 8 \text{ cm}$

Water Depth (H) = 12 cm Gate Opening (G) = 5 cm
Length of Tank (L) = 40 cm Head Over the
Height of Weir = 8.5 cm Weir = 3.4 cm

Elev. (cm)	VELOCITY (volts)		r.m.s. (volt) Average
	\bar{U}_{max}	\bar{U}_{min}	
1	5.03	4.75	0.22
2	5.20	5.08	0.25
3	5.50	5.30	0.30
4	6.00	5.60	0.35
5	5.80	5.40	0.32
6	3.90	1.70	0.30
7	1.15	0.95	0.13
8	1.13	0.95	0.09
9	1.05	0.85	0.15
10	1.03	0.75	0.10
11	1.03	0.72	0.10
12	1.02	0.70	0.10

TABLE 3.18

Measured Longitudinal Mean Velocity and (r.m.s.)
Profiles for, $q = 111 \text{ cm}^3/\text{sec}/\text{cm}$ at $X = 18 \text{ cm}$

Water Depth (H) = 12 cm Gate Opening = 5 cm
Length of Tank (L) = 40 cm Head Over the
Height of Weir = 8.5 cm Weir = 3.4 cm

Elev. (cm)	VELOCITY (volts)		r.m.s. (volt) Average
	\bar{U}_{max}	\bar{U}_{min}	
1	5.04	4.60	0.25
2	5.23	4.95	0.25
3	5.50	5.15	0.25
4	5.30	4.85	0.25
5	5.11	4.19	0.19
6	4.25	2.60	0.15
7	3.80	1.15	0.15
8	1.15	0.98	0.10
9	1.13	0.80	0.05
10	1.13	0.80	0.09
11	1.13	0.65	0.10
12	1.10	0.60	0.10

TABLE 3.19

Measured Longitudinal Mean Velocity and (r.m.s.)
Profiles for, $q = .111 \text{ cm}^3/\text{sec}/\text{cm}$ at $X = 28 \text{ cm}$

Water Depth (H) = 12 cm Gate Opening (G) = 5 cm
Length of Tank (L) = 40 cm Head Over the
Height of Weir = 8.5 cm Weir = 3.4 cm

Elev. (cm)	VELOCITY (volts)		r.m.s. (volt) Average
	\bar{U}_{max}	\bar{U}_{min}	
1	4.01	3.59	0.12
2	4.57	4.09	0.30
3	4.70	4.20	0.25
4	4.82	4.03	0.13
5	4.75	4.08	0.30
6	4.55	3.15	0.30
7	3.75	2.15	0.23
8	2.65	1.15	0.20
9	2.14	1.10	0.20
10	1.65	0.65	0.15
11	1.03	0.55	0.15
12	1.01	0.90	0.15

TABLE 3.20

Measured Longitudinal Mean Velocity and (r.m.s.)
Profiles for, $q = 111 \text{ cm}^3/\text{sec}/\text{cm}$ at $X = 33 \text{ cm}$

Water Depth (H) = 12 cm Gate Opening (G) = 5 cm
Length of Tank (L) = 40 cm Head Over the
Height of Weir = 8.5 cm Weir = 3.4 cm

Elev. (cm)	VELOCITY (volts)		r.m.s. (volt) Average
	\bar{U}_{max}	\bar{U}_{min}	
1	2.60	1.15	0.45
2	3.60	2.10	0.45
3	3.90	3.18	0.40
4	4.05	3.75	0.27
5	4.20	3.75	0.30
6	4.70	3.00	0.32
7	4.11	2.70	0.50
8	3.85	1.60	0.45
9	2.75	1.40	0.47
10	2.35	1.38	0.40
11	1.70	1.10	0.40
12	1.50	1.10	0.40

TABLE 3.21

Measured Longitudinal Mean Velocity and (r.m.s.)
Profiles for, $q = 147 \text{ cm}^3/\text{sec}/\text{cm}$ at $X = 8 \text{ cm}$

Water Depth (H) = 12.7 cm Gate Opening (G) = 5 cm
Length of Tank (L) = 73 cm Head Over the Weir = 4.1
Height of Weir = 8.5 cm

Elev. (cm)	VELOCITY (volts)		r.m.s. (volt) Average
	\bar{U}_{max}	\bar{U}_{min}	
1	5.48	4.96	0.25
1.5	5.85	5.48	0.25
2.5	6.14	5.90	0.15
3.5	6.32	5.98	0.20
4.5	6.45	5.32	0.10
5.5	3.67	2.03	0.10
6.5	1.15	0.95	0.10
7.5	1.10	0.95	0.08
8.5	1.10	0.89	0.08
9.5	1.10	0.65	0.08
10.5	1.09	0.65	0.08
11.5	1.09	0.65	0.08
12	1.09	0.55	0.08
12.5	1.09	0.55	0.07

TABLE 3.22

Measured Longitudinal Mean Velocity and (r.m.s.)
Profiles for, $q = 147 \text{ cm}^3/\text{sec}/\text{cm}$ at $X = 18 \text{ cm}$

Water Depth (H) = 12.7 cm Gate Opening (G) = 5 cm
Length of Tank (L) = 73 cm Head Over the
Height, of Weir = 8.5 cm Weir = 4.1 cm

Elev. (cm)	VELOCITY (volts)		r.m.s. (volt) Average
	\bar{U}_{max}	\bar{U}_{min}	
1	5.85	5.19	0.25
2	6.35	5.45	0.25
3	6.35	5.60	0.20
4	6.32	5.45	0.18
5	5.70	4.25	0.18
6	4.36	2.25	0.13
7	3.90	2.20	0.10
8	1.35	0.83	0.10
9	1.17	0.83	0.10
10	1.10	0.80	0.10
11	1.09	0.80	0.05
12	1.09	0.80	0.05

TABLE 3.23

Measured Longitudinal Mean Velocity and (r.m.s.)
Profiles for, $q = 147 \text{ cm}^3/\text{sec}/\text{cm}$ at $X = 28 \text{ cm}$

Water Depth (H) = 12.7 cm Gate Opening (G) = 5 cm
Length of Tank (L) = 73 cm Head Over the
Height of Weir = 8.5 cm Weir = 4.1 cm

Elev. (cm)	VELOCITY (volts)		r.m.s. (volt) Average
	\bar{U}_{max}	\bar{U}_{min}	
1	5.70	4.20	0.25
2	6.08	4.90	0.30
3	6.25	4.98	0.30
4	6.03	4.45	0.15
5	5.82	4.35	0.20
6	5.08	3.55	0.20
7	4.90	3.40	0.10
8	4.40	1.04	0.10
9	1.23	0.85	0.10
10	1.23	0.85	0.10
11	1.20	0.65	0.10
12	1.20	0.50	0.05

TABLE 3.24

Measured Longitudinal Mean Velocity and (r.m.s.)
Profiles for, $q = 147 \text{ cm}^3/\text{sec}/\text{cm}$ at $X = 38 \text{ cm}$

Water Depth = 12.7 cm Gate Opening (G) = 5 cm
Length of Tank (L) = 73 cm Head Over the
Height of Weir = 8.5 cm Weir = 4.1 cm

Elev. (cm)	VELOCITY (volts)		r.m.s. (volt) Average
	U_{max}	U_{min}	
1	5.25	4.19	0.30
2	5.30	4.07	0.30
3	5.35	3.85	0.35
4	5.35	3.85	0.20
5	5.40	3.27	0.20
6	4.78	3.06	0.15
7	4.75	3.03	0.10
8	4.37	2.28	0.15
9	4.37	1.85	0.15
10	4.03	1.01	0.15
11	4.03	0.97	0.15
12	4.01	0.95	0.15

TABLE 3.25

Measured Longitudinal Mean Velocity and (r.m.s.)
Profiles for, $q = 147 \text{ cm}^3/\text{sec}/\text{cm}$ at $X = 70 \text{ cm}$

Water Depth = 12.7 cm Gate Opening (G) = 5 cm
Length of Tank (L) = 73 cm Head Over the
Height of Weir = 8.5 cm Weir = 4.1 cm

Elev. (cm)	VELOCITY (volts)		r.m.s. (volt) Average
	\bar{U}_{max}	\bar{U}_{min}	
1	2.13	1.10	0.20
2	2.70	1.50	0.30
3	2.85	1.65	0.32
4	3.10	1.70	0.30
5	3.15	2.10	0.35
6	3.40	2.20	0.40
7	3.50	2.50	0.35
8	3.75	2.70	0.28
9	4.15	2.85	0.30
10	4.27	3.20	0.20
11	4.36	3.60	0.20
12	4.45	3.72	0.22

TABLE 3.26

Measured Longitudinal Mean Velocity and (r.m.s.)
Profiles for, $q = 106 \text{ cm}^3/\text{sec}/\text{cm}$ at $X = 0.0$

Water Depth (H) = 11.9 cm Gate Opening (G) = 7 cm
Length of Tank (L) = 30 cm Head Over the
Height of Weir = 8.5 cm Weir = 3.3 cm

Elev. (cm)	VELOCITY (volts)		r.m.s. (volt Average)
	\bar{U}_{max}	\bar{U}'_{min}	
1	3.95	3.65	0.25
1.5	3.98	3.70	0.18
2	3.85	3.55	0.10
2.5	3.85	3.55	0.20
3	3.65	3.50	0.10
3.5	3.50	3.40	0.13
4	3.50	3.40	0.13
4.5	3.50	3.40	0.15
5	3.50	3.40	0.20
5.50	3.50	3.35	0.20
6	3.48	3.35	0.15
6.5	3.48	3.35	0.15
6	3.48	3.35	0.15

Reference:

Velocity, $U_R = 3.62 \text{ volts}$

TABLE 3.27

Measured Longitudinal Mean Velocity and (r.m.s.)
Profiles for, $q = 106 \text{ cm}^3/\text{se}/\text{cm}$ at $X = 18 \text{ cm}$

Water Depth (H) = 11.9 cm Gate Opening (G) = 7 cm
Length of Tank (L) = 30 cm Head Over the
Height of Weir = 8.5 cm Weir = 3.3 cm

Elev. (cm)	VELOCITY (volts)		r.m.s. (volt) Average
	\bar{U}_{max}	\bar{U}_{min}	
1	3.61	3.42	0.28
2	3.62	3.40	0.25
3	3.55	3.35	0.25
4	3.35	3.19	0.20
5	3.25	3.09	0.20
6	3.25	3.09	0.25
7	3.19	3.05	0.30
8	2.85	2.19	0.35
9	2.15	1.65	0.35
10	1.75	1.15	0.25
11	1.15	0.98	0.20

TABLE 3.28

Measured Longitudinal Mean Velocity and (r.m.s.)
Profiles for, $q = 106 \text{ cm}^3/\text{sec}/\text{cm}$ at $X = 28 \text{ cm}$

Water Depth (H) = 11.9 cm Gate Opening (G) = 7 cm
Length of Tank (L) = 30 cm Head Over the
Height of Weir = 8.5 cm ~ Weir = 3.3 cm

Elev. (cm)	VELOCITY (volts)		r.m.s. (volt) Average
	\bar{U}_{max}	\bar{U}_{min}	
1	2.85	2.69	0.30
2	3.00	2.75	0.25
3	3.00	2.85	0.20
4	3.00	2.85	0.20
5	3.00	3.85	0.20
6	3.00	2.90	0.20
7	3.00	2.90	0.18
8	3.12	3.07	6.18
9	3.25	3.18	0.20
10	3.25	3.05	0.20
11	3.05	2.80	0.20

TABLE 4.1
Average Values of A and B for
Different Flow Conditions

Flow Characteristics	A	B
G = 3 cm, L = 30 cm, q = 87.41 cm ³ /sec/cm	0.0060	19
G = 5 cm, L = 30 cm, q = 101.32 cm ³ /sec/cm	0.0120	21.5
G = 7 cm, L = 30, q = 106 cm ³ /sec/cm	0.0060	22.3
G = 5 cm, L = 73 cm, q = 147 cm ³ /sec/cm	0.0022	29
G = 3 cm, L = 73 cm, q = 111 cm ³ /sec/cm	0.0130	23
G = 5 cm, L = 40 cm, q = 111 cm ³ /sec/cm	0.0220	23
G = 7 cm, L = 30 cm, q = 53.9 cm ³ /sec/cm	0.0060	9.8
G = 5 cm, L = 30 cm, q = 53.9 cm ³ /sec/cm	0.0082	9.8
G = 3 cm, L = 30 cm, q = 53.9 cm ³ /sec/cm	0.0095	9.8
G = 3 cm, L = 40 cm, q = 61.74 cm ³ /sec/cm	0.0070	10.9

APPENDIX B

Computer Programmes

```

1. //AMAL JOB ( ,2), 'AMAL SEBAKHY', CLASS=A
2. // EXEC PLOT
3. //FORT.SYSIN DD *
4. DIMENSION IBUF(1000),VEL(21),DIST(21),R(21),VE1(21),VAU(20)
5. CALL PLOTS (IBUF,1000)
6. READ 20,C,C1
7. 20 FORMAT (2F6.3)
8. READ 25, (DIST(I),I=1,19)
9. READ 25, (VEL(I),I=1,19)
10. 25 FORMAT (12F6.3)
11. DO 5 I=1,19
12. VEL(I)=(VEL(I)-1.0)/C
13. PRINT 4,VEL(I),DIST(I)
14. 4 FORMAT (2F8.3)
15. 5 CONTINUE
16. CALL PLOTID('AMAL , SEBAKHY ', ' ')
17. CALL PLOT (1.,1.,-3)
18. CALL SCALE (VEL,5.0,19,1)
19. VEL(20)=-0.4
20. VEL(21)=0.4
21. CALL SCALE (DIST,9.0,19,1)
22. DO 40 II=1,5
23. CALL AXIS (0.0,0.0,8HVELOCITY,-8,5.0,0.0,VEL(20),VEL(21))
24. CALL AXIS (0.0,0.0,8HDEPTH ,8,9.0,90.0,DIST(20),DIST(21))
25. CALL LINE (VEL,DIST,19,1,0,0)
26. 40 CONTINUE
27. VE1(20)=VEL(20)
28. VE1(21)=VEL(21)
29. READ 26,(VE1(J),J=1,19)
30. 26 FORMAT(12F6.3)
31. DO 30 J=1,19
32. VE1(J)=(VE1(J)-1.0)/C
33. PRINT 6,VE1(J),DIST(J)
34. 6 FORMAT (2F10.3)
35. 30 CONTINUE
36. DO 50 II=1,5
37. CALL LINE (VE1,DIST,19,1,0,0)
38. 50 CONTINUE
39. CALL SYMBOL(.5,9.,0.21,20HVELOCITY VS DEPTH ,0.0,20)
40. DO 11 N=1,19
41. VAV(N)=(VEL(N)+VE1(N))/2.
42. 11 CONTINUE
43. SUM=0
44. DO 12 I=1,18
45. A=(VAV(I)+VAV(I+1))*(DIST(I+1)-DIST(I))/2.
46. SUM=SUM+A
47. 12 CONTINUE
48. PRINT 13,SUM
49. 13 FORMAT (50X,5HAREA=,F10.5)
50. READ 8 , (R(K),K=1,19)
51. 8 FORMAT (12F6.3)

```

```

52.      DO 7 K=1,19
53.      R(K)=R(K)/C
54.      PRINT 9,R(K),DIST(K)
55.      9 FORMAT (2F6.3)
56.      7 CONTINUE
57.      CALL PLOT (7.,0.,-3)
58.      CALL SCALE (R,5.0,19,1)
59.      CALL SCALE (DIST, 9.0 ,19 ,1)
60.      DO 60 II=1,5
61.      CALL AXIS (0.0,0.0,8HR.M.S. , -8,5.0,0.0,R(20),R(21))
62.      CALL AXIS (0.0,0.0,8HDEPTH , 8,9.0,90.0,DIST(20),DIST(21))
63.      CALL LINE (R,DIST,19,1,0,0)
64.      60 CONTINUE
65.      CALL SYMBOL (.5,9.,0.21,20HR.M.S. VS DEPTH ,0.0 ,20)
66.      SUMR=0
67.      DO 16 I=1,18
68.      A1=(R(I)+R(I+1))*(DIST(I+1)-DIST(I))/2.
69.      SUMR=SUMR+A1
70.      16 CONTINUE
71.      PRINT 17 ,SUMR
72.      17 FORMAT (50X,6HAREAR=,F10.5)
73.      CALL PLOT (0.0,-2.0,-3)
74.      CALL PLTEND(6.)
75.      DO 21 I=1,19
76.      VAV(I)=VAV(I)/SUM
77.      PRINT 22 ,VAV(I)
78.      22 FORMAT (40X,'VELOCITY CORRECTED=',F7.3)
79.      21 CONTINUE
80.      SUMM=0
81.      DO 41 I=1,18
82.      AM=(VAV(I)+VAV(I+1))**(DIST(I+1)-DIST(I))/2.
83.      SUMM=SUMM+AM
83.1     PRINT 100,I,SUMM
83.2     100 FORMAT(' ****DEPTH=',I5,10X,' AREA=',F10.6)
84.      41 CONTINUE
85.      PRINT 42 ,SUMM
86.      42 FORMAT (40X,15HAREA CORRECTED=,F10.5,/)
87.      SUM2=0
88.      DO 23 I=1,18
89.      A2=(VAV(I)**3+VAV(I+1)**3)*(DIST(I+1)-DIST(I))/2.
90.      SUM2=SUM2+A2
91.      23 CONTINUE
92.      SUM2=SUM2/C1
93.      PRINT 24,SUM2
94.      24 FORMAT(40X,' AREA TOTAL =',F10.5)
95.      DO 31 I=1,19
96.      R(I)=R(I)/SUM
97.      PRINT 27 , R(I)
98.      27 FORMAT (30X,'R.M.S.CORRECTED=',F7.3)
99.      31 CONTINUE
100.     SUM3=0
101.     DO 28 I=1,18
102.     A3=(R(I)**2*VAV(I)+R(I+1)**2*VAV(I+1))*(DIST(I+1)-DIST(I))/2.
103.     SUM3=SUM3+A3
104.     28 CONTINUE
105.     SUM3=SUM3/C1
106.     PRINT 29 ,SUM3
107.     29 FORMAT (30X,' AREA OF R.M.S. CORRECTED=',F9.5)
108.     STOP
109.     END

```



```

1. //HALA JOB ( ) , 'SEBAKHY' , CLASS=W
2. // EXEC WATFIV
3. //GO.SYSIN DD *
4. $JOB WATFIV HALA
5. REAL*8 Y(25),W(25),DY(25)
6. EXTERNAL VECTOR
7. COMMON / AREA1 / TL,XN,G,A,C,D,B,U
8. C=0.01200
9. D=2.500
10. A=-0.134
11. B=0.000
12. N=-0.629
13. G=3.00
14. TL=55.0
15. DX=0.25
16. X =0.25
17. XN=TL/DX
18. V=.00450
19. PRINT ,X,V
20. NX=XN
21. Y(1)=V
22. DO 1 K=1,NX
23. DX=0.25
24. N =1
25. CALL RK5ES(X,Y,DY,DX,N,VECTOR)
26. PRINT , X,Y(1)
27. 1 CONTINUE
28. STOP
29. END
30. C *****
31. SUBROUTINE VECTOR (X,Y,W,N )
32. COMMON / AREA1 / TL,XN,G,A,C,D,B,U
33. REAL*8 X, Y(25),W(25),DY(25)
34. C=.0120
35. D=2.500
36. A=-.134
37. B=0.000
38. AN=-0.629
39. G=3.0
40. DX=0.25
41. W(1)=-C*(A*(X/G)**AN+B)-D*(V)**1.5
42. RETURN
43. END

```

```

1. //RAM      JOB (           ), 'SEBAKHY', CLASS=A
2. // EXEC    WATFIV
3. //GO.SYSIN DD *
4. $JOB      WATFIV          RAM
5.          DIMENSION U(50),V(50)
6.          READ 5 , X , DX , UB , UD , G , D
7.          PRINT 5,X,DX,UB,UD,G,D
8.          5 FORMAT ( 6F6.3 )
9.          N = ( X + 1 ) / DX
10.         W = UD * G / D
11.         READ , ( U(I) , V(I) , I = 1,N )
12.         PRINT , (U(I),V(I) , I = 1,N )
13.         NN = N - 2
14.         DO 15 I = 1,NN
15.         U1 = UB * ( V(I+1) - V(I) ) / DX
16.         V1 = W * ( U(I+1) - U(I) ) / DX
17.         D1 =      ( ( V(I+1) + V(I) ) / 2. ) ** 1.5
18.         U2 = UB * ( V(I+2) - V(I+1) ) / DX
19.         V2 = W * ( U(I+2) - U(I+1) ) / DX
20.         D2 =      ( ( V(I+2) + V(I+1) ) / 2. ) ** 1.5
21.         Z=(D2*V1-D1*V2)
22.         IF(Z.EQ.0.0) GO TO 15
23.         A = ( D1 * U2 - D2 * U1 ) / Z
24.         B = ( U1 * V2 - U2 * V1 ) / Z
25.         J = I
26.         PRINT 20 , J , A , B
27.         20 FORMAT (10X,'SEC.NO.',I2, 5X,'A=',1F10.5,5X,'B=',1F10.5,/)
28.         15 CONTINUE
29.         STOP
30.         END

```

NOMENCLATURE

A	Constant of the generation term, Eq. 4.10
B	Constant of the decay term, Eq. 4.10
C	Empirical constant, Eq. 4.13
C_D	Constant appearing in the dissipation term of turbulence energy, Eq. 2.9
C_D	Empirical constant, Eq. 2.13
D	Empirical constant; Eq. 4.13
E	Output voltage of frequency tracker
E_s	Output voltage of frequency tracker at zero velocity
f_d	Frequency
f_k	Mean kinetic energy flux
g_i	The gravitational acceleration in direction x_i , Eq. 2.11
G	Gate opening in cm.
H	Water depth of the tank
h_w	Head over end-weir
h_B	Baffle height
i, j	Tensor-notation subscripts taking values 1, 2 or 3 and u_1' and u_2' denote u' and v' respectively, x_1 denotes x , etc. Eq. 2.6
K	Half the intersection angle of laser beams
k'	The instantaneous value of turbulence energy
k	Kinetic energy of turbulence
L	Effective length of the tank

l	Length scale of turbulence proportional to the size of the energy containing motions.
L_p	Length of potential core
L_r	Length of eddies
P	The fluctuations about the mean value of the time-mean pressure field
P'	Fluctuating pressure
q	Flowrate per unit width
R_N	Reynolds number
\bar{U}	The mean velocity at a point in the x-direction
$\overline{U'^2}$	Representative turbulent kinetic energy
\bar{U}_m	Depth-averaged mean velocity q/H
\bar{U}_O	Depth averaged mean velocity at the gate, q/G
\bar{U}_R	The reference velocity calculated as the average value at the gate
$U, V, W,$	Velocity components in x, y, z direction
u', v', w'	Fluctuating components of velocity in x, y and z directions
$\overline{u'^2}, \overline{v'^2}, \overline{w'^2}$	Mean-square fluctuating components of velocity in x, y, and z directions
V_t	Eddy (or turbulent) viscosity. Eq. 2.12.
β	Volumetric expansion coefficient. Eq. 2.11
ϵ	Turbulence dissipation rate
Δ	The space increment
λ	Laser light wave length, nm
μ	Molecular viscosity. Eq. 2.6

μ_t	Turbulent viscosity. Eq. 2.7
ν	Molecular kinematic viscosity, Eq. 2.5
ρ	Density of fluid
ψ	Fluctuating scalar quantity. Eq. 2.11
σ_k	Empirical diffusion constant. Eq. 2.12
σ_k	The effective Prandtl number for the diffusion turbulence energy. Eq. 2.7

REFERENCES

1. Bayazit, M. "Random Walk Model for Motion of a Solid Particle in Turbulent Open-Channel Flow." *Journal of Hydraulic Research*, Vol. 10, No. 1, 1972, pp. 1-14.
2. Bradshaw, P. "Turbulence Research Progress and Problems." *Proc. of the Heat Transfer and Fluid Mech. Inst.*, 25th. Univ. of Calif., Davis, June 21-23, 1976, Stanford University Press, 1976, pp. 128-139.
3. Camp, T. R. "Studies of Sedimentation Basin Design." *Sewage and Industrial Wastes*, Vol. 25, 1953, pp. 1-12.
4. Cenedese, A., Lannetta, S., Mele, P., and Pietrogiacomini, D. "Non Stationary Analysis of Velocity Field Around a Square Section Bluff Body." 2nd Symposium on Turbulent Shear Flow, London, 1979.
5. Cenedese, A., Mele, P., and Morganti, M. "Boundary Layer Separation Analysis Around a Square Section Bluff Body." *International Association for Hydraulic Research*,
6. Clements, M. S., and Price, G. A. "A Two-Float Technique for Examination of Flow Characteristics of Sedimentation Tanks." *Journal Instn. Municipal Engrs.*, Vol. 99, February 1972, pp. 53-58.
7. Crosby, R. M., and Bender, J. H. "Hydraulic Considerations that Affect Secondary Clarifier Performance." *U.S. EPA Technology Transfer*, March 1980.
8. Dobbins, W. E. "Solid-Liquid Separation, Advances in Sewage Treatment Design." *Proceedings of a Symposium held at Manhattan College, New York, May 1961*, pp. 1-23.
9. Durst, F., Melling, A., and Whitelaw, J. H. *Principles and Practice of Laser Anemometry*. Academic Press, 1976.
10. Durst, F., and Rastogi, A. K. "Theoretical and Experimental Investigations of Turbulent Flows with Separation." *Symposium on Turbulent Shear Flows*, Pa. State Univ., April 18-20, 1977, Pennsylvania State Univ. Press. p. 18.1-18.9.
11. El-Baroudi, H. M. "Characterization of Settling Tanks by Eddy Diffusion." *J. of Sanitary Eng., ASCE*, No. SA3, Vol. 95, June 1969, pp. 327-344.

12. El-Baroudi, H. M., and Fuller, D. R. "Tracer Dispersion of High Rate Settling Tanks." ASCE, Vol. 99, No. EE3, June 1973, pp. 347-368.
13. Galin, N. M. "Calculation of the Dissipation of Turbulent Energy in Incompressible Fluid Flows." Moscow Power Int., USSR, V. 14, No. 1, Jan-Feb. 1976, pp. 109-115.
14. Ginevskii, A. S., Kolesnikov, A. V., and Ukhanova, L. N. "Decay of Turbulence Behind a Double Grid of Cylinders with Opposite Motion of the Grids." Fluid Dyn, Vol. 14, No. 3, May-June 1979, pp. 334-338.
15. Griffith, O. F., and Grimwood, C. "Turbulence Measurement Study." ASCE, Vol. 107, No. HY3, March, 1981, pp. 311-326.
16. Hirsch, A. A. "Basin Tracer Curves Interpreted by Basin Analytics." J. of Sanitary Eng., ASCE, No. 5A6, Vol. 95, Proc. Paper 6951, Dec. 1969, pp. 1031, 1050.
17. Imam, E. H. "Numerical Modelling of Rectangular Clarifiers." Ph.D. Thesis, University of Windsor, Windsor, Ontario Canada, 1981.
18. Ingersoll, A. C., McKee, J. E., and Brooks, N. H. "Fundamental Concepts of Rectangular Settling Tanks." ASCE, Trans., Paper No. 2837, 1956 (with discussions).
19. Khattab, A.F.M. "Flow Patterns in Circular Sedimentation Tanks." Ph.D. Thesis, Sheffield University, 1967.
20. Larsen, P. "Research on Settling Basin Hydraulics." Tenth Anniversary Paper on Research in Progress, Dept. of Water Res. Eng., Lund Inst. of Tech., Bull. Series A No. 55, Lund, Sweden, July 1976, pp. 137-149.
21. Larsen, P. "On the Hydraulics of Rectangular Settling Basins- Experimental and Theoretical Studies." Department of Water Resources Engineering, Report No. 1001, Lund, Sweden, 1977.
22. Launder, B. E., and Spalding, D. B. Lectures in Mathematical Models of Turbulence. Third Printing. Academic Press, London, 1979.
23. McCorquodale, J. A. "Hydraulic Study of the Circular Settling Tanks at the West Windsor Pollution Control Plant." Report submitted to Lafontaine, Cowie, Buratto and Associates, Ltd. Consulting Engineers, Windsor, Ontario. 1977.

24. McQuivey, R. S. (1972). Summary of Turbulence Data from Rivers, Conveyance Channels and Laboratory Flumes. U.S. Department of the Interior Geological Survey, Water Resources Division, Open-File Report, St. Louis, Mississippi.
25. Melling, A., and Whitelaw, J. H. "Turbulent Flow in a Rectangular Duct." J. Fluid Mech., Vol. 78, Part 2, Nov. 23, 1976, pp. 289-315.
26. Ming Li, R., Schall, J. D., and Simons, D. B. "Modeling of Turbulent Intensity in Open Channel Flows." Proc. of the First International Conference, Univ. College Swansea, Swansea SA2 8PP, U.K., July 17-21, 1978. Halsted Press, New York, 1978, pp. 317-328.
27. Ming Li, R., and Shen, H. W. "Solid Particle Settlement in Open-Channel Flow." ASCE, Vol. 101, No. HY7, July, 1975, pp. 917-931.
28. Morrill, A. B. "Sedimentation Basin Research and Design." J.A.W.W.A., Vol. 24, No. 9, 1932, pp. 1442-1463.
29. Orton, J. W. "Discussion on Sedimentation Basin Research and Design, by A. B. Morrill," J.A.W.W.A, Vol. 24, No. 9, pp. 1442-1463.
30. Price, G. A. "Influence of Inlet Changes, Wind Effects and Density Currents in Rectangular Sedimentation Tanks." Ph.D. Thesis, Univ. of Sheffield, 1970.
31. Rajaratnam, N., and Subramanya, K. "Flow Immediately Below Submerged Sluice Gate." ASCE, Vol. 93, No. HY4, July 1967, pp. 57-77.
32. Rajaratnam, N. Turbulent Jets. Elsevier Scientific Co., New York, 1976.
33. Rankin, G. W. "Developing Region of Laminar Jets." Ph.D. Thesis, University of Windsor, Windsor, Ont. Canada, 1980.
34. Reynolds, A. J. Turbulent Flows in Engineering. John Wiley and Sons, 1974.
35. Rodi, W. "Turbulence Models and Their Application in Hydraulics." State-of-the-Art Paper, IAHR, 1980.
36. Schall, J. D., Ming Li, R. and Simons, D. B. "Prediction of Turbulent Intensity in Open Channel Flows." Int. Assoc. for Hydraulic Research

37. Schamber, D. R., and Larock, B. E. "Numerical Analysis of Flow in Sedimentation Basins." ASCE, Vol. 107, No. HY5, May 1981, pp. 575-591.
38. Schamber, D. R., and Larock, B. E. "A Finite Element Model of Turbulent Flow in Primary Sedimentation Basins." Proceeding, Finite Elements in Water Resources, Imperial College, Longon, July 1978, pp. 3.3-3.22.
39. Singhal, A. K. and Spalding, D. B. "Predictions of Two-Dimensional Boundary Layers with the Aid of the K- ϵ Model of Turbulence." Comput. Methods Appl. Mech. Eng. V25, No. 3, Mar. 1981, pp. 365-383.
40. Smyth, R. "Turbulent Flow Over a Plane Symmetric Sudden Expansion." J. Fluids Eng. Trans. ASME, Vol. 101, No. 3, Sept. 1979, pp. 348-353.
41. Wylie, C. Differential Equations. McGraw-Hill Book Co., New York, 1979.

VITA AUCTORIS

Amal M. Moursy (El-Sebahky)

The author was born on June 28, 1951, in Elzakazik, Egypt. In 1969, she completed her secondary school education and joined the Department of Civil Engineering, Alexandria University, Alexandria, Egypt. In 1974, she graduated from Alexandria University with a degree of Bachelor of Civil Engineering. After graduation, the author spent two years working as research engineer with UNESCO in seashore protection.

In 1979, she joined the Civil Engineering Department at the University of Windsor, Windsor, Ontario, Canada, as a teaching and research assistant. The author prepared this thesis in partial fulfillment for the requirements for the degree of Master of Applied Science at the University of Windsor.